SAND REPORT
SAND2003-0411
Unlimited Release
Printed February 2003

Final Report on LDRD Project: Heterogeneous Integration of Optoelectronic Arrays and Microelectronics

Kent M. Geib, Darwin K. Serkland, Kent D. Choquette, Gregory M. Peake, Terry W. Hargett, Jana J. Hindi, Victoria M. Montano, Gary D. Karpen, Ronald D. Briggs, G. Ronald Hadley, Sayan D. Mukherjee, Charles T. Sullivan, Andrew A. Allerman, Sally Samora, Tony R. Carter, Dennis J. Rieger, Arthur J. Fischer, Vincent M. Hietala

Prepared by
Sandia National Laboratories
Albuquerque, New Mexico 87185 and Livermore, California 94550

Sandia is a multiprogram laboratory operated by Sandia Corporation, a Lockheed Martin Company, for the United States Department of Energy's National Nuclear Security Administration under Contract DE-AC04-94-AL85000.

Sandia National Laboratories

Issued by Sandia National Laboratories, operated for the United States Department of Energy by Sandia Corporation.

Available to DOE and DOE contractors from
U.S. Department of Energy
Office of Scientific and Technical Information
P.O. Box 62
Oak Ridge, TN 37831

Telephone: (865)576-8401
Facsimile: (865)576-5728
E-Mail: reports@adonis.osti.gov
Online ordering: http://www.doe.gov/bridge

Available to the public from
U.S. Department of Commerce
National Technical Information Service
5285 Port Royal Rd
Springfield, VA 22161

Telephone: (800)553-6847
Facsimile: (703)605-6900
E-Mail: orders@ntis.fedworld.gov
Online order: http://www.ntis.gov/help/ordermethods.asp?loc=7-4-0#online

SAND2003-0411
Unlimited Release
Printed February 2003

Final Report on LDRD Project: Heterogeneous Integration of Optoelectronic Arrays and Microelectronics

Kent M. Geib, Darwin K. Serkland, Kent D. Choquette*, Gregory M. Peake, Terry W. Hargett**, Jana J. Hindi***, Victoria M. Montano**, Gary D. Karpen, Ronald D. Briggs, G. Ronald Hadley, Sayan D. Mukherjee*, Charles T. Sullivan
RF Microsystems Technologies

Andrew A. Allerman
Chemical Processing Science

Sally Samora** and Tony R. Carter**
Photonic Microsystems Technologies

Dennis J. Rieger
Microdevice Technologies

Arthur J. Fischer
Semiconductor Material & Device Science

Vincent M. Hietala
Integrated Microsystems

Sandia National Laboratories
P.O. Box 5800
Albuquerque, NM 87185-0603

Abstract

Integrated microsystems provide the benefits of small size, low power consumption, robustness, and potentially inexpensive manufacture. However, multifunctional advanced microsystems often require a combination of microelectronic and photonic technologies. For example, high-density 2-dimensional integrated optoelectronic arrays are the basic components necessary to construct real-time electro-optical signal processing and analog information processing microsystems. In corresponding

*no longer at Sandia **L&M Technologies, Inc.

applications such as digital and neural computing, data mining, and data communication switching, there is a critical need to provide local electronic processing in each optoelectronic element. Moreover, to achieve the required functionality in these systems, highly sophisticated devices with state-of-the-art performance are necessary. Thus, large numbers of densely packed high performance devices originating from disparate technologies are needed to achieve the next generation of information processing, interconnect, and intelligent sensing microsystems.

This project produced a number of first-ever research prototypes. The hybrid integration work was the first demonstration of GaAs drivers and receivers integrated with VCSELs for spatially multiplexed multi-channel high-speed data links. The flip-chip integration was the first demonstration of flip-chipped 850 nm VCSELs onto GaAs drivers showing the possibility of using such arrays under the current short distance datacom standards. The matrix addressable array work demonstrated the largest number of lasers and detectors ever integrated onto a single chip, opening the way for scannerless VCSEL based imaging systems. Fiber image guides show great promise for use in short range highly parallel array-to-array data transmission compatible with the current 850 nm datacom standards. Lastly, integration of VCSELs with high performance heat sinks shows potential for even higher device performance in the future.

Acknowledgments

Sandia is a multiprogram laboratory operated by Sandia Corporation, a Lockheed Martin Company, for the United States Department of Energy under contract DE-AC04-94AL85000.

Heterogeneous Integration of Optoelectronic Arrays and Microelectronics

Table of Contents

Introduction

Integration of microelectronic and photonic technologies can take on many forms depending on the particular needs of the driving application. We have concentrated on the integration of vertical-cavity surface-emitting lasers (VCSELs) with drive electronics and/or detectors thus building on our VCSEL expertise, although the techniques can be used for the integration of many other optoelectronic devices. We first investigated hybrid integration in which separate electronic and optoelectronic chips were attached to a common chip carrier and connected to each other using wire bonds. This hybrid approach requires the least sophisticated processing while allowing the optimization of all of the electronic and optoelectronic components but has limitations in size and performance that can be overcome by doing flip-chip integration, which was investigated next. Homogeneous integration of VCSELs and photodetectors was also investigated to maximize the integration density for imaging applications. As array densities increase, heat dissipation from the VCSELs becomes increasingly important. Thus, we have also looked at various techniques for the integration of high performance heat sinks. The report is organized according to the integration technique with the majority of details being contained in the appendices, which include the published references from this project.

Hybrid packaging

Massively parallel optical interconnects may be appropriate to ease the data bandwidth bottleneck that may occur in future computing applications. For example, the use of guided wave or free space optical interconnects to provide a high-speed parallel bus between a microprocessor and memory may enable faster computing speeds. However, there are stringent performance requirements that must be imposed on an optical interconnect within the computing environment, such as high reliability, high modulation rate, and operation at elevated temperature. Vertical cavity surface emitting lasers (VCSELs) are promising optical sources for 2-dimensional optical systems such as free space and guided wave optical interconnects. VCSELs have already been enthusiastically adopted into Gigabit Ethernet applications in a remarkably short period of time due to their reduced threshold current, circular output beam, and inexpensive and high volume manufacture. Extending VCSEL sources from single devices to 2-dimensional arrays will enable high density optical interconnects suitable for emerging computing applications.

We assembled hybrid packages of 8x8 VCSEL arrays with GTL logic compatible digital drivers. The VCSELs were fabricated at Sandia using our advanced wet thermal oxidation process. The drivers were Sandia designed and foundry fabricated. An industrial partner tested the components and found 100% functionality. The VCSEL and driver arrays were mounted together in a large pin-grid-array package and were electrically connected together using fine gold wire. Arrays of compatible detectors were also designed, foundry fabricated, and tested. Details can be found in the following references that are included as Appendix A.

High Performance 2-Dimensional VCSEL Arrays for Interconnect and Imaging Applications, K. D. Choquette, R. D. Briggs, K. M. Geib, A. A. Allerman, J. J. Hindi, and S. Samora, in International Symposium on Ultra-Parallel Optoelectronics (Post Proceedings): 2/3/00 thru 2/4/00, Kawasaki, Japan (2000).

Hybrid Integrated VCSEL and Driver Arrays for Optical Interconnects, K.D. Choquette, V.M. Hietala, K.M. Geib, S.D. Mukherjee and A.A. Allerman, in IEEE Lasers and Electro-Optics Society 2000 Annual Meeting: 11/13/00 thru 11/16/00, Rio Grande, Puerto Rico (2000).

Two-Dimensional 8x8 Photoreceiver Array and VCSEL Drivers for High-Throughput Optical Data Links, V.M. Hietala, Carl Chun, Joy Laskar, K.D. Choquette, K.M. Geib, A.A. Allerman and J.J Hindi, IEEE Journal of Solid-State Circuits, vol. 36, no. 9, pp. 1297-1302, Sept. (2001).

High-performance vertical-cavity laser, driver, and receiver arrays for optical interconnects, K.D. Choquette, V.M. Hietala, K.M. Geib, R.D. Briggs, A.A. Allerman, and J.J.Hindi, Proceedings of the SPIE - The International Society for Optical Engineering, vol. 4089, pp. 704-707, (2000).

Flip-chipped 2-D VCSEL arrays

Combinations of large numbers of densely packed high performance photonic and microelectronic devices originating from disparate technologies are needed to achieve the next generation of information processing, interconnect, and intelligent sensing microsystems. Flip-chip integration promises even higher densities than hybrid integration. Previous flip-chip VCSELs integrated to microelectronic circuitry were accomplished as isolated individual VCSEL islands and often emit at longer wavelengths to allow emission through the GaAs substrate. However, 850 nm VCSELs are the most mature commercial technology, and high count/high density 2-dimensional arrays are desired for emerging applications. We report the fabrication techniques for flip-chip integration of selectively oxidized 850 nm 8x8 individually addressable VCSEL arrays.

A novel gold coated silver post flip-chip bonding process was developed for the bonding of 2-dimensional VCSEL arrays to high-speed driver circuits. This thin film process provides better planarity between the VCSELs and drive electronics than can be achieved using gold ball bonding and is less time consuming to fabricate as well. We have designed a 64-channel driver circuit to accept a flip-chipped VCSEL array and have had it fabricated at a commercial foundry. All of the flip-chip processes that were individually developed have been brought together to demonstrate lasing devices bonded onto a test coupon. Details of this work are contained in Appendix B.

Flip-chip Integration of Selectively Oxidized 850 nm VCSEL Arrays, K.M. Geib, K.D. Choquette, A.A. Allerman, and J.J. Hindi in IEEE Lasers and Electro-Optics

Society 2000 Annual Meeting: 11/13/00 thru 11/16/00, Rio Grande, Puerto Rico (2000).

VCSEL light coupling to fiber bundles

While 1-D data links based on VCSELs and linear fiber ribbons have seen significant commercial success, parallel links that take advantage of the two-dimensionality of VCSEL arrays on planar substrates are at an early stage of development. Getting light from the VCSELs into optical fibers often requires sophisticated focusing optics and small alignment tolerances. We investigated a more straightforward approach using a flexible imaging fiber bundle light guide with a 1.8 mm hexagonal cross-section consisting of 15379 fibers each with a 9.1-μm core at a 13.5-μm pitch and a 2-μm-thick cladding to transmit the VCSEL light to the detector without the need for focusing optics or accurate alignment. In spite of apparent simplicities, the fiber image guide is a complex medium for parallel optical data transmission. There are several characteristics that are unique to a 2-D array of fibers that are not present in the case when a single fiber is used. These are: multiple large angle reflections at the input facet contributing to optical cross-talk, a three-segment transmission medium, high-index coupling of cladding modes to adjacent fibers, high divergence of fiber modes and extreme divergence of cladding modes at the output. Our investigation showed that this technology is, however, insensitive to VCSEL/fiber alignment making it ideally suited for light transmission over short distances (several meters). The results of this effort are shown in Appendix C.

Input Coupling Measurements for Parallel Optical Interconnects using Imaging Fiber Bundles and VCSEL Arrays, Sayan D. Mukherjee, Kent M. Geib and Kent D. Choquette, CLEO-Europe, 10-15 September, 2000, Nice, France (2000).

Characterization of Cross-Talk Sources in Massively Parallel Datalinks using VCSEL arrays and Fiber Image Guides, S.D. Mukherjee, K.D. Choquette, K.M. Geib, G.R. Hadley, T. Carter, A.J. Fischer, C.T. Sullivan and K. Tatah, Optics in Computing topical meeting 2001: 1/9/2001 thru 1/11/2001, Lake Tahoe, NV (2001).

Critical Parameters For Parallel Interconnects Using VCSEL Arrays and Fiber Image Guides, Sayan D. Mukherjee, G. Ron Hadley, Kent M. Geib, Kent D. Choquette, Tony R. Carter, Arthur J. Fischer, Matt Robinson, and Charles T. Sullivan, in VCSELs and Optical Interconnects SPIE Photonics Fabrication Europe 2002: 10/28/02 thru 11/1/02, Brugge, Belgium: (2002).

Two Dimensional Guided Wave Optical Interconnect, H. P. Chen, K. D. Choquette, V. M. Hietala, and K. M. Geib, J. Sel. Top. Quan. Electron., submitted (2003).

Integrated VCSEL/detector arrays

Early in the development of vertical-cavity surface-emitting lasers (VCSELs), large 2-dimensional arrays were recognized as an enabling technology for many applications. The inclusion of photodetectors within such a VCSEL array enables a variety of applications including high-density interconnects, position sensors and imaging devices. To reach the device densities required for scannerless imaging applications, we investigated the homogeneous integration of resonant cavity photodiodes within the VCSEL array.

We have successfully fabricated 4096 element arrays (64x64) containing alternating rows of selectively-oxidized 850 nm VCSELs and resonant-cavity photodetectors (RCPDs) on a 55 micron pitch monolithically integrated on semi-insulating GaAs substrates. We employ a matrix addressable architecture to reduce the input and output electrical connections to the array, where all the VCSELs (or RCPDs) in each row are connected by a common metal trace at the base of their mesas. The columns are connected by metal traces that bridge from mesa top to mesa top, connecting every other row (i.e., only VCSELs or only RCPDs). An industrial partner has demonstrated that the array functions as both the light emitter and detector in a prototype scannerless scanning confocal microscope (see SPIE Photonics Fabrication Europe, 2002). Publications are included in Appendix D.

Monolithic Integration of Vertical-Cavity Surface-Emitting Lasers and Wavelength-Shifted Resonant-Cavity Photodetectors, D.K. Serkland, K.M. Geib, A.A. Allerman, and T.W. Hargett, in IEEE LEOS 2001 Annual Meeting: 11/12/01 thru 11/15/01, La Jolla, CA (2001).

Fabrication and Performance of Large (64x64) Arrays of Integrated VCSELs and Detectors, K.M. Geib, K.D. Choquette, D.K. Serkland, A.A. Allerman, and T.W. Hargett, in Vertical Cavity Emitting Lasers Symposium SPIE Photonics West 2002: 1/20/02 thru 1/25/02, San Jose, CA (2002).

Fabrication and Performance of Two-Dimensional Matrix Addressable Arrays of Integrated Vertical-Cavity Lasers and Resonant Cavity Photodetectors, K.M. Geib, K.D. Choquette, D.K. Serkland, A.A. Allerman, and T.W. Hargett, IEEE Journal of Selected Topics in Quantum Electronics, Vol. 8, No. 4, July/Aug, pp. 943-947 (2002).

High Density Interleaved VCSEL-RCPD Arrays for Optical Information Processing, K.M. Geib, D.K. Serkland, A.A. Allerman, T.W. Hargett, and K.D. Choquette in VCSELs and Optical Interconnects SPIE Photonics Fabrication Europe 2002: 10/28/02 thru 11/1/02, Brugge, Belgium (2002).

Heat sinking VCSELs

Temperature rise in VCSELs due to the electrical drive current limits the light output power possible from any given device. By increasing the thermal conductivity of the VCSEL substrate, higher light output powers can be achieved. We have successfully demonstrated high power VCSELs on silicon heat sinks where VCSEL epitaxial material was bonded to silicon using an indium metal thin film. The GaAs substrate was partially removed to reduce absorption but approximately 50 μm was left to aid in current spreading across the large aperture devices. The process was accomplished using either electron beam evaporated or electroplated indium and a flip-chip bonder modified with a nitrogen purge to allow melting of the indium without oxidation (which prevents bonding). This work will be published, however, the manuscript is not yet complete so the details are included below.

> *Optimization of External Cavity VCSELs,* Darwin K. Serkland, Peter Esherick, Kent M. Geib, Gregory M. Peake, and Andrew A. Allerman, to be presented at SPIE Photonics West 2003: 1/25/02 thru 1/31/02, San Jose, CA (2003).

Indium is a soft low melting point metal that is ideally suited for thin film solder applications where intimate thermal contact, high adhesion strength and low temperature processing are required, thus making it the logical starting point for this investigation. Indium can be deposited either by vacuum evaporation or electroplating and we have investigated the pro's and con's of both processes.

Indium can be readily electroplated onto gold coated substrates in a room temperature bath containing indium sulfamate. The solution is placed in a beaker on a magnetic stirrer with the sample placed orthogonal to the fluid motion for best uniformity. The smoothest and most uniform films were obtained using a 50% duty cycle plating current at 500 Hz and 0.124 mA/mm^2 current density. Patterned electroplating is possible using AZ9260 photoresist for depositions of less than 6 μm although the gold metalization before photoresist patterning must be continuous to provide the proper current path for plating.

Electroplating provides thick films at a high rate, however, the films tend to be rough and oxidize readily in air making them unusable within a few days of air exposure. We have, however, found that a short etch in dilute HF acid will make the films useable again. Thermal evaporation of indium provides a smoother film which can be capped with a thin gold layer prior to air exposure to prevent oxidation. However, the process is slower, thick films are more difficult to deposit and the evaporation system is easily contaminated with indium which is a problem for other system users. Evaporation also does not need the initial continuous gold film that electroplating does so that isolated devices are easier to fabricate.

If the fresh indium film is deposited on both the heat sink and the device prior to placing them in contact, only pressure is required to get good mechanical adhesion. This is very

useful for the appliqué technique where the sample is attached to a temporary substrate with wax, the GaAs substrate is chemically removed from the sample, and then the sample is coated with indium and transferred to the heat sink by mechanically pressing the two indium coated pieces together. After dissolving the wax holding the sample to the temporary substrate, the heat sink and sample are pressed together and heated above the indium melting point to get excellent electrical and thermal contact. Using this technique, the device epitaxial material alone can be transferred to a high performance heat sink to provide outstanding heat extraction.

The high power single element VCSELs that we are developing need to have about 50 μm of the substrate left on the device to provide current spreading across the large device diameters. Thus, heat sinking these devices requires a modification of the above process using the indium as a solder in a flip-chip bonder rather than as a uniform film between the devices and heat sink. Indium is deposited only on the heat sink to avoid modification of the VCSEL processing. We have found that a 4 μm thick indium film is required to get good adhesion of the flip-chip bond thus making electroplating the preferred indium deposition technique. The gold film required for electroplating also serves as the common contact to the heat sink side of the VCSELs. An oxide free indium surface is formed by a 10 sec dip in a dilute HF acid solution (1:6 BOE) immediately prior to the flip-chip bond. The flip-chip bond must then be performed in an inert environment to prevent oxidation of the indium. This is provided by a simple nitrogen purge modification to the flip-chip alignment system. Once the devices are flip-chip bonded onto the patterned heat sink, the device substrate can be lapped and polished to provide the 50 μm thick current spreading layer and the back side contacts can be deposited using the pattern on the heat sink for alignment. The VCSELs are then antireflection coated and electrically isolated from one another by a deep dry etch process.

This process results in devices that are both electrically and mechanically connected to the heat sink. A typical light-voltage versus current (LIV) curve for a device with an 18 μm implant aperture is shown in Fig. 1. Similar devices on a GaAs substrate would experience thermal rollover around 50 mA while this device does not roll over until about 90 mA, thus indicating the thermal conductivity of the heat sink is higher than that of the GaAs substrate. The kinks in the light curve are due to different lateral modes turning on in the VCSEL.

The heat sink work is to be continued in conjunction with other projects and this data is quite preliminary, however, it looks very encouraging and should provide a path to single VCSELs with more than 50 mW of continuous wave output power.

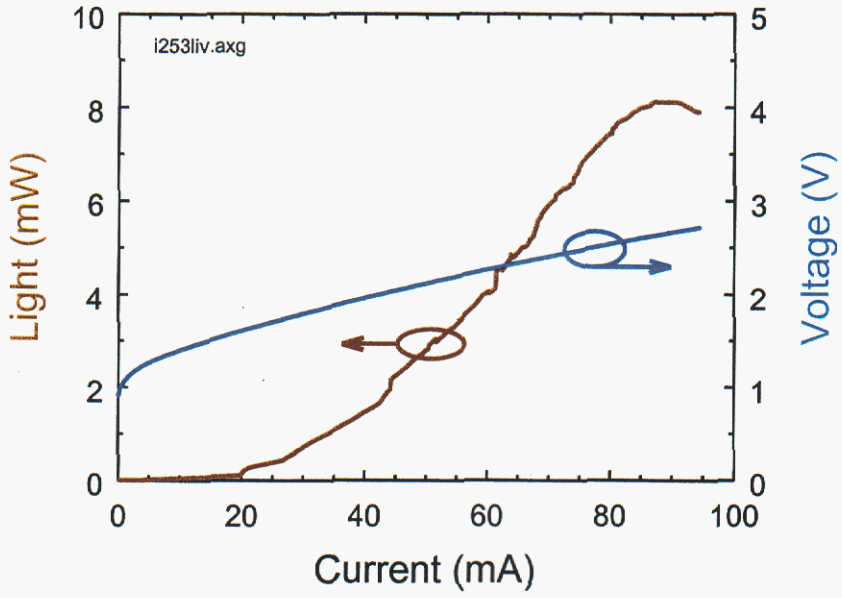

Figure 1. LIV curve from an 18μm diameter 980nm VCSEL flip-chipped onto a silicon heat sink.

Summary

This project produced a number of first-ever research prototypes. The hybrid integration work was the first demonstration of GaAs drivers and receivers integrated with VCSELs for spatially multiplexed multi-channel high-speed data links. The flip-chip integration was the first demonstration of flip-chipped 850 nm VCSELs onto GaAs drivers showing the possibility of using such arrays under the current short distance datacom standards. The matrix addressable array work demonstrated the largest number of lasers and detectors ever integrated onto a single chip, opening the way for scannerless VCSEL based imaging systems. Fiber image guides show great promise for use in short range highly parallel array-to-array data transmission compatible with the current 850 nm datacom standards. Lastly, integration of VCSELs with high performance heat sinks shows potential for even higher device performance in the future.

Heterogeneous integration is a must for many current and future Sandia projects and this work has added significantly to that database. The integration techniques developed in this work have been transferred to a number of other groups at Sandia as well as being used in a number of our ongoing projects.

Appendix A

High Performance 2-Dimensional VCSEL Arrays for Interconnect and Imaging Applications, K. D. Choquette, R. D. Briggs, K. M. Geib, A. A. Allerman, J. J. Hindi, and S. Samora, in International Symposium on Ultra-Parallel Optoelectronics (Post Proceedings): 2/3/00 thru 2/4/00, Kawasaki, Japan (2000).

Hybrid Integrated VCSEL and Driver Arrays for Optical Interconnects, K.D. Choquette, V.M. Hietala, K.M. Geib, S.D. Mukherjee and A.A. Allerman, in IEEE Lasers and Electro-Optics Society 2000 Annual Meeting: 11/13/00 thru 11/16/00, Rio Grande, Puerto Rico (2000).

Two-Dimensional 8x8 Photoreceiver Array and VCSEL Drivers for High-Throughput Optical Data Links, V.M. Hietala, Carl Chun, Joy Laskar, K.D. Choquette, K.M. Geib, A.A. Allerman and J.J Hindi, IEEE Journal of Solid-State Circuits, vol. 36, no. 9, pp. 1297-1302, Sept. (2001).

High-performance vertical-cavity laser, driver, and receiver arrays for optical interconnects, K.D. Choquette, V.M. Hietala, K.M. Geib, R.D. Briggs, A.A. Allerman, and J.J.Hindi, Proceedings of the SPIE - The International Society for Optical Engineering, vol. 4089, pp. 704-707, (2000).

High Performance 2-Dimensional VCSEL Arrays for Interconnect and Imaging Applications

Kent D. Choquette, R. D. Briggs, K. M. Geib, A. A. Allerman, J. J. Hindi, and S. Samora
Center for Compound Semiconductor Science & Technology
Sandia National Laboratories
Albuquerque, NM 87185
Voice: (505)844-7287 FAX: (505)844-8985 e-mail: kdchoqu@sandia.gov

Vertical-cavity surface emitting laser (VCSEL) arrays are promising optical sources for emerging 2-dimensional (2-D) optical systems such as parallel optical interconnect, optical display and projection, confocal microscopy, and smart pixel applications. Aside from the relative simplicity of 2-D array fabrication, VCSELs also have the advantages of circular output beams, efficient operation, low dissipation power, and excellent tolerance to radiation. For optical systems which require 100 s to 1000 s of optical signals, the laser modal characteristics, output power, efficiency, and thermal budget are critical attributes. We will discuss 850 nm 2-D VCSEL arrays which exhibit efficient high power (> 2 mW) single mode operation per channel. We will also report our progress toward 2-D VCSEL array structures, ranging in size from 8x8 to 128x128, under development for novel parallel channel microsystem applications.

The superior efficiency of monolithic selectively oxidized VCSELs [1] is critical to attain high count 2-D VCSEL arrays with low power dissipation. However, selectively oxidized VCSELs tend to emit in multiple transverse modes, which is inappropriate for many applications. Thus we have pursued strategies to maintain singe mode operation. Shown in Fig. 1 is the maximum power in the fundamental mode for two selectively oxidized VCSEL structures. Note that a standard p-up VCSEL with a quarter wavelength thick oxide surrounding the active region will operate multimode, even for the smallest device diameter, due to excessive optical confinement. As shown in Fig. 1, the reduced index confinement afforded by thin oxide apertures positioned at field nulls on both sides of the active region of a p-up VCSEL enables a single mode cavity for oxide apertures as large as about 2x2 m. As a second option, n-up VCSELs with a quarterwave length oxide on each side of the active region exhibit single mode operation up to apertures <3x3 m (see Fig. 1). In this case the higher electron mobility in the top n-type mirror provides better overlap between the carrier injection and the fundamental mode. In addition, common anode VCSELs are attractive for high speed npn transistor driver circuitry.

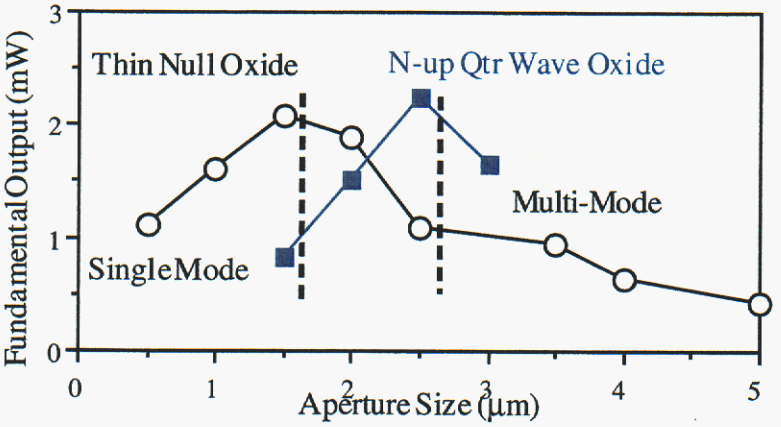

Fig. 1. Fundamental mode output for p-up VCSELs with thin null oxides and n-up VCSELs with quarter wave oxides; to left (right) of dotted lines VCSELs operate in single (multiple) transverse mode(s).

We have fabricated and packaged 8x8 individually addressable VCSEL arrays whose elements are separated by 250 m. We employ dry etched mesas to define the oxide apertured VCSELs, and use an air bridge for the interconnect metal level. We have previously reported that uniform VCSEL characteristics can be achieved, specifically < 2% variation in the threshold current, threshold voltage, and output power. Using the strategies described above, we have also demonstrated 8x8 VCSEL arrays which produce > 2mW of single mode output per channel. These arrays are presently being inserted into a multiple channel guided wave optical interconnect, targeted for a high speed data bus linking a computer processor to memory.

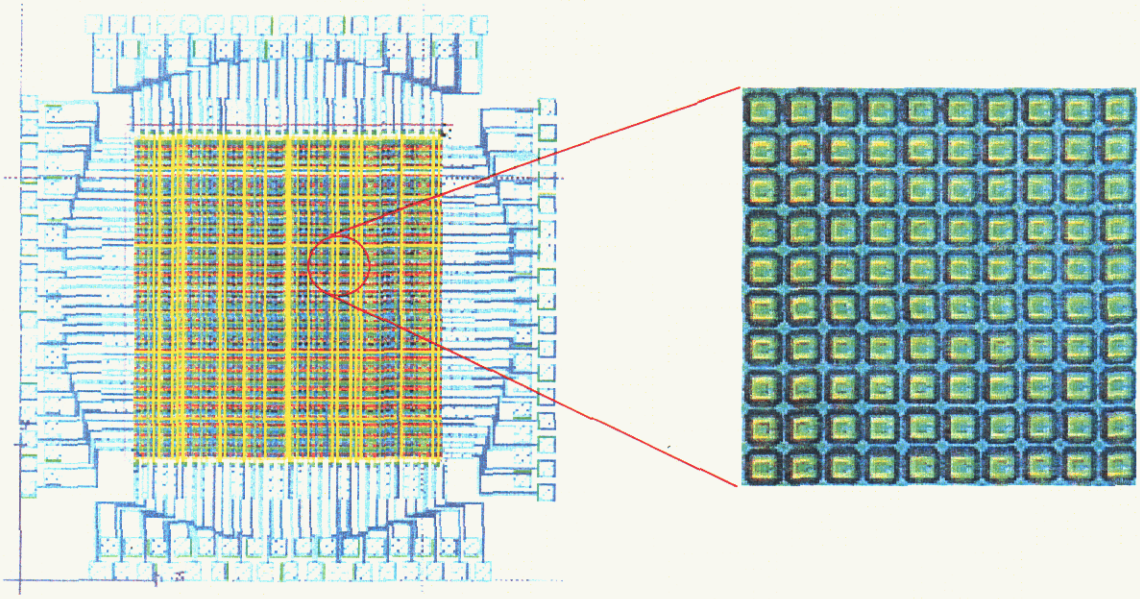

Fig. 2. 64x64 matrix addressable VCSEL array with 30 m pitch; inset shows mesa tops without interconnect metal.

Shown in Fig. 2 is the layout of a 64x64 matrix addressable VCSEL array. In this array structure we wish to achieve a device pitch as small as 30 m. We are also fabricating similar matrix addressable arrays as large as 128x128. Moreover, for confocal microscopy applications, intermeshed detectors within the array are required. Resonant cavity photodetectors (RCPDs) are suitable for integration with VCSELs since they share essentially the same epitaxial structure. To achieve interleaved VCSEL/RCPD 2-D arrays, we have incorporated an appropriate etch stop layer and developed a three etch fabrication sequence which leverages the separate advantages of reactive ion etching, inductively coupled plasma etching, and reactive ion beam etching.

In summary, high performance selectively oxidized 2-D VCSEL arrays and their required fabrication technologies are under development at Sandia. Individually addressable arrays with >2 mW single mode output/channel as well as high count/high density matrix addressable arrays will be appropriate for emerging parallel channel optoelectronic applications. Sandia is a multiprogram lab operated by Sandia Corporation for the U. S. Dept. of Energy under Contract DE-AC04-94AL85000.

References

[1] K. D. Choquette, R. P. Schneider, Jr., K. L. Lear, and K. M. Geib, "Low Threshold Voltage Vertical-Cavity Lasers Fabricated by Selective Oxidation," Electron. Lett. **30**, 2043 (1994).

[2] K. M. Geib, K. D. Choquette, H. Q. Hou, and B. E. Hammons, Uniformity and Performance of Selectively Oxidized VCSEL Arrays, Proc. SPIE **3286**, 72 (1998).

Hybrid Integrated VCSEL and Driver Arrays for Optical Interconnects

Kent D. Choquette*, Vincent M. Hietala, Kent M. Geib,
Sayan Mukherjee, and A. Andy A. Allerman

Sandia National Laboratories,
Albuquerque, NM, 87185-0603

*University of Illinois
Electrical and Computer Engineering Dept.
208 N. Wright Street
Urbana, IL 61801
FAX: (217)244-7645
e-mail: choquett@uiuc.edu

Abstract

We discuss the performance of hybrid integrated 2-dimensional VCSEL arrays and 1-dimensional MESFET driver arrays coupled to fiber image guides for parallel channel optical interconnects.

Hybrid Integrated VCSEL and Driver Arrays for Optical Interconnects

Kent D. Choquette*, Vincent M. Hietala, Kent M. Geib,
Sayan Mukherjee, and Andy A. Allerman

Sandia National Laboratories,
Albuquerque, NM, 87185-0603
FAX: (217)244-7645 e-mail: choquett@uiuc.edu

Massively parallel optical interconnects will ease the bandwidth bottleneck that may occur in future data communication applications. However, there are stringent performance requirements that must be imposed on an optical interconnect such as high reliability, high modulation rate, and elevated temperature operation. The integration of 2-dimensional VCSEL arrays with III-V microelectronics is promising for development of high aggregate bandwidth optical interconnects. VCSELs have already been enthusiastically adopted into Gigabit Ethernet applications due to their reduced threshold current, circular output beam, and inexpensive and high volume manufacture. GaAs-based MESFET circuits have the potential to operate at multi-gigabit rates. We discuss the performance of hybrid integrated VCSEL and MESFET driver arrays coupled to fiber image guides for parallel channel optical interconnects.

Shown in Fig. 1 is an 8x8 individually addressable selectively oxidized VCSEL array [1] hybrid packaged with four 16 channel driver chips. Since VCSELs can modulate at speeds > 10 Gbit/sec. [2], we have designed GaAs MESFET chips to drive the VCSEL arrays at > 1 Gbit/sec. The drivers are designed to respond to GTL logic input, as depicted in Fig. 2, where the bias and drive currents can be separately adjusted between 0-3 and 0-10 mA, respectively. The inset of Fig. 3 shows the response of our top emitting "n-up" 850 nm VCSEL array. The VCSEL light output versus driver voltage input characteristics for the hybrid source component (see Fig. 1) is shown in Fig. 3 at various bias currents from below to above threshold current. The optical output rise time for the hybrid component has been measured to be ≤ 520 psec.

Finally, we have begun to examine fiber image guides (FIG) as a guided wave approach for parallel channel optical interconnects [3]. Fig. 4 shows a butt-coupled FIG to a packaged VCSEL array. The FIG is composed of microfibers with 9 μm core on approximately 13 μm centers. The high numerical aperture of the FIG (NA=1.0) enables efficient collection of the VCSEL output. Shown in Fig. 5 is the intensity profile measured at the output end of the FIB with 13 channels operating. Note that single microfibers guide the VCSEL emission in Fig. 5.

In summary, we have designed VCSEL and MESFET driver arrays which have been hybrid integrated for parallel channel optical interconnects. Initial transmission experiments are underway to characterize the use of fiber image guides for parallel optical interconnects. Continued development of such an optical system will enable a path toward massively parallel optical interconnections for future communication and computing applications.

References

* Presently at the University of Illinois, Electrical and Computer Engineering Dept., 208 N. Wright St., Urbana, IL

[1] K. M. Geib, K. D. Choquette, A. A. Allerman, R. D. Briggs, and J.J. Hindi, Proc. SPIE **3946**, 36 (2000).

[2] K. L. Lear, A. Mar, K. D. Choquette, S. P. Kilcoyne, R. P. Schneider, Jr., and K. M. Geib, Electron. Lett. **32**, 457 (1996).

[3] H. Kasaka, M. Kajita, Y. Li, and Y. Sugimoto, IEEE Photon. Tech. Lett. **9**, 253 (1997).

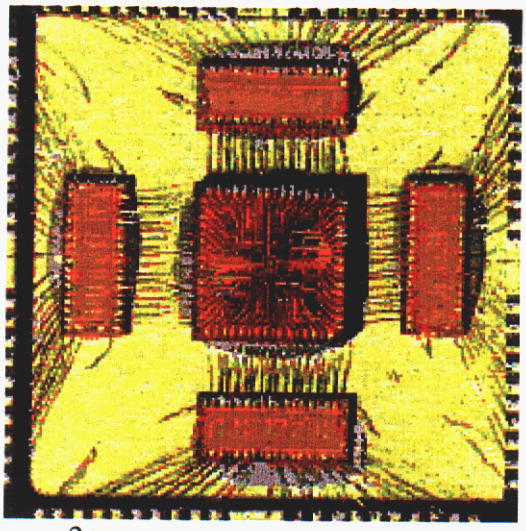

Fig. 1. Hybrid wire-bond packaged 8x8 VCSEL array with four 16 channel MESFET driver die.

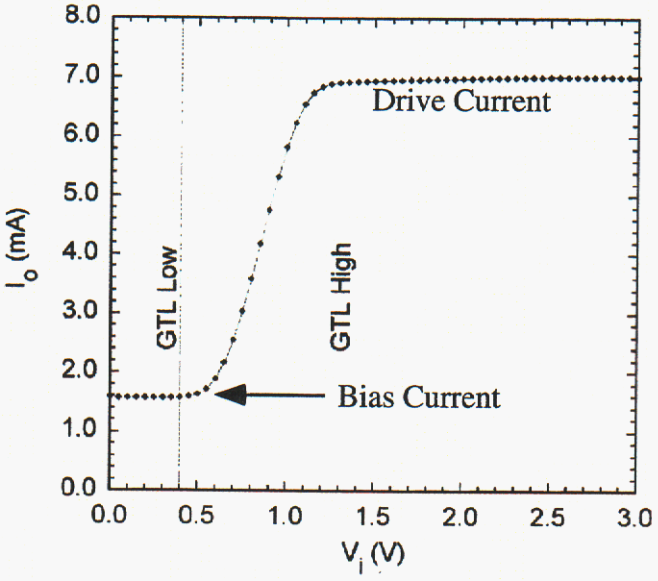

Fig. 2. MESFET driver response.

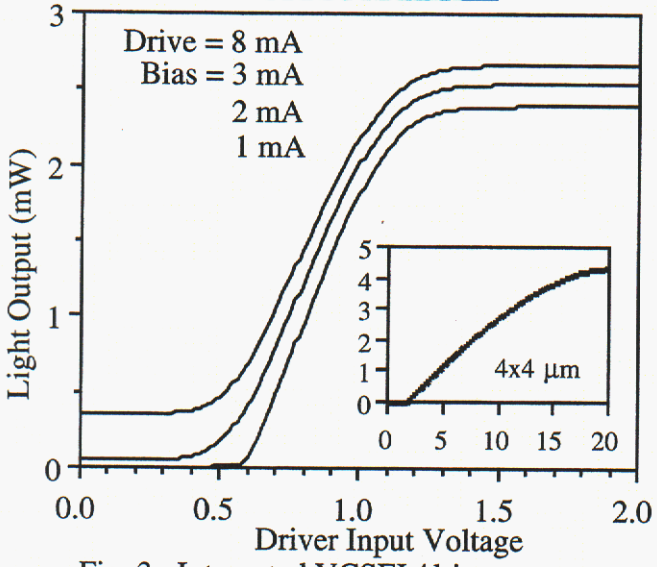

Fig. 3. Integrated VCSEL/driver response; inset shows VCSEL characteristics.

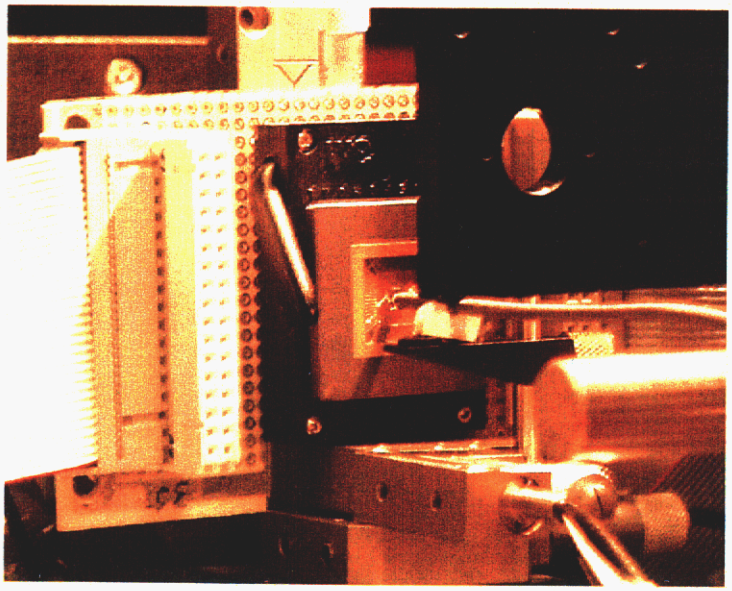

Fig. 4. Fiber image guide butt-coupled to packaged VCSEL array.

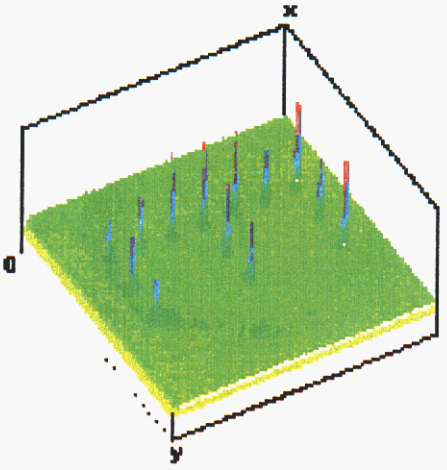

Fig. 5. Image of output facet of fiber guide showing a single fiber is illuminated in each channel.

TWO-DIMENSIONAL 8X8 PHOTORECEIVER ARRAY AND VCSEL DRIVERS FOR HIGH-THROUGHPUT OPTICAL DATA LINKS

Vincent M. Hietala[1], Carl Chun[2], Joy Laskar[2], K. D. Choquette[3], K. M. Geib, A. A. Allerman, and J. J. Hindi
Sandia National Laboratories, Albuquerque, NM 87185-0874
[1]QDI, Yorba Linda, CA 92887
[2]Georgia Institute of Technology, Atlanta, GA 30332
[3]University of Illinois, Electrical and Computer Eng. Dept. Urbana, IL 61801

Abstract

Two custom GaAs integrated circuits have been developed for enabling vertical cavity surface emitting laser (VCSEL) arrays to be used for high throughput spatially-multiplexed optical data links. The present 8x8-array size along with an estimated usable channel speed of 1 Gbps allows for an aggregate throughput of 64 Gbps.

I. Introduction

Modern digital systems are pushing the data-rate limits of conventional interconnects. For example, current personal computers have data at rates of 10^9 to 10^{10} bytes per second. With these present needs, optical interconnects represent a possible solution. This paper describes a GaAs power-efficient chip set, which enables VCSEL's to satisfy current and future throughput needs.

Fig. 1 shows a Sandia 8x8 850nm oxide confined VCSEL array [1], which is the basis of this work. Shown in Fig. 2 is the performance of a single channel that demonstrates high-efficiency (>10%) at moderate power levels (several mW's). The design target was for an array size of 8x8 (64 channels) with a data rate of 1 Gbps per channel. The VCSEL pitch is 250 μm with direct connections to the laser's cathodes at contact pads around the periphery of the array chip.

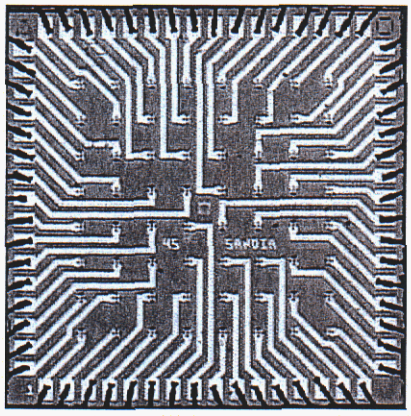

Fig. 1. Photograph of Sandia's 8x8 850 nm VCSEL array.

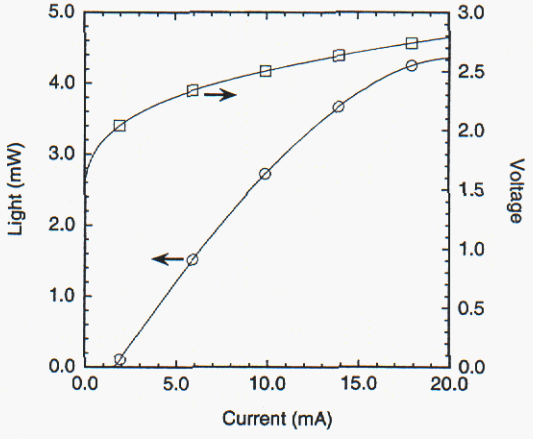

Fig. 2. Typical measured oxide-confined VCSEL performance of an element from the 8x8 850 nm array.

Since VCSEL's have been demonstrated to speeds approaching 20 GHz [2], future links based on 8x8 arrays could exceed aggregate data rates of Terabits per second (Tbps). Spatial multiplexing offers simplified interface electronics due to lower channel data rates as compared to serial (TDM) approaches. However spatial multiplexing does create more challenges with the added necessity of many parallel channels introduces new demands on integration levels and power dissipation.

II. Array Photoreceiver

Power dissipation was a primary design issue for the photoreceiver array. An 8x8 detector array with 64 transimpedance amplifiers requires careful consideration in keeping power levels practical (<3 W total). The desired bandwidth of the photoreceivers along with the large number of channels dictates a monolithic solution. Shown in Fig. 3 is a microphotograph of the resulting 8x8 photoreceiver array with a total die size of 3800 μm x 3800 μm and a total power dissipation of less than 2W using a 3 V supply.

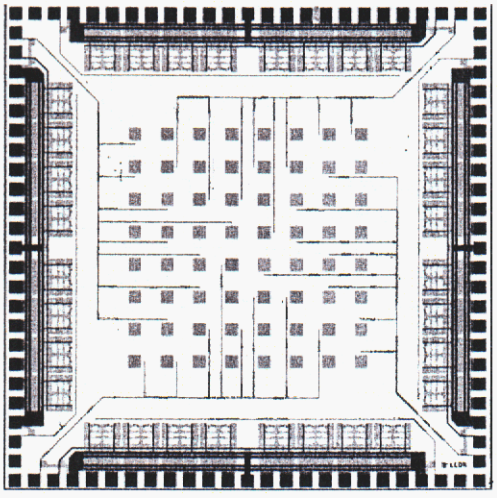

Fig. 3. Microphotograph of the 8x8 photo-receiver array. Center squares are the MSM photodiodes and 64 electronic amplifiers are located around the periphery.

This photoreceiver was fabricated in TriQuint Semiconductor's TQTRx process (www.triquint.com) using a custom "parasitic" metal-semiconductor-metal (MSM) photodiode. The 100μm x 100μm MSM photodetector is formed from an interdigitated electrode structure with 1μm finger widths and 2μm gaps on SI GaAs. Fig. 4 shows the measured extrinsic quantum efficiency of the MSM photodiodes.

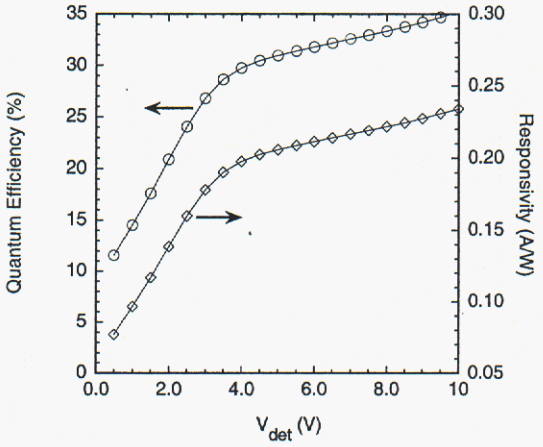

Fig. 4. Measured quantum efficiency and responsivity of the MSM photodetector.

A transimpedance amplifier, decision circuit and GTL output buffer follow the MSM photodetector in each channel. A schematic diagram of the photoreceiver circuit is shown in Fig. 5. The input transimpedance amplifier is comprised of Q1 and Q2, and is based on a design from ref. [3]. A simple decision circuit comprised of Q3 and D1 follows the transimpedance amplifier. Q4 is an output buffer that drives a large open drain GTL output buffer (Q5). The resistor R_2 sets the transimpedance of the input stage and was selected to provide a basic light threshold level of approx. 100μW. An additional input offset current can be injected through resistor R_1 to adjust the receiver threshold level. Fig. 6 shows the

measured transfer characteristics of one photoreceiver channel.

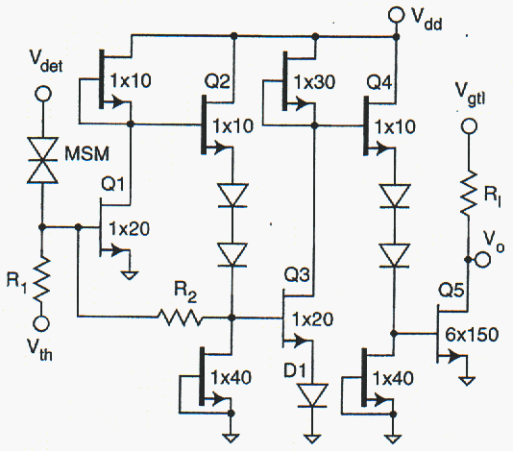

Fig. 5. Single channel schematic diagram of the photoreceiver.

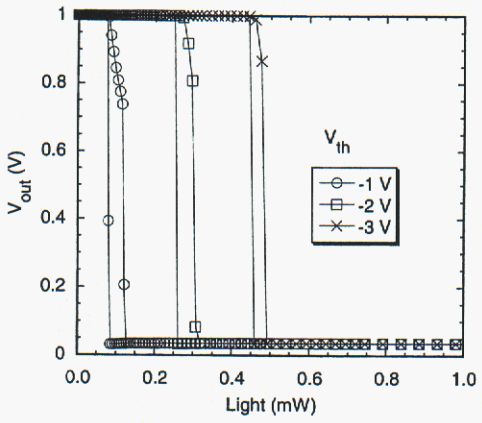

Fig. 6. Measured transfer characteristics (O-E). V_{th} is an input that controls the decision point of the receiver.

III. Array VCSEL Drivers

To drive the 8x8 VCSEL array, special 16 channel driver arrays (4 used per VCSEL array) were developed. A simplified schematic of a single channel is shown in Fig. 7. Each individual driver is comprised of two current sources (one for pre-bias and the other for the pulse current) and a differential switch. The current sources are made from enhancement-mode and the switch from depletion-mode MESFETs. The input to the drivers uses GTL logic levels. The drivers are designed to provide programmable bias currents of up to 3 mA and a maximum pulse currents of 8 mA. With a 5 V supply voltage, the total power dissipation of the transmitter assembly is projected to be less than 2.5 W (worst case). Fig. 8 shows an eye diagram of the driver operating into a 50Ω load (1 mA/div.) at 200 Mbps. Fig. 9 shows the measured light output of one channel as the input is swept from 0 to 2 V under various operating points.

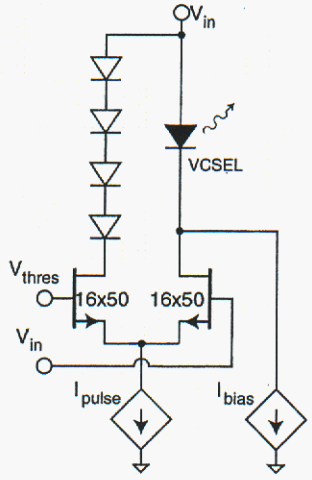

Fig. 7. Simplified schematic diagram of one channel of the driver circuit.

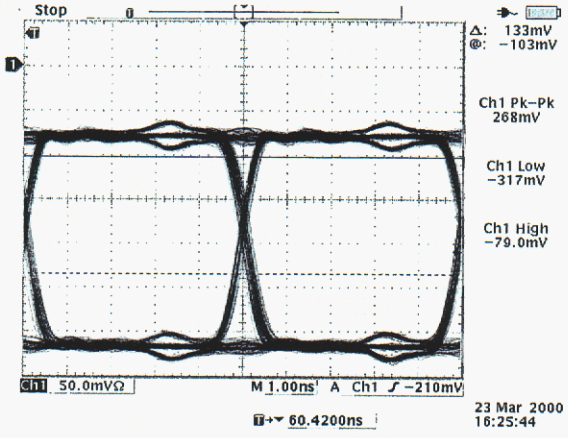

Fig. 8. Measured eye diagram of one channel of the VSCEL driver IC operated into a 50 Ω load (1 mA/div.) at 200 Mbps.

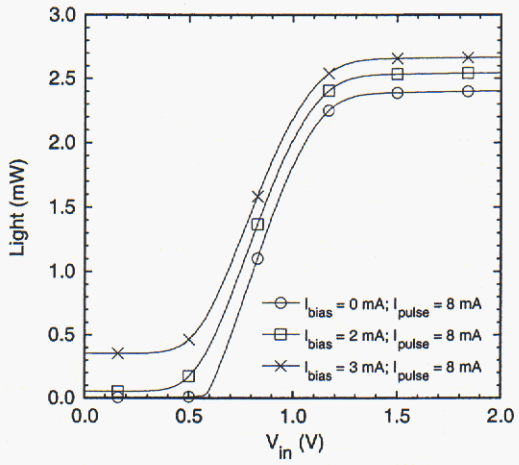

Fig. 9. VSCEL output power (E-O) at various bias conditions.

Fig. 10 shows a microphotograph of the completed 16-channel driver IC (1025 µm x 2650 µm). Fig. 11 shows the completed hybrid transmitter assembled in an 84-pin FPGA package.

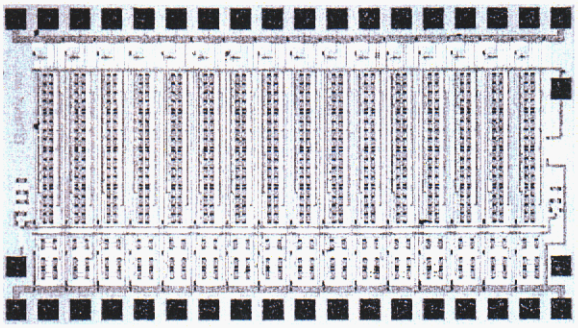

Fig. 10. Microphotograph of the 16-channel VCSEL driver IC.

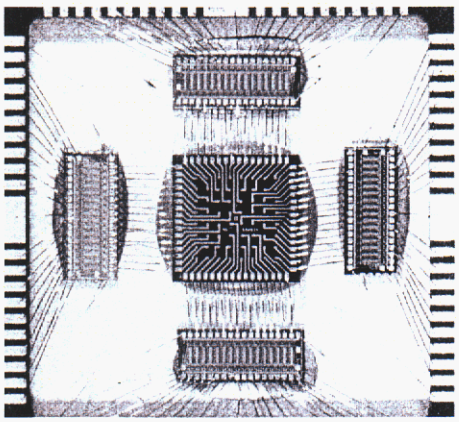

Fig. 11. Photograph of an 8x8 VCSEL transmitter.

IV. Conclusions

Two custom GaAs integrated circuits have been developed to allow for spatially multiplexed 8x8 VCSEL data link. An 8x8 photoreceiver array based on a commercial foundry process using parasitic MSM photodiodes has been demonstrated. A 16-channel driver array with programmable drive currents compatible with the requirements of high-efficiency oxide confined VCSELs has been realized.

Acknowledgements

Sandia is a multiprogram laboratory operated by the Sandia Corporation, a Lockheed Martin company, for the United States Department of energy under Contract DE-AC04-94AL85000.

References

[1] K. M. Geib, K. D. Choquette, A. A. Allerman, R. D. Briggs, and J. J. Hindi, Proc. SPIE 3946, 36 (2000).

[2] V. M. Hietala, K. L. Lear, M. G. Armendariz, C. P. Tigges, H. Q. Hou, and J. C. Zolper, "Electrical Characterization and Application of Very High Speed Vertical Cavity Surface Emitting Lasers (VCSELs)," 1997 IEEE MTT-S International Microwave Symposium Digest 1, Vol. 1, pp. 355-358, 1997.

[3] O. Wada, H. Hamaguchi, M. Makiuchi, T. Kumai, M. Ito, K. Nakai, T. Horimatsu, and T. Sakurai, "Monolithic Four-Channel Photodiode/Amplifier Receiver Array Integrated on a GaAs Substrate," Journal of Lightwave Technology, Vol. LT-4, No. 11, pp. 1694-1703, 1986.

High Performance Vertical Cavity Laser, Driver, and Receiver Arrays for Optical Interconnects

Kent D. Choquette*, Vincent M. Hietala, Kent M. Geib, Ronald D. Briggs,
Andy A. Allerman, and Jana Jo Hindi
Center for Compound Semiconductor Science and Technology
Sandia National Laboratories, Albuquerque, NM 87185-0603

ABSTRACT

Massively parallel optical interconnects are appropriate to ease the data bandwidth bottleneck that will occur in future computing applications. Vertical cavity surface emitting lasers (VCSELs) are promising sources for emerging 2-dimensional optical systems such as free space and guided wave optical interconnects. We discuss the development of high performance VCSEL arrays, including individually addressable and matrix addressable arrays. We also show the characteristics of GaAs microelectronic driver and photoreceiver chips that have been designed to interface with Si-based CMOS circuitry. Finally, the potential of these source and receiver modules for use in free space or guided wave parallel channel optical interconnect architectures will be described.

Keywords: VCSEL, laser drivers, photoreceivers, 2-dimensional arrays, optical interconnects

1. INTRODUCTION

Massively parallel optical interconnects may be appropriate to ease the data bandwidth bottleneck that may occur in future computing applications. For example the use of guided wave or free space optical interconnects to provide a high-speed parallel bus between a microprocessor and memory may enable faster computing speeds. However, there are stringent performance requirements that must be imposed on an optical interconnect within the computing environment, such as high reliability, high modulation rate, and operation at elevated temperature. Vertical cavity surface emitting lasers (VCSELs) are promising optical sources for 2-dimensional optical systems such as free space and guided wave optical interconnects [1]. VCSELs have already been enthusiastically adopted into Gigabit Ethernet applications in a remarkably short period of time due to their reduced threshold current, circular output beam, and inexpensive and high volume manufacture. Extending VCSEL sources from single devices to 2-dimensional arrays will enable high density optical interconnects suitable for emerging computing applications.

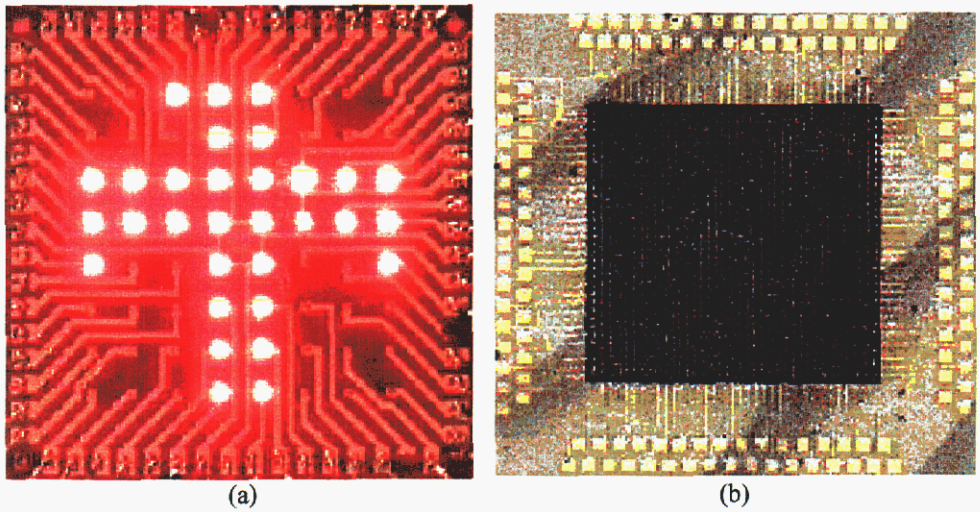

(a) (b)

Figure 1. 2-dimensional VCSEL arrays: (a) 8x8 individually addressable 670 nm array; and (b) 64x64 matrix addressable 850 nm array.

*Email: kdchoqu@sandia.gov; voice: (505)844-7287; FAX: (505)844-8985

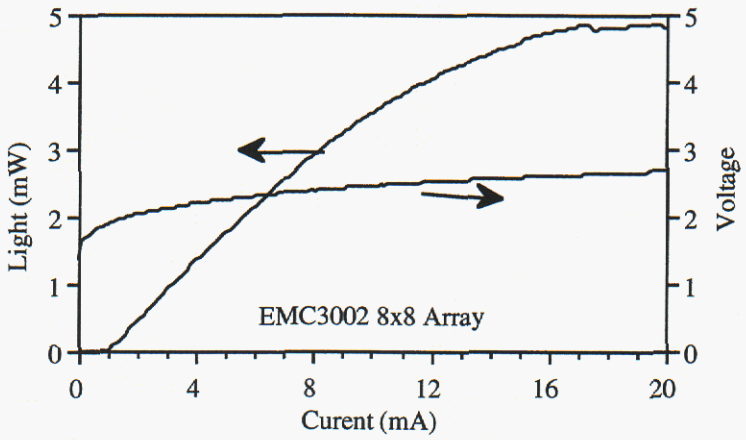

Figure 2. Light output and voltage versus injected current for N-up VCSEL.

For optical systems which require 100 s to 1000 s of optical signals, the laser modal characteristics, output power, efficiency, and thermal budget are important laser source attributes. We discuss the development of high performance VCSEL arrays suitable for optical interconnects. Several array structures have been pursued, including individually addressable and matrix addressable VCSEL arrays. It is also important that the source arrays have appropriate microelectronic drivers which can interface with the computing processor chip. We show the characteristics of GaAs MESFET driver and photoreceiver chips that have been designed to interface with Si-based CMOS circuitry. Finally, the potential of these source and photoreceiver modules for use in free space or guided wave parallel channel optical interconnect architectures will be described.

2. VCSEL ARRAYS

Shown in Fig. 1(a) is a packaged 8x8 individually addressable selectively oxidized VCSEL array operating continuous wave at room temperature [2]. The oxide aperture 670 nm VCSELs in the array are positioned on a 250 m pitch, and the die is wirebonded to a pin-grid-array package. We have produced similar VCSEL arrays at other wavelengths such as 780, 850, and 980 nm [3]. VCSELs that emit at short wavelength (< 870 nm) can be matched with Si photodetectors, while longer wavelength VCSELs can transmit through their substrate. The latter VCSEL arrays would simplify flip-chip integration with CMOS circuitry, although the substrate can also be removed from the VCSEL arrays. For our prototype activity, we have chosen to utilize 8x8 individually addressed top emitting 850 nm VCSELs [4]. In Fig. 2 we show the representative operating characteristics of a common cathode (N-up) 8x8 VCSEL. This VCSEL array has been integrated into a hybrid assembly with separate driver chips described in the next section.

Alternative VCSEL array structures have also been pursued, such as the matrix addressable array shown in Fig. 1(b). The elements of this 64x64 array are on 30 m pitch. Array elements in each row and column of the matrix addressable arrays are electrically in series, which can significantly reduce the number of connections (wirebonds) necessary to the array, and can dramatically increase the array density. (Note the arrays in Fig. 1 have nearly the same area, but Fig. 1(b) has more than an order of magnitude greater number of elements!) However, a limitation is imposed on the array elements that can be simultaneously operated, and thus rastering (and likely multiplexing) would be necessary to utilize a matrix addressable array within an interconnect application.

3. DRIVER ARRAYS

Although VCSELs with low operating current (and voltage) could be directly integrated with Si-based CMOS, there are advantages to utilizing distinct laser drivers. For example, since VCSELs can modulate at speeds >10 Gbit/sec., we have designed GaAs MESFET chips to drive the VCSEL arrays at > 1 Gbit/sec. 1-dimensional arrays of 16 channel driver chips have been fabricated through a foundry. Thus four driver chips are mounted around the 8x8 array and wire-bonded together to form a source module. In the future we plan to flip-chip the VCSEL arrays onto matching 8x8 arrays of drivers. The driver characteristics are depicted in Fig. 3. Note that the drivers respond to GTL logic input, while the bias and switching

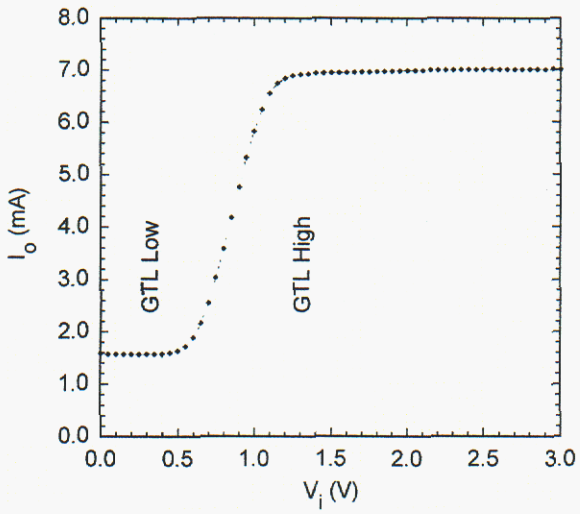

Figure 3. Output current (I_o) as a function of input signal (V_i) for the MESFET driver chips. The bias and switching currents were held at 1.5 and 5 mA respectively. The appropriate switching levels for GTL input are also shown.

currents from the driver can be separately adjusted between 0-3 and 0-10 mA, respectively. From Fig. 2 this implies that the maximum 13 mA drive current can produce 4 mW from the VCSEL.

4. RECEIVER ARRAYS

Matching receiver arrays have also been designed and fabricated, as shown in Fig. 4. The amplifier circuitry is integrated with metal-semiconductor-metal (MSM) detectors that are incorporated into the foundry fabrication process. The MSM detectors are 100 m in size to ease optical alignment and are separated by 250 m to match the 8x8 VCSEL arrays (see Fig. 1(a)). The output voltage as a function of input light level from a receiver channel is shown in Fig. 5. The light switching threshold can be adjusted to greater than 0.5 mW. Since the VCSEL arrays can provide several mW/channel, the optical power budget should be relaxed in our initial prototype interconnect experiments.

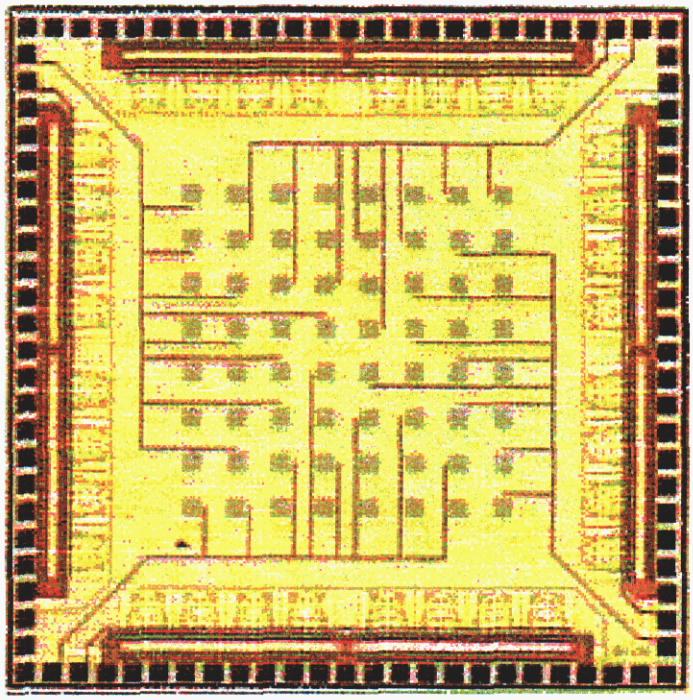

Figure 4. GaAs MESFET Photoreceiver with integrated MSM detectors. Note the detector array is on 250 m pitch to match the VCSEL array in Fig. 1(a).

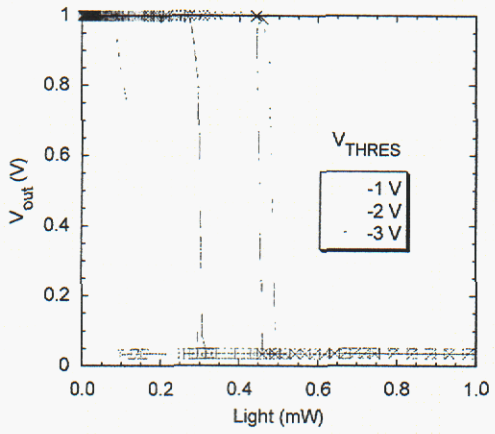

Figure 5. Measured photoreceiver output voltage as a function of input light level onto the MSM detector. Note the switching threshold can be adjusted.

5. SUMMARY

High speed interconnects will be foundational to future computing systems. We have begun to develop optical source and receiver prototype components that could compose a 2-dimensional optical interconnect. Individually addressable 8x8 VCSEL arrays have been demonstrated with suitable performance. Appropriate 1-dimensional driver array chips, which potentially operate at > 1 Gbit/sec, have been designed and fabricated. Matching photoreceiver arrays have also been demonstrated, which consist of 8x8 MSM detectors with monolithic amplifiers. Finally, we have also begun to investigate methods to robustly optically couple the source and receiver arrays, including the use of fiber image bundles and other guided wave techniques. Continued development of such an optical system will enable a path toward massively parallel optical interconnections for future computing applications.

6. ACKNOWLEDGEMENTS

Sandia National Laboratories is a multiprogram laboratory operated by Sandia Corporation for the United States Department of Energy under contract No. DE-AC04-94AL85000.

7. REFERENCES

[1] *Vertical Cavity Surface Emitting Lasers-New Technologies and Applications*, ed. C. Wilmsen, H. Temkin, and L. Coldren, Cambridge University Press (Cambridge, UK) 1999.

[2] K. D. Choquette, K. M. Geib, A. A. Allerman, D. K. Serkland, J. A. Nevers, and J. J. Hindi, "Integrated VCSEL/detector Arrays for 2-Dimensional Microsystems," Spatial Light Modulators and Integrated Optoelectronic Arrays, Snowmass, CO (March 1999).

[3] W. W. Chow, K. D. Choquette, M. Haggerot Crawford, K. L. Lear, and G. R. Hadley, "Design, Fabrication, and Performance of Infrared and Visible Vertical-Cavity Surface Emitting Lasers," J. Quan. Electron. **33**, 1810 (1997).

[4] K. M. Geib, K. D. Choquette, H. Q. Hou, and B. E. Hammons, Uniformity and Performance of Selectively Oxidized VCSEL Arrays, K. D. Choquette and R. Morgan, Editors, Proc. SPIE **3286**, 72 (1998).

Appendix B

Flip-chip Integration of Selectively Oxidized 850 nm VCSEL Arrays, K.M. Geib, K.D. Choquette, A.A. Allerman, and J.J. Hindi in IEEE Lasers and Electro-Optics Society 2000 Annual Meeting: 11/13/00 thru 11/16/00, Rio Grande, Puerto Rico (2000).

Flip-chip Integration of Selectively Oxidized 850 nm VCSEL Arrays

K. M. Geib, K. D. Choquette, A. A. Allerman and J. J. Hindi

Sandia National Laboratories,
Albuquerque, NM, 87185-0603
Voice: (505)844-8214
FAX: (505)844-8985
kmgeib@sandia.gov

Abstract

We report reliable bonding and mechanically stable packaging techniques for flip-chip integration of selectively oxidized 8x8 bottom emitting 850 nm VCSEL arrays for novel microsystem applications.

Flip-chip Integration of Selectively Oxidized 850 nm VCSEL Arrays

K. M. Geib, K. D. Choquette, A. A. Allerman and J. J. Hindi

Sandia National Laboratories,
Albuquerque, NM, 87185-0603
kmgeib@sandia.gov

Combinations of dense numbers of high performance photonic and microelectronic devices originating from disparate technologies are needed to achieve the next generation of information processing, interconnect, and intelligent sensing microsystems. Previous flip-chip VCSELs integrated to microelectronic circuitry were accomplished as isolated individual VCSEL islands, and often emit at longer wavelengths to allow emission through the GaAs substrate [1,2]. However, 850 nm VCSELs are the most mature commercial technology, and high count/high density 2-dimensional arrays are desired for emerging applications. We report the fabrication techniques for flip-chip integration of selectively oxidized 850 nm 8x8 individually addressable VCSEL arrays.

For robust integration of 2-dimensional 850 nm VCSEL arrays to microelectronics, there are three challenges to overcome: 1) reliable bonding; 2) mechanically stable packaging; and 3) substrate side emission of 850 nm light. To achieve robust bonding of VCSELs to Si or III-V electronic circuitry, we have developed a silver post flip-chip process after Goossen, *et al.* [3]. The selectively oxidized 2-dimensional VCSEL arrays are fully fabricated [4] and tested prior to flip-chipping. The top facet of the VCSEL mesas are coated with a Au film, then a Ag post, and finally another thin Au layer to provide the bonding contact. The flip-chip test coupon has matching electrical interconnections which extend Au contact pads out beyond the periphery of the VCSEL array die as shown in Fig. 1. Eventually, this coupon will be replaced with an integrated circuit driver chip. To ensure mechanical stability between the VCSEL die and the underlying coupon we employ an unfilled Dexter epoxy under fill that readily wicks from the edges into the ~6μm gap between the ~2x2 mm^2 square die. The voidless epoxy adhesion to the die is evident from the cross section scanning electron microscope picture in Fig. 2.

Finally, to enable 850nm emission we remove the optically absorbing GaAs substrate by wet chemical jet etching. A 100 nm thick AlAs layer is utilized as an etch stop to preserve the VCSEL epitaxial material. Flip-chipped VCSEL assemblies have been tested on a probe station, as depicted in the inset of Fig. 3. The representative performance of a flip-chipped bottom emitting 850nm VCSEL with an oxide aperture of $14x14^2$ μm is shown in Fig. 3. We will also report on efforts to improve uniformity and yield, as well as the performance of fully packaged flip-chipped VCSEL arrays.

References

[1] R. Pu, E. M. Hayes, R. Jurrat, C. W. Wilmsen, K. D. Choquette, H. Q. Hou, and K. M. Geib, IEEE Photon. Tech. **9**, 1622 (1997).

[2] A. V. Krishnamoorthy, L. M. F. Chirovshy, W. S. Hobson, R. E. Leibenguth, S. P. Hui, G. J. Zydzik, K. W. Goossen, J. D. Wynn, B. J. Tseng, J. Lopata, J. A. Walker, J. E. Cunningham, and L A. D'Asaro, IEEE Photon. Tech. **11**, 128 (1999).

[3] K. W. Goossen, IEEE Trans. on Advanced Packaging **22**, 561 (1999).

[4] K. M. Geib, K. D. Choquette, A. A. Allerman, R. D. Briggs, and JJ Hindi, Proc. SPIE **3946**, 36 (2000).

Sandia is a multiprogram laboratory operated by Sandia Corporation for the United States Department of Energy under Contract DE-ACO4-94AL85000.

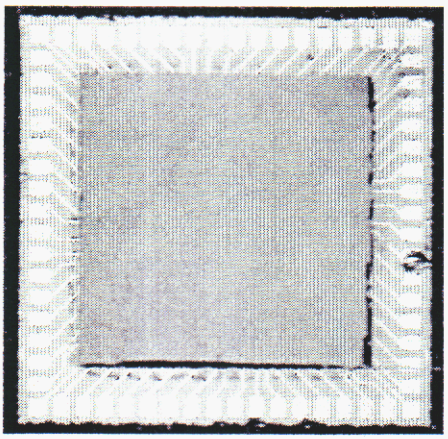

Fig. 1. VCSEL array flip-chipped onto test coupon prior to substrate removal.

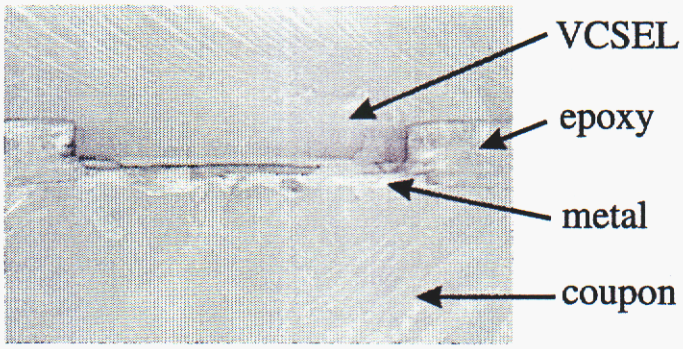

Fig. 2. Cross section photomicrograph of the flip-chipped and epoxy under filled VCSEL mesa.

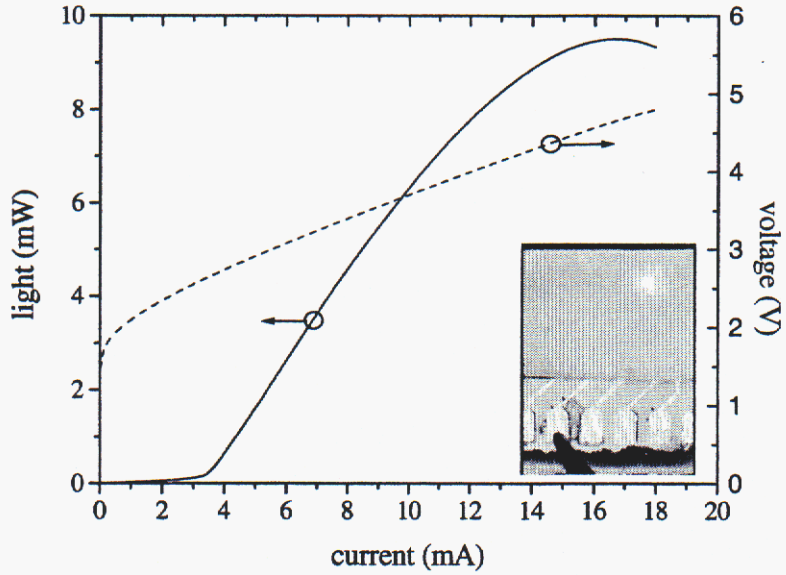

Fig. 3. The array elements have threshold currents of 3.5 mA and threshold voltage of 2.7 V.

Appendix C

Input Coupling Measurements for Parallel Optical Interconnects using Imaging Fiber Bundles and VCSEL Arrays, Sayan D. Mukherjee, Kent M. Geib and Kent D. Choquette, CLEO-Europe, 10-15 September, 2000, Nice, France (2000).

Characterization of Cross-Talk Sources in Massively Parallel Datalinks using VCSEL arrays and Fiber Image Guides, S.D. Mukherjee, K.D. Choquette, K.M. Geib, G.R. Hadley, T. Carter, A.J. Fischer, C.T. Sullivan and K. Tatah, Optics in Computing topical meeting 2001: 1/9/2001 thru 1/11/2001, Lake Tahoe, NV (2001).

Critical Parameters For Parallel Interconnects Using VCSEL Arrays and Fiber Image Guides, Sayan D. Mukherjee, G. Ron Hadley, Kent M. Geib, Kent D. Choquette, Tony R. Carter, Arthur J. Fischer, Matt Robinson, and Charles T. Sullivan, in VCSELs and Optical Interconnects SPIE Photonics Fabrication Europe 2002: 10/28/02 thru 11/1/02, Brugge, Belgium: (2002).

Two Dimensional Guided Wave Optical Interconnect, H. P. Chen, K. D. Choquette, V. M. Hietala, and K. M. Geib, J. Sel. Top. Quan. Electron., submitted (2003).

Input Coupling Measurements for Parallel Optical Interconnects using Imaging Fiber Bundles and VCSEL Arrays

Sayan D. Mukherjee, Kent M. Geib and Kent D. Choquette
Sandia National Laboratories, P.O. Box 5800, Albuquerque, NM 87185-0603, USA, and
Matthew Robinson, Schott Fiber Optics, Inc., 122 Charlton Street, Southbridge, MA 01550-1960, USA.

Imaging fiber bundles from Schott Fiber Optics [1] and 8x8 individually addressable vertical cavity surface emitting laser (VCSEL) arrays from Sandia National Laboratories [2] have been investigated for their mutual compatibility for flexible parallel optical interconnects. The 2-D array (250 μm x 250 μm pitch) of selectively oxidized 850 nm VCSELs have 3 μm x 3 μm active area, threshold current around 0.5 mA and maximum power of 3.5 mW with wallplug efficiency at 2mW output of about 25%. Three kinds of fiber bundles were tested each containing 15379 fibers with 9 μm core diameter and 13.5 μm pitch in a close-packed hexagonal (honeycomb) pattern, and the core to total cross-sectional area ratio of 0.45. The distinguishing features were the numerical apertures: 0.25 (half acceptance angle, $\theta a = 14.5^{\circ}$), 0.55 (33.4°) and 1.0 (90°). The maximum lateral extent of the fiber-bundle was less than the inner dimension of the VCSEL-array facilitating butt coupling of the fibers.

Parallel imaged transfer of laser emissions for several VCSELs operating simultaneously were demonstrated for fiber to VCSEL-array distances between 0 to 300 μm. This study was undertaken to quantify VCSEL emission propagating through the common clad to reach adjacent photodetectors (PDs) at the receiver plane contributing to possible crosstalk and noise. Figure 1 shows light output plots for one VCSEL without and with fiber (NA = 1.0) coupling at 0 μm, and into the central cladding area between three neighboring fibers. Figures 2 and 3 show respectively the beam-profile representations of emission into one fiber versus that into the clad over an area of 370 μm square. The scale of Figure 3 is < –30dB below that of Figure 2 and this indicates, for instance, that for 0 μm separation the emission from one VCSEL would be reduced to < – 40dB at adjacent PD sites. Fiber bundles with smaller numerical apertures showed somewhat greater inter-element light. The difference in transmitted power between aligned emission and misaligned emission disappeared at distances between 250 μm and 300 μm for all the fibers. Crosstalk and coupling issues, as well as influence of fiber feedback into the VCSELs will be presented.

References

1. K. Tatah, D. Filkin, B. Greiner and M. Robinson, Technical Digest, Optics in Computing, Snowmass, Aspen, CO, USA, April 13-16, 1999. ISBN 1-55752-588-9 (1999) pp. 115-117.
2. K.D. Choquette, K.M. Geib, A.A. Allerman, D.K. Serkland, J.A. Nevers and J.J. Hindi, paper STuA3-1, Technical Digest, Spatial Modulators and Integrated Optoelectronic Arrays, Snowmass, Aspen, CO, USA, April 12-14, 1999. ISBN 1-55752-601-X (1999) pp. 59-61.

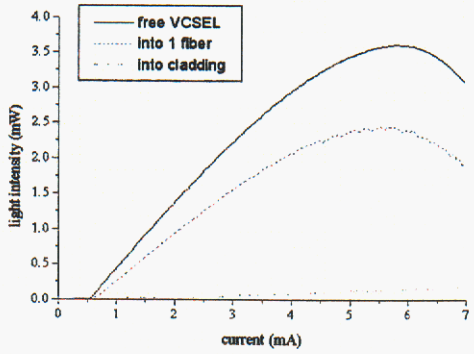

Figure 1. Light output from VCSEL.

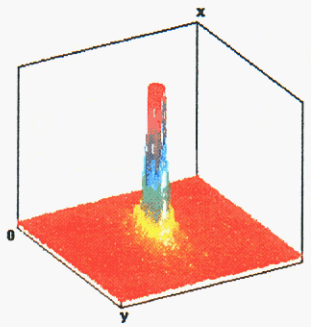

Figure 2. VCSEL emission into single fiber in bundle.

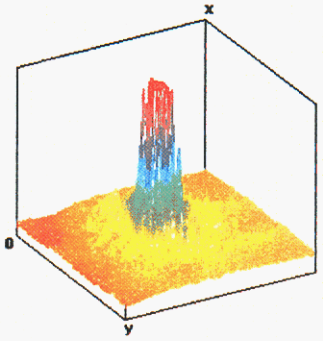

Figure 3. VCSEL emission into clad, at +31 dB magnification.

Characterization of Crosstalk Sources in Massively Parallel Datalinks Using VCSEL Arrays and Fiber Image Guides

S.D. Mukherjee[1,2,*], K.D. Choquette[3], K.M. Geib[2], G.R. Hadley[2], T.R. Carter[2], A.J. Fischer[2], C.T. Sullivan[2] and K. Tatah[4]

[1] Electrical and Computer Engineering, University of New Mexico, Albuquerque, NM 87131-1356, USA and The Norwegian University of Science and Technology, 7491 Trondheim, Norway. *sdmukhe@sandia.gov
[2] Sandia National Laboratories, CSRL, Albuquerque, NM 87185-0603, USA
[3] Department of Electrical and Computer Engineering, University of Illinois, Urbana, IL 61801, USA.
[4] Schott Fiber Optics, Inc., 122 Charlton Street, Southbridge, MA 01550, USA.

Abstract

Sources of possible optical crosstalk in parallel datalinks comprised of VCSEL-arrays and imaging fiber guides have been characterized using L-I-V, near field, far field measurements and simulations using beam propagation method. Input coupling, propagation through the fiber-guide and output spreading are evaluated quantitatively for their contribution to the degradation of link properties for high-density, massively parallel 2-D optical link systems.

Introduction

While 1-D links based on VCSELs and linear fiber ribbons have seen some commercial successes [1,2], parallel links that take advantage of the two-dimensionality of VCSEL arrays on planar substrates are at an early stage of development. Fiber image guide (FIG) based links have been demonstrated at up to 1 Gb/s [3,4] and 3 GHz [4], but a detailed understanding of link parameters and limits is unavailable. Recently VCSEL array coupling experiments to Schott imaging fiber guides with numerical aperture NA = 0.25, 0.55 and 1.00 have been reported [5].

The current goal for the ongoing work is to identify critical parameters for massively parallel optical interconnects of medium distances (0.5 to 10 meters) comprised of 2-D fiber image guides & VCSEL arrays. The long-term goal is to develop co-design rules for 2-D VCSEL, optical receiver and fiber image guides for optimized parallel optical interconnections of size from 2^6 (8x8) to 2^{10} (32x32 = 1024) or 2^{14} (128x128 = 16384). This paper explores quantitatively the sources of crosstalk due to VCSEL emission angles, reflections at the FIG input facet, spreading of the uncoupled beam through the length of the FIGs including core and cladding-mode guiding and, finally, spreading of the beam once it emerges from the output side of the FIG.

Figure 1a. Fiber output for with VCSEL emission into a single NA = 0.55 fiber at z = 0 μm. Photo at −59dB attenuation..

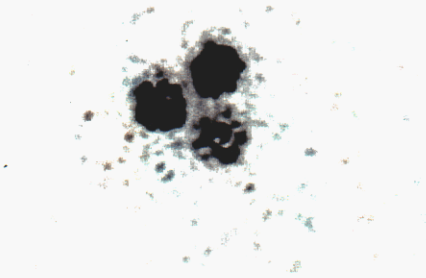

Figure 1b. Fiber output with VCSEL emission aimed into cladding in between three NA = 0.55 fibers at z = 0 μm. Note cladding modes. Photo at −20dB attenuation.

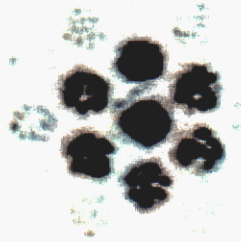

Figure 1c. Fiber output with VCSEL emission axis aligned to a single NA = 0.55 fiber at z = 100 μm. Photo at −59dB.

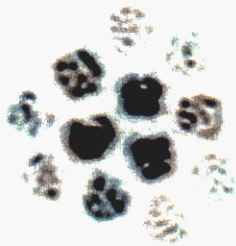

Figure 1d. Fiber output with VCSEL emission axis aligned to the clad in between three NA = 0.55 fibers at z = 100 μm. Near field photo at −59dB attenuation.

Experimental details

Fiber image guides of 20-cm length and of numerical apertures 0.25, 0.55 and 1.00 were used with 4x4 μm square oxide confined VCSEL arrays mounted on a x-y-z θ–ϕ–φ stage. The ~1.8 mm hexagonal cross-section FIG consisted of 15379 fibers with 9.1-

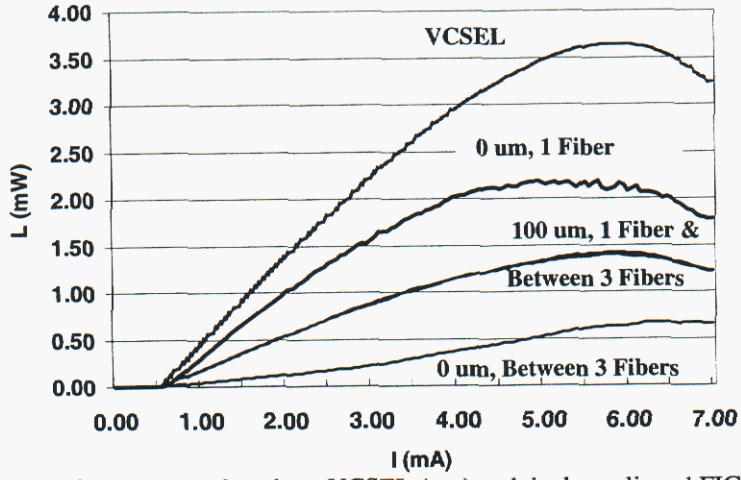

Figure 2. L-I curves for a bare VCSEL (top) and the best aligned FIG output vs. maximum-misaligned conditions for z = 0 and 100 μm.

μm core at a 13.5- μm pitch, with 2 μm thick clad. The space between the individual fibers is filled with acid soluble glass (ASG). The ASG is etched away in the long central part of the finished FIG for flexibility while the two ends containing ASG remain solid for ease of handling and the end facets are polished for light input and output. Light and voltage versus current (L-I-V), near and far field patterns were then recorded for a selection of input conditions. In particular, two specific lateral (x-y) positions were chosen to determine the extremes for coupling differences. For these two lateral conditions the value of z, the separation between the FIG input facet and the VCSEL, was varied from 0 μm to 300 μm. Figure 1 describes the conditions. In 1a & 1c: z = 0 and 100 μm, the VCSEL emission is aligned to one fiber within the fiber image guide. In 1b & 1d: z = 0 and 100 μm, the VCSEL emission peak is aligned to the cladding material so that most of the light is injected into the clad. This was done in order to measure how efficient the cladding materials were in transmitting "stray" light through the length of the FIG.

Results

Figures 2 and 3 describe the differences for transmission through FIGs corresponding to the four conditions in Figure 1. The top curve in Fig. 3 shows that at z = 0 μm the ratios of transmitted powers, shown as the lateral coupling variation, for the best and the worst aligned conditions are between 8 and 12 dB. These large differences become very small, e.g., ~0.3 dB, for z = 100 μm (bottom curve, Fig.3). Therefore, unidirectional links may be constructed with an input separation of ~ 100 μm with an accompanying high lateral positional tolerance. The associated input coupling loss is between 4 and 6 dB (top dashed line in Fig. 3), which is about 3 dB worse than the best coupling condition at z = 0 μm (bottom dashed line in Fig. 3). This differential loss appears to be an acceptable penalty for achieving an undemanding lateral alignment requirement.

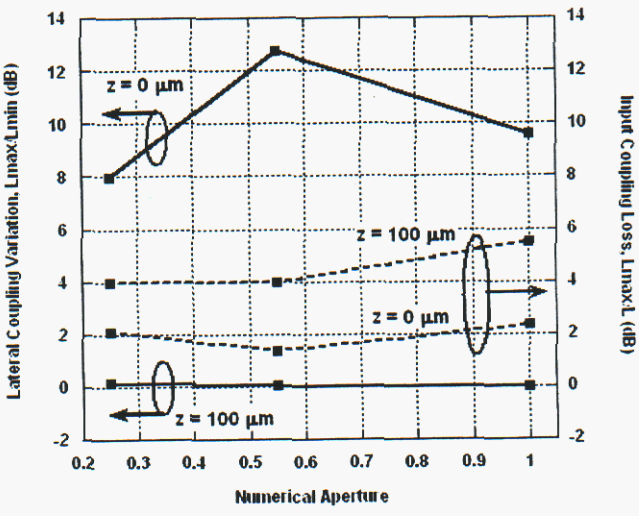

Figure 3. Numerical aperture dependence of coupling efficiency (ratio of light coupled into the fiber and VCSEL emission) and coupling error (ratio of maximum to minimum coupling for a change in lateral position).

The output far field patterns shown in Figure 4, however, indicate that the z = 100 μm condition is unsuitable for bi-directional links because of the large spreading angles observed for all the FIGs with the $1/e^2$ angle increasing almost linearly from NA = 0.25 to NA = 1.00. In addition, the cladding modes (Figure 1b), observed only for NA = 0.55 and 1.00, contributed to the greater than 100^0 total angular spread at the output. The cladding modes form as high-angle spreading leaky modes in high-differential refractive index systems [6], such as the two high NA FIGs here. These modes tend to congregate at the clad at the expense of being in the cores while continuing to expand and couple into adjacent cladding regions even if the two cladding regions are not in physical contact with each other.

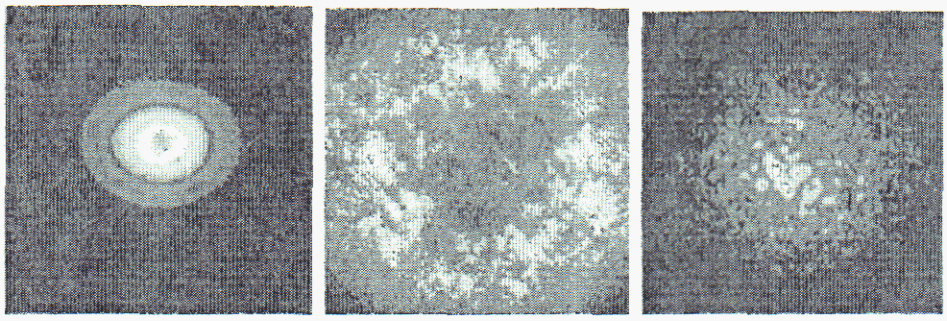

Figure 4. Far field patterns at 2.50 mA. Left: bare VCSEL Middle: z = 0 μm aligned to the clad. Right: z = 100 μm, aligned to the clad. NA for fiber image guide = 0.55. Scale: 62^0 x 62^0.

Discussion

The cladding modes could only be seen when all the VCSEL light was purposely injected into the clad and only for NA = 0.55 and 1.00. The corresponding total transmitted light is ~10 dB lower than when a VCSEL is aligned to a fiber at z = 0 μm. So the inadvertent propagation of light through the cladding media in a real link is expected to be less than that recorded in these ideal experiments at z = 0 μm. The ratio of the core area to the total cross-sectional area for all the FIGs is about 41%. Therefore the resulting 59% of injected light for z = 100 μm would contribute to cladding modes and would cause cumulative cross-talk (increase of the random noise floor) when many VCSELs are operated at once in a real link system. The FIG with NA = 0.25 showed only fiber modes for light injected into the clads and carried higher intensities than those carried by the cladding modes for NA = 0.55 and 1.00. Estimates for these contributions to both cumulative and local cross have been made and will be presented.

A detailed analysis of the quantity of light transmitted as leaky modes needs to take into account in the way the FIG is constructed. Three are separate regions of the FIG, namely the solid portion at the input side with the ASG still in place, the long flexible region where the ASG is replaced with air, and finally the output solid portion with ASG. These need to be considered both separately and together in order to estimate their respective contributions to cross talk. In this work the polished end facets of the FIGs were uncoated, i.e., without anti-reflection coatings (ARC). It is likely that the use of ARC would reduce input leakage caused by multiple large-angle reflections between the input facet and the VCSEL array surfaces. These are topics for further investigations.

Conclusion

In spite of apparent simplicities, the FIG is a complex medium for parallel optical data transmission. There are several characteristics that are unique to a 2-D array of fibers that are not present in the case when a single fiber is used. These are: multiple large angle reflections at the input facet contributing to optical cross talk, a three-segment transmission medium, high-index coupling of cladding modes to adjacent fibers, high divergence of fiber modes and extreme divergence of cladding modes at the output. This work provides some evidence to suggest that high NA fibers (i.e., those with high differential refractive indices between cladding and guide media) are generally unsuitable for bidirectional link applications of a massive scale, namely upward of 2 x 2^{10} (2 x 1024) bi-directional links within a diameter of around 3 mm. It is expected that these critical and unique parameters will be identified, characterized and be used for developing complete models for massively parallel data links.

Sandia is a multiprogram laboratory operated by Sandia Corporation, a Lockheed Martin Company, for the United States Department of Energy under Contract DE-AC04-94AL85000. SayanMukherjeeCrossTalkPaperOC2001-092200

References

1. W.S. Ishak, K.H. Hahn, B.L. Booth, C. Mueller, A.A.J. Levi and R. Craig, "Optical interconnects – The POLO approach", Proc. SPIE vol. 2400 (Optical Interconnects III) (1995) pp. 214-221.
2. M. Lebby, C.A. Gaw, W. Jiang, P.A. Kiely, C.L. Shieh, P.R. Claisse, J. Ramadani, D.H. Hartman, D.B. Scwartz and J. Grula, "Use of VCSEL arrays for parallel optical interconnects," Proc. SPIE vol. 2683 (Fabrication, Testing and Reliability of Semiconductor Lasers) (1996) pp. 81-91.
3. T. Maj, A. Kirk, D. Plant, J. Ahadian, C. Fonstad, K. Lear, K. Tatah, M. Robinson and J.A. Trezza, "Interconnection of a 2D VCSEL array to a receiver array via a fiber image guide," Optics in Computing OC-1999, Abstracts, Snowmass, Aspen, CO, USA, April 13-16, 1999, paper PD2-1.
4. H. Kosaka, M. Kajita, Y. Li and Y. Sugimoto, "A two-dimensional optical parallel transmission using a vertical-cavity surface-emitting laser array module and an image fiber," IEEE Photonics Technol. Lett. 9 (1977) 253-255.
5. S.D. Mukherjee, K.M. Geib, K.D. Choquette and M. Robinson, "Input Coupling Measurements for Parallel Optical Interconnects using Imaging Fiber Bundles and VCSEL Arrays," Conference Digest 2000 CLEO-Europe (Conference on Lasers and Electro-Optics, Europe), 10-15 September 2001, Nice, France, paper CWJ2, pp. 267.
6. G.R. Hadley, "Index-guided arrays with a large index step." Optics Letters 14 (1989) 308-310.

Invited Paper
Symposium Photonics Fabrication Europe, Brugge, Belgium, 28 October – 1 November 2002
SPIE Vol. 4942 (VCSELs and Optical Interconnects) (2002) Paper 37

Critical Parameters For Parallel Interconnects Using VCSEL Arrays And Fiber Image Guides

Sayan D. Mukherjee[1,2], G. Ron Hadley[2], Kent M. Geib[2], Kent D. Choquette[3,2], Tony R. Carter[2], Arthur J. Fischer[2], Matt Robinson[4], and Charles T. Sullivan[2]
[1] Linköping University – ITN, SE-60174 Norrköping, Sweden,
[2] Sandia National Laboratories, PO Box 5800 MS 0603, Albuquerque, NM 87185, USA,
[3] Dept of Electrical and Computer Engineering, University of Illinois, Urbana, IL 61801, USA,
[4] Schott Optovance, 15 Sandersdale Road, Southbridge, MA 01550, USA

ABSTRACT

Several thousand glass optical fibers fused together is routinely used as fiber image guides for medical and other image remoting applications. Fiber image guides also offer possibility for flexible optical interconnect links with potentially thousands of bi-directional parallel channels with data rates as high as 10 Gbps per channel, leading to more than Tera bits per second aggregate data transfer rates. A fair number of fiber image guide based link demonstrations using vertical cavity surface emitting lasers have been reported. However, little is known about designable parameters and optimization paradigms for applications to massively parallel optical interconnects. This paper discusses critical optical parameters that characterize a massively parallel link. Experimental characterizations were carried out to explore some of the fundamental interactions between single-mode 850 nm VCSELs and fiber image guides having different numerical apertures, 0.25, 0.55 and 1.00. Preliminary optical simulation results are given. Finally, potential directions for further experimental and analytical explorations, and for applicability into designable link systems are suggested.

Keywords: Optical interconnects, fiber image guides, parallel datalink, VCSEL, optical feedback, fiber modes, multimode fibers

INTRODUCTION

According to a popular article [1], inter-board optical data links and optical backplanes are expected to enter the personal computer market in 2 to 5 years, and intra-board – such as, inter-CPU, CPU-to-memory, or more generally, inter-module – optical interconnections may become viable in 5 to 10 years. These are the predictions for the mass market. Meanwhile, there are high-value systems-oriented uses, somewhat hidden from the mass media, where parallel optical links are being applied. These are rack-to-rack connections among servers, storage and local area networks (LAN). Both clustered processors and distributed processors also require parallel optical links. These datalinks are essentially of two kinds: those that use fiber ribbons – generally 10 or 12 fibers parallel, and those that position separate fibers using either silicon V-grooves or molded plastic ferrules and thus create proprietary transmission media [2]. There are two other possible methods for parallel transmission of optical data. These are free space optical interconnects (FSOI) and those that attempt to mimic it using a potentially lower cost, and mechanically forgiving, alternative by using fiber image guides (FIGs). This paper discusses critical optical parameters that characterize FIG-based massively parallel links. The paper then proceeds to describe near-field, far-field, L-I-V and spectral characterizations carried out to explore some of the fundamental interactions between single-mode vertical cavity surface emitting lasers – VCSELs – and fiber image guides having different numerical apertures: 0.25, 0.55 and 1.00.

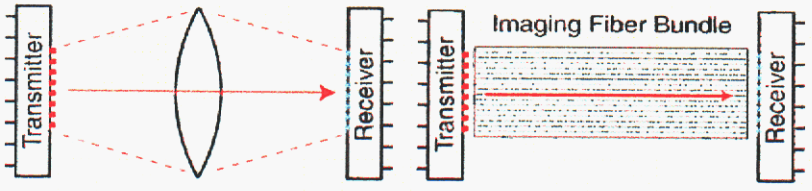

Figure 1 A fiber image guide is expected to replace lens-based imaging of the transmitter plane upon the receiver plane. FIGs would provide additional advantage of mechanical flexibility, e.g., going round corners and lack of sensitivity to mechanical deformation of the sending and the receiving planes caused by thermal expansion and contraction.

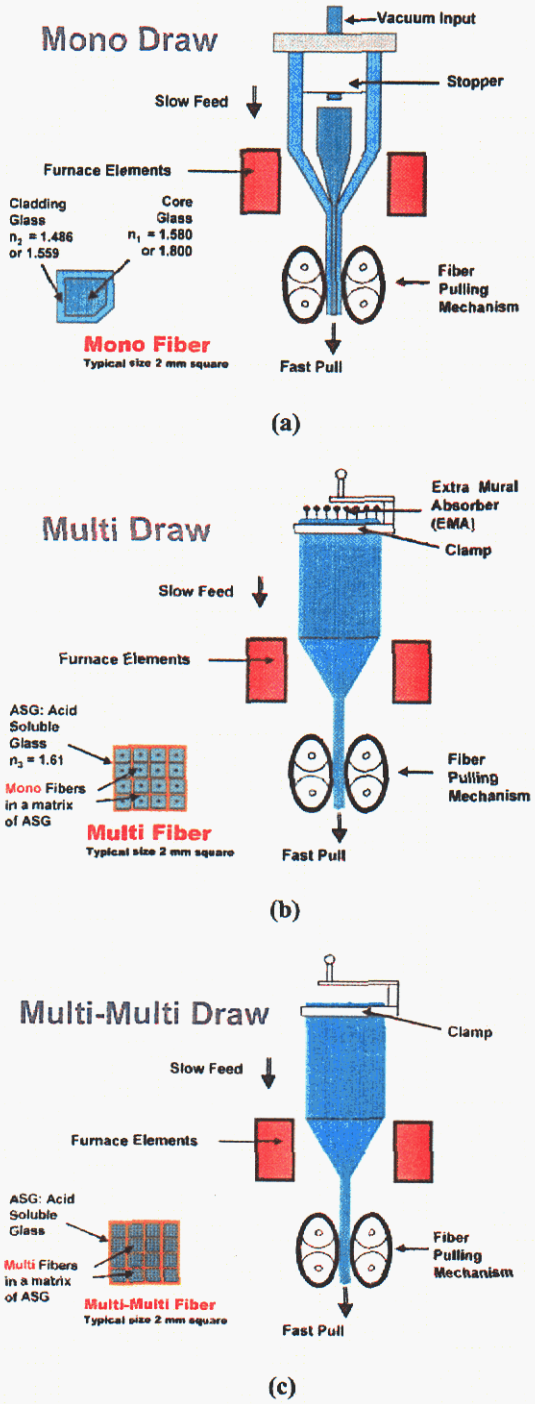

Figure 2 Production of fiber image guide rods through three fiber-drawing stages. Both hexagonal and rectangular fiber arrays can be produced. The final drawing creates a long rod with fibers embedded in acid soluble glass (ASG). The ASG is removed from a long central portion of the rod to produce flexible FIGs.

BACKGROUND

Fiber ribbon-based optical datalink products have their genesis in the traditional optical interconnects fraternity and rises technology up from R&D that began in the late 1980s and ended in the late 1990s. National consortia, such as the OptoElectronic Technology Consortium (OETC) in the US [3-5], and several industries produced parallel fiber links. Some examples are: HP – POLO [6,7] and PONI [8], Motorola – OPTOBUS™ [9-12], IBM – Jitney [13-14] and Litebus™ [15], Vixel Corp – P-VixeLink™ [16], Siemens – PAROLI™ [17], and link-demonstrations and products from NEC [18], NTT [19,20], Hitachi [21], and others.

Datalinks that use separately positioned (and passively aligned) individual fibers – as opposed to fiber ribbons – are market-driven and systems-driven. User industries that deal with LAN, wide area network (WAN) and metro area network (MAN) tend to require such links. Producing industries leverage technologies originanated in the domains of long-haul optical fiber communications. However, unlike cost-insensitive long-haul businesses, these use production techniques that are potentially of low cost [2,22].

For most short-haul applications, the optical transmitter of choice is the 850 nm VCSEL with its bit-parallel (i.e., several VCSELs modulated side-by-side) data handling capability of up to 10 Gb/s per VCSEL. Ostensibly, however, this wavelength is expected to change to 1550 nm in order to accommodate 40 Gb/s LAN/MAN/WAN links where the distance-bandwidth product becomes an issue. There are no fibers that would carry even externally modulated 40 Gb/s signals at 850 nm wavelengths over 100-300-meter distance. This is due to dispersion-induced pulse spreading. For shorter distances, dispersion in fibers and other waveguide media is manageable and so the 850 nm wavelength is preferred. For even shorter distances, such as 10s of centimeters to 10s of meters, multimode waveguides and fibers are the norm. Here, modal dispersion [23] and modal noise [24] can be managed with suitable engineering of both the VCSEL and the transmission medium.

VCSEL-FIG based parallel interconnects offer higher potential data throughput that cannot be readily achieved using either fiber ribbons, separately (passively) positioned fibers or free-space optical interconnects. Fiber ribbons provide too few channels and can only grow in number along one dimension. Separately (and passively) aligned fibers eventually run out of cost effectiveness and cross-sectional space. Free space optical interconnects uses imaging techniques to connect the receiver plane to the transmitter plane (Fig. 1 top). FSOIs can be loosely divided into two types. The first employs material

Table 1 Optical parameters for Fiber Image Guides used in this work

Numerical Aperture (NA)	Core refractive index (n_1)	Cladding refractive index (n_2)	Refractive index for acid soluble glass – ASG (n_3)	Core-clad refractive index difference (Δn)	Index difference ratio ($\Delta n/n_{avg}$)	Acceptance half angle ($\psi_{½}$)	Fiber V-number at 850 nm wavelength (V)
0.25	1.580	1.559	1.61	0.021	1.34%	15°	16
0.55	1.580	1.486	1.61	0.094	6.13%	32°	37
1.00	1.800	1.486	1.61	0.324	19.7%	90°	66

transmission media such as slab waveguides with diffractive, holographic or refractive optical elements (DOEs, HOEs or ROEs) [25]. These require novel technologies and reconfiguration of the board and backplane-based electronic systems. Their projected use in a multiplicity of products in large volume is uncertain. Several specialized functional sub-systems that take advantage of the slab waveguide have been proposed and demonstrated. The second type of FSOI incorporates bulk or microlenses and makes use of air as the optical transmission medium. These generally require positional precision and maintenance of such precision over the operating life of the system. Such solutions can be small in size but require special fabrication and micropositioning techniques [26,27]. Bulk lens-based FSOI links are large and heavy in weight [28,29], but use commercially available lenses. Their applications are expected to be limited to systems where these overheads are tolerable.

Superficially, FIG-based optical interconnects are replacements for lens-based systems [30-38], but with added advantages such as going round bends and being impervious to dimensional changes and buckling due to localized heating/cooling of the optical transceive board or module (Fig. 1). Butt coupling the FIG upon the transceive planes eliminates the need for focusing lenses. Thus, butt coupling is but one option [33,37,38]. The second option is to move the input facet of the FIG somewhat away from the VCSEL plane. Here, light coupling is distributed over many fibers,

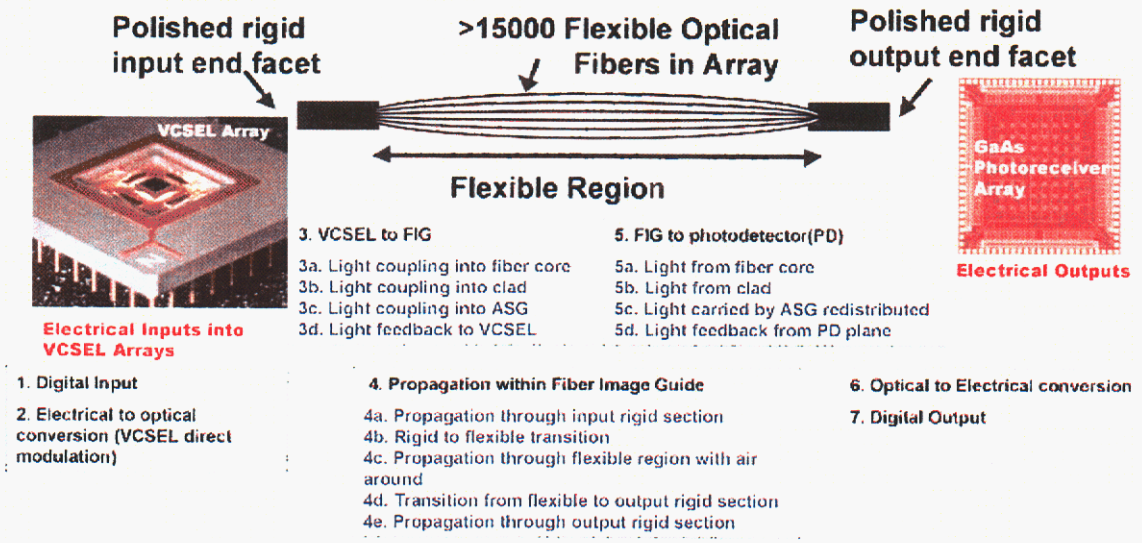

Figure 3 Classification of regions where propagating data may suffer degradation. Degradation is possible from electrical means (drivers to VCSELs and amplifiers in the photoreceivers), due to electrical to optical conversion and vice-versa, optical reflections from at least five interfaces and optical propagation through a complex medium, the FIG, segmented into three separate regions. Noise from the VCSELs due to optical feedback-induced effects should also be considered. Some are understood. Others are just being recognized. Here, ASG is acid soluble glass – see Fig. 2.

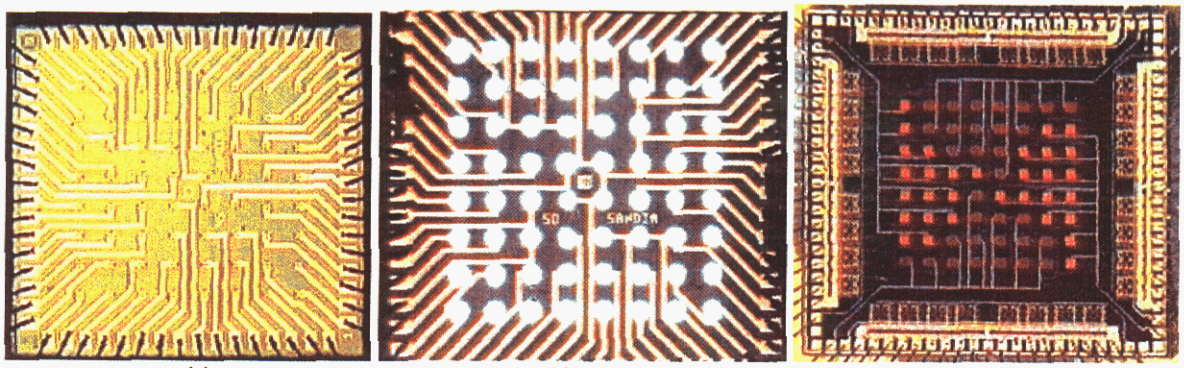

(a) (b) (c)

Figure 4 (a) Wire-bonded 8x8 VCSEL array with ~0.5 mA threshold and 3.5+ mW maximum output singlemode power. **(b)** All VCSELs powered up. **(c)** Wire-bonded GaAs MESFET IC photoreceiver with large 50 microns square MSM photodetectors.

and each cluster would carry almost equal amount of light from each separate VCSEL [31]. In addition, however, at least four kinds of input-output optics have been used for bringing VCSEL light into the FIG and for taking the output light on to the photodetector. These are: linear fiber tapers [30], large (macro- and mini-) lens-based focusing optics [30,32,35,36], microlens-arrays [34] and separate fibers attached to the output facet of the FIG [34]. Like FSOI, FIG-based optical interconnects that depend on large lens assemblies are bulky and may suffer from both high cost and long-term thermal-mechanical instability. Simplicity dictates butt coupling or short distance coupling with or without microlens arrays.

Fiber image guide based links have been demonstrated at up to 1 Gb/s [31,35] and 3 GHz [35], but a detailed understanding of link parameters and design limits are unavailable. Gaussian beam input coupling analyses [39,40] have reported first order estimation of the coupling efficiency between laser emissions and FIG input facets.

Our work identifies additional VCSEL-FIG coupling issues and FIG parameters of relevance. These are categorized but only some are addressed in this paper.

EXPERIMENTAL & SIMULATION DETAILS

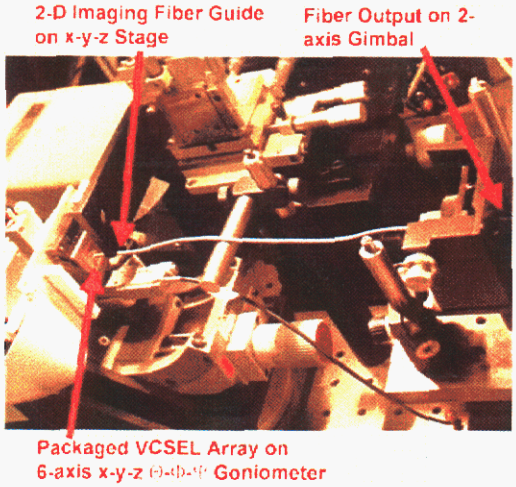

Figure 5 VCSEL-array-FIG experimental setup.

The Fiber Image Guide (FIG)

Fiber image guides of 20-cm length and of numerical apertures 0.25, 0.55 and 1.00 were used. These numerical apertures correspond to core and clad refractive indices respectively of [1.58, 1.56], [1.58, 1.486] and [1.80, 1.486] (**Table 1**). The ~1.8 mm hexagonal cross-section FIGs consists of 15379 fibers with 9.1-μm core at a 13.5- μm pitch, with 2 μm thick clad. The space between the individual fibers is filled with acid soluble glass (ASG) with a 1.61 refractive index. Schott Fiber Optics manufactured them by using a three-stage fiber pulling technique shown in Fig. 2. At the end of the production process, the long, solid rod with embedded fibers is optically polished to produce the input and the output facets. The two ends are then dipped in an etch mask polymer to few to ~10 mm in length. The entire rod is dipped in an acid that dissolves the ASG from the long, central part. The fibers are therefore embedded in ASG at the two ends but have air between them in the central part that gives the FIG its flexibility. The polymer is then removed and the FIG encased in a protective, but flexible, shield for use. For applications with known connector types, the polished ends are connectorized.

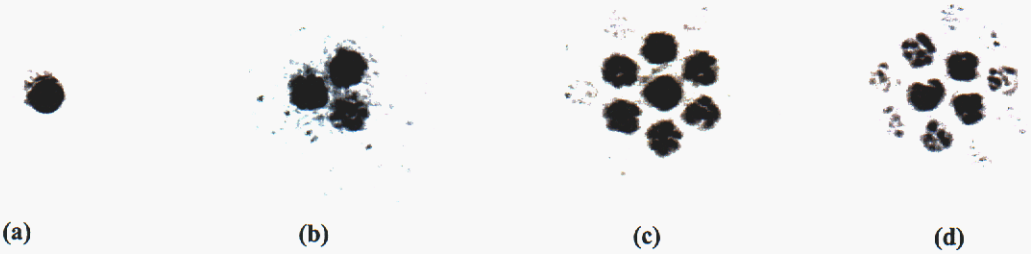

(a) (b) (c) (d)

Figure 6 Image reversed near-field photomicrographs. Here, dark implies more light. **(a)** Fiber output for with VCSEL emission into a single NA = 0.55 fiber at z = 0 μm. Recorded at attenuation −59dB. **(b)** Fiber output with VCSEL emission aimed into cladding in between three NA = 0.55 fibers at z = 0 μm. Note cladding modes. Recorded at attenuation −20dB. **(c)** Fiber output with VCSEL emission axis aligned to a single NA = 0.55 fiber at z = 100 μm. Recorded at attenuation −59dB. **(d)** Fiber output with VCSEL emission axis aligned to the clad in between three NA = 0.55 fibers at z = 100 μm. Recorded at attenuation at −59dB.

Qualitative Description Of The Link

Let us consider a FIG-based datalink with butt- or short-distance-coupled VCSEL-FIG-receiver combination (Fig. 3). The light must travel through several interfaces and media types to reach its destination. Upon leaving the VCSEL, the light would travel through a finite distance in air – unless the FIG is immersed in index matching fluid, a method impractical to implement in a product. The light then hits the air-FIG interface, suffers some reflection, and the reflected light comes back to the VCSEL. The FIG's optically polished input plane thus forms a Fabry-Perot cavity with the planar VCSEL top surface. This may very well be the dominant source of optical feedback.

The light entering into the solid portion of the FIG is divided into three parts: into the core, clad and ASG. This is so if the VCSELs are not aligned to one core at a time, a requirement that probably would make the FIG not as attractive a link medium. These three components are:

(i) Light originally launched and guided within the core. This is expected to continue to the end unless the FIG is bent too much.

(ii) Light launched in the clad. This would have a tendency of straying into the core and the ASG. This is because the clad has the lowest refractive index and so is unable to guide any light in the presence of the ASG around it and the core within it.

(iii) Light launched into the ASG and is guided. Only the forward scattered portion will follow the fibers after air replaces ASG.

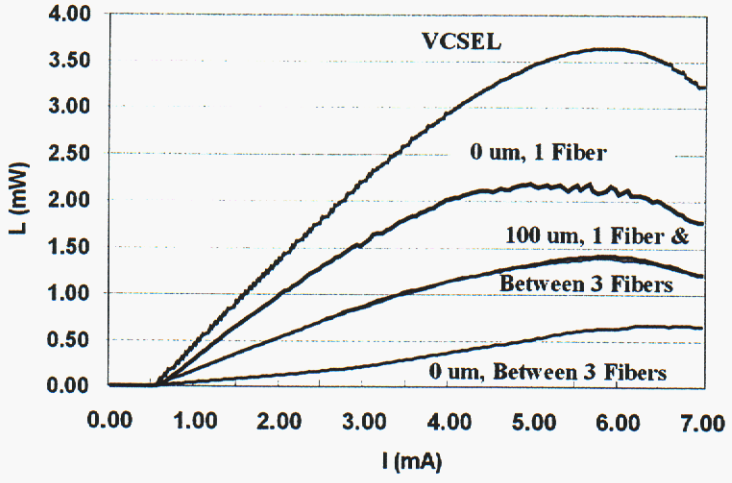

Figure 7 L-I curves for a bare VCSEL (top) and the best aligned FIG output vs. maximum-misaligned conditions for z = 0 and 100 μm. FIG numerical aperture NA = 0.25.

It has been assumed that only the light entering the core would appear at the output end, and the other propagating light could be neglected [39,40]. We have seen cladding modes for NA = 0.55 and 1.00 for light injected purposely into the region in-between three neighboring fiber cores [41-43]. For some specialized applications, Schott produces FIGs with some parts of the ASG embedded with dark glass that absorbs most visible and 850 nm

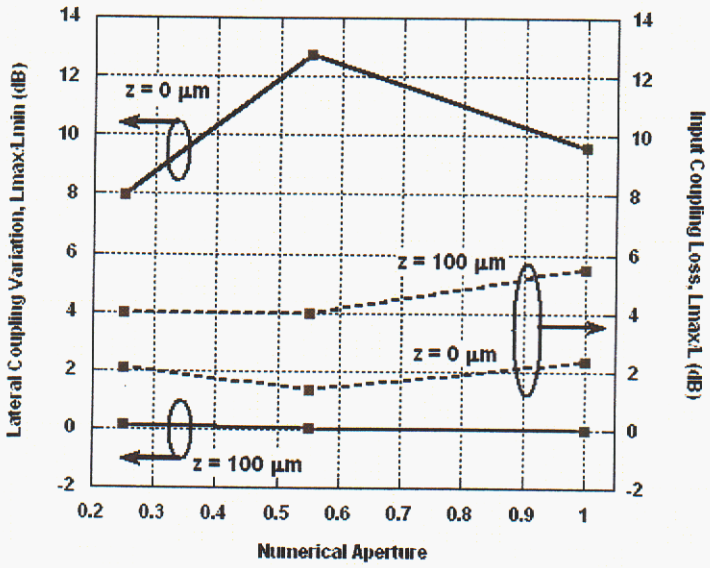

Figure 8 Dependence of coupling efficiency (ratio of light coupled into the fiber and VCSEL emission) and coupling error (ratio of maximum to minimum coupling for a change in lateral position) upon numerical aperture of FIGs.

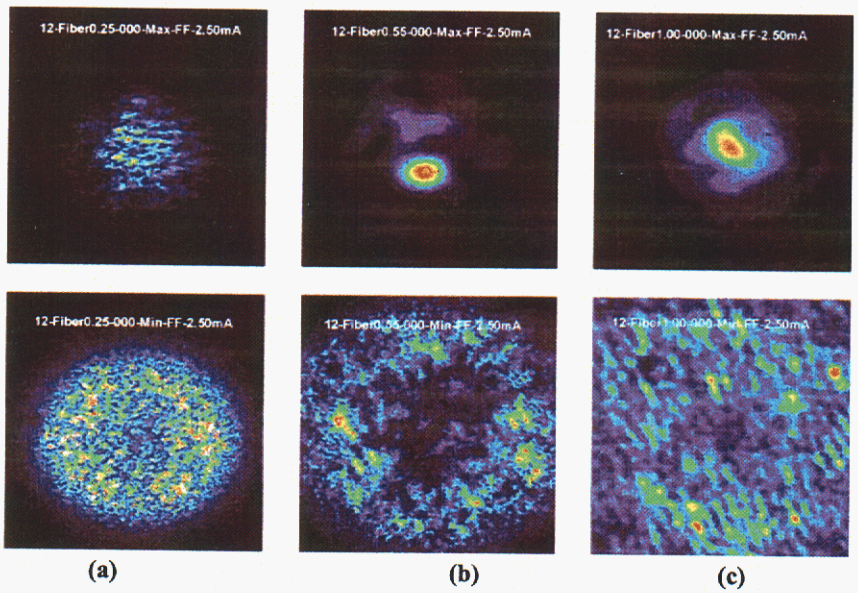

Figure 9 Far-field patterns for FIGs with three NAs under butt-coupled (z = 0 µm) conditions. **(a)** VCSEL centered on one fiber core (top) and into the ASG in-between 3 cores (bottom) for FIG with NA = 0.25. **(b)** Same for FIG with NA = 0.55. **(b)** Same for FIG with NA = 1.00. Both NA = 0.55 and 1.00 transmit single mode pattern when VCSEL is centered on one fiber core, but not NA = 0.25.

stray radiation. This is not so for the FIGs used here.

After passage through the first solid section, the light carried by the three separate materials, the core, clad and the ASG, enters the second – flexible – portion of the FIG. Here the ASG disappears and the fibers are surrounded by air. It is expected, therefore, that light carried by the ASG would be scattered at this discontinuity with three possible outcomes. Part of it would radiate out into air, part reflected back towards the input facet and the VCSEL, and part scattered forward into the clad-core combination of the individual fibers that make up the flexible portion of the FIG. From this point onwards, light is carried by the core confined by the clad, and by the clad confined by air. In effect, there are now two concentric waveguides one inside the other. Within these two waveguides are components from three original propagating lightwaves:

At the end of flexible portion, the light enters the solid output segment of the FIG. Exactly how the different components of light under (ii) and (iii) above would become redistributed is not clear. There is a discontinuity from air to the start of ASG in this final segment. Evanescent light field traveling along the outside perimeters of the fibers would experience a large jump in refractive index – from 1.00 to 1.61. Some reflection is expected. A part of this reflected light would constitute optical feedback not only for the VCSEL that produced the light but also for all other VCSELs in the input array.

The light would now travel through the solid output section of the FIG and, finally, would emerge into a

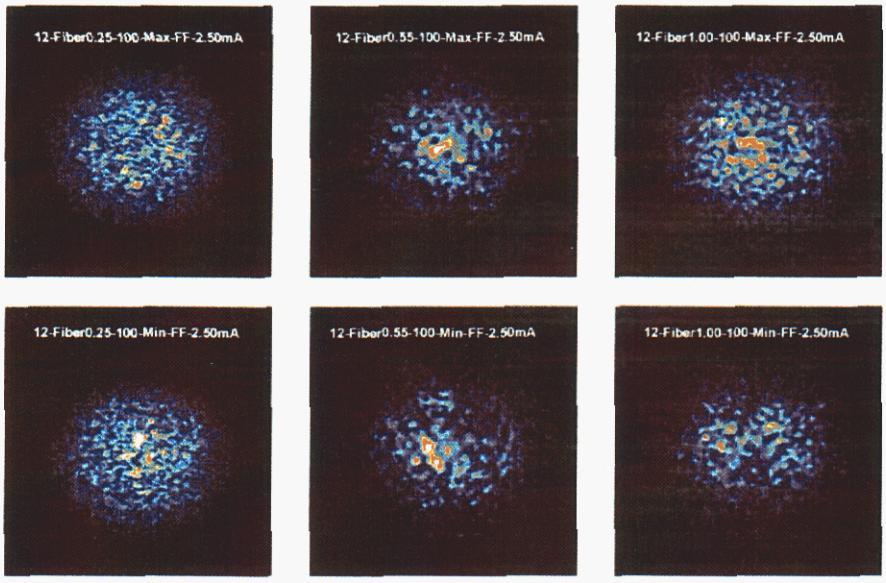

Figure 10 Far-field patterns for FIGs for z = 100 μm conditions. **(a)** VCSEL centered on one fiber core (top) and into the ASG in-between 3 cores (bottom) for FIG with NA = 0.25. **(b)** Same for FIG with NA = 0.55. **(b)** Same for FIG with NA = 1.00. For the top row 13 cores take part in transmitting light, and for the bottom row it is 12 fibers. Both the cases have a number of nearest neighbors that carry light at between – 20 to – 30 dB-attenuated levels relative to the central peaks. The average $1/e^2$ cone full angles are 33° for NA = 0.25, 37° for NA = 0.55 and 41° for NA = 1.00. These angles are not well represented in the patterns due to different neutral density filters used in each case. Free-space VCSEL emission full angle is 22°.

finite thickness of air that separates the optically polished output facet of the FIG and the surface of the photodetector in the receiver array. Reflection from the FIG-air interface would result in some light traveling backwards and constitute optical feedback for the VCSEL that produced the light and optical disturbances to the neighboring VCSELs having very similar cavity lengths and emission wavelengths. For 850-nm detection, GaAs metal-semiconductor-metal (MSM) photodetectors are generally used. This is due to their ease of fabrication and ease of integration with standard GaAs MESFET (metal semiconductor field effect transistor) circuits with no or minimal modification to the fabrication process. Generally, a simple, anti-reflection coating (ARC) made with just one silicon nitride layer suffices to provide acceptable suppression (low reflection) of return optical signal. However, the MSM photodetector also has metal lines with uneven surfaces. Given the high numerical apertures of common FIGs, it is conceivable that some light would get reflected and would go back to the source/s as optical feedback and disturbance.

The light may, therefore, get reflected back into the VCSEL/s from five interfaces. These are: (i) air to FIG input facet, (ii) FIG input solid section to flexible section transition, (iii) flexible to final solid section transition, (iv) FIG output facet to air interface, and, finally, (v) the receiver plane.

Considering that single-transverse mode VCSELs tend to have CW coherence lengths ~ 30 – 40 cm [44], a 20 cm long FIG with minimum refractive index ~ 1.58, and double the path for return signals, would probably not produce coherent optical feedback from the receiver plane. But there are many other reflection planes of shorter distances described above. These reflections may cause random mode locking resulting in uneven emitted power that would amount to high source noise. The case for a VCSEL dynamically modulated may even be more complex due to chirping if the VCSEL is single longitudinal and transverse mode, and due to modal fluctuations if the VCSEL is capable of oscillating in multiple transverse modes. We found evidence that free running single-mode VCSELs would demonstrate multi-transverse-mode behavior under CW optical feedback [41]. In addition, dynamically operated (i.e., the input current modulated to produce digital pulses) multimode VCSELs show effective lowering of coherence length [44] when all possible transverse and chirped modes are taken together. Separately, each mode would have longer coherence lengths each, and the possibility for random mode-locking type noise may remain.

The light emerging from the output facet is complex. Most FIGs reported in the literature for link applications are multimoded and have large V-numbers implying their capacity to carry a large number of modes. These can be easily observed using near-field techniques [36,40-43,45]. In addition, there are other modes carried by the 2-micron wide cladding material [41,43] to be discussed later. Overall, therefore, light transmission through FIGs, and its possible interactions with VCSELs, are complex and require detailed evaluations.

VCSEL-FIG Coupling Experiments

Oxide confined, 4x4 μm square aperture, single mode VCSEL arrays emitting nominally at 850 nm were used. The VCSELs operate in a single transverse optical mode, as determined by both far field (~22° full angle) and spectral measurements, with ~0.5 mA threshold current and a maximum of 3.5+ mW output power at ~5.5 mA drive current [46]. VCSEL arrays were wire bonded in open packages (Fig. 4) and mounted on a 6-axis goniometer (Fig. 5). The input of the FIG was mounted on a precision 3-axis translation stage and the output on a 2-axis gimbal. Two specific lateral (x-y) positions were chosen to determine the extremes of coupling differences. For these two lateral conditions the value of z, the separation between the FIG input facet and the VCSEL, was varied from 0 μm to 300 μm. Light and voltage versus current (L-I-V), near-field and far-field patterns were recorded for a selection of input conditions. The FIGs were 20 cm long each with numerical apertures NA = 0.25, 0.55 and 1.00 as described earlier.

Simulations using Beam Propagation Method (BPM)

Semivectorial 2-D Pade (1.1) wide-angle BPM codes, developed internally, were used to simulate a 10-μm waist diameter Gaussian beam of 850 nm wavelength. The beam was injected at the aligned-to-the-core and aligned-to-the-clad states for butt-coupled (z = 0 μm) and z = 100 μm conditions. The computation was carried out with a 600-μm propagation distance into the solid input portion of the FIG. Equilateral triangular grids of ~0.5 μm pitch were allowed to relax around circular fibers to enable smoother transitions for optical E-field calculations.

RESULTS AND DISCUSSION

Near-Field Patterns

Fig. 6 shows examples of near-field patterns for FIG with NA = 0.55. In (a) & (c): z = 0 and 100 μm, the VCSEL emission is aligned to one fiber within the FIG. In (b) & (d): z = 0 and 100 μm, the VCSEL emission peak is aligned to the cladding material so that most of the light is injected into the clad. This was done in order to measure how efficiently the cladding materials transmit "stray" light through the length of the FIG. When VCSEL emission was injected purposely into the ASG and the cladding material at the center of three fiber cores at near-zero separation (butt-coupled condition), two dissimilar near field patterns were obtained at the output plane for low NA (here 0.25) and high NA (here 0.55 and 1.00) cases. In the former, the cladding regions did not carry any light but the stray light was present only in the core. Many cores were illuminated that were several neighbors away from the point of light entry. In contrast, for high NA FIGs, the stray light was carried not by the cores at all but was carried by the cladding material – see Fig. 6(b). In both cases, there was a high-intensity region at the center of the three fibers. The VCSELs have about 10 μm Gaussian waist diameter upon exiting the VCSEL surface. A 10-μm diameter $1/e^2$ circle (with 86.5% intensity inside the circle) would most adequately encompass parts of three fibers surrounding the point of entry – so the peaking here is not surprising. However, both the presence of core light for NA = 0.25 and cladding light for NA = 0.55 and 1.00 require explanations. BPM simulations shed some insight into these issues – see later – but the reason for this difference is not fully understood yet.

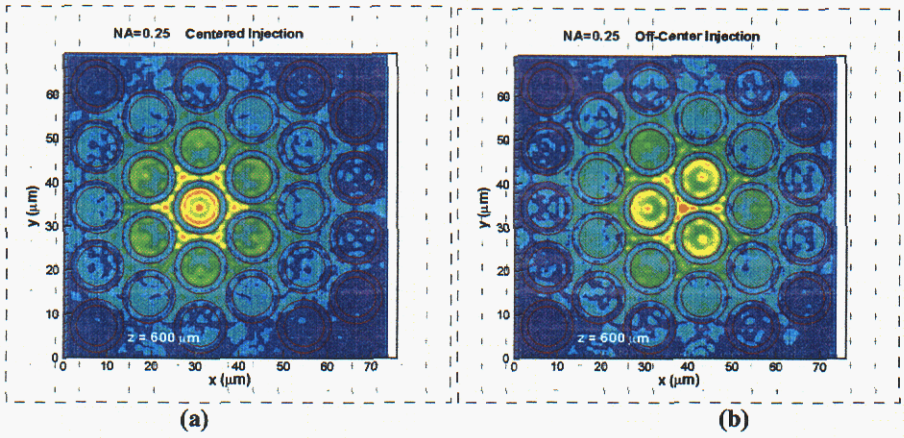

Figure 11 Near field patterns calculated using beam propagation method (BPM) simulation for 850 nm VCSEL emission into FIG with 600 μm propagation distance. FIG NA = 0.25 and z = 100μm. **(a)** VCSEL centered on one core. **(b)** VCSEL centered on the ASG in between three cores. The input Gaussian mode waist diameter is 10 μm.

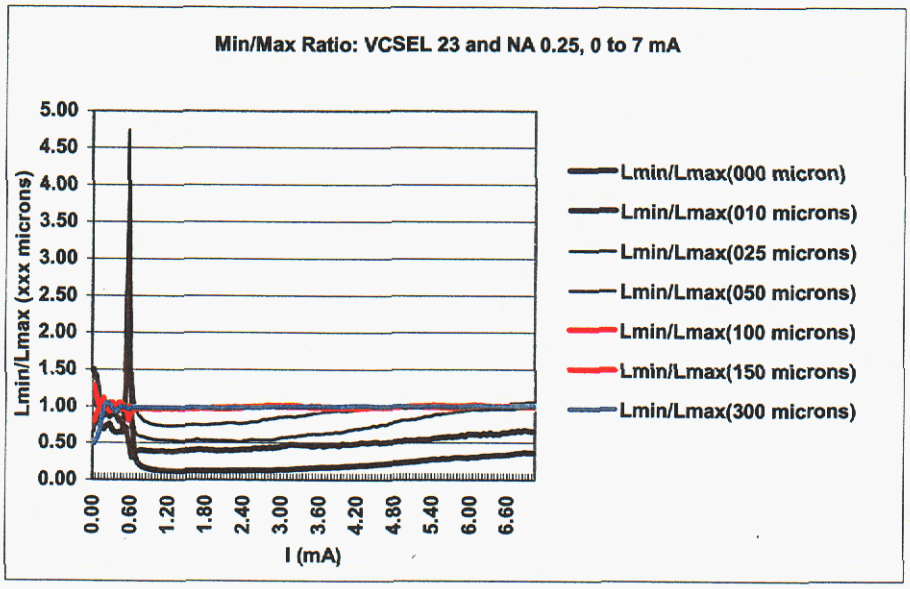

Figure 12 Ratio of minimized output optical power (i.e. VCSEL centered to the ASG in between three fiber cores) to maximized output optical power (i.e., VCSEL aligned to one fiber core) as a function of input current at various VCSEL to FIG separations for NA = 0.25.

L-I-V Measurements

Figures 7 and 8 describe the differences for transmission through FIGs corresponding to the four conditions in Fig. 6. The top curve in Fig. 7 shows that at z = 0 μm the ratios of transmitted powers, shown as the lateral coupling variation, for the best and the worst aligned conditions are between 8 and 12 dB. These large differences become very small, e.g., ~0.3 dB, for z = 100 μm (bottom curve, Fig. 8). Therefore, unidirectional links may be constructed with an input separation of ~ 100 μm with an accompanying high lateral positional tolerance. The associated input coupling loss is between 4 and 6 dB (top dashed line in Fig. 8), which is about 3 dB worse than the best coupling condition at z = 0 μm (bottom dashed line in Fig. 8). This differential loss appears to be an acceptable penalty for achieving an undemanding lateral alignment requirement.

The combined L-I-V and near-field measurements show that for the separation z ~ 100 μm the difference between best and worst aligned conditions disappear completely. For the best aligned case at z = 100 μm, with the VCSEL centered upon one fiber core, there are 6 additional cores that carry the most light and another 6 carry a little light each. For the worst aligned case at z = 100 μm, which started with the VCSEL center aligned to the center in between three cores, the three central cores carry most of the light, the immediate-neighbor 3 carry some, and the next 6 nearest neighbors carry a little. The total number of fiber cores that would carry the signal is between 12 and 13, in approximate agreement with an earlier estimate of about 14 μm radius of illumination [40]. In our case at z ~ 100 μm the Gaussian beam radius is ~ 19 μm, calculated using the measured far field full-angle of about 22° for the VCSELs.

Other work [39,40] calculated the overlap integral of in input Gaussian beam and the circular cross-sectional input openings of the fiber cores of the FIG. This method is applicable when the VCSEL numerical aperture (emission angle) is less than the fiber or FIG numerical aperture (acceptance angle), which was the case there as well as is here. It assumed the fiber mode to be Gaussian only and did not account for the light carried by the cladding regions, also transparent to 850 nm radiation. It then proceeded on to calculate optical crosstalk due solely to the lateral tail ends of the input Gaussian beams collected by neighboring fiber cores adjacent, but very close, to the main channel fiber cores. It estimated the minimum allowable channel separation – 3 to 4 fibers per channel. In effect, it addressed only item 3a in Fig. 3. Our experiments shows that an estimation of cross talk and maximum allowable channel density would require careful consideration of the light carried by the cladding material and the ASG. It should also include the influence of all the intermediate interfaces described under "Qualitative Description Of The Link" above. Moreover, the VCSEL-FIG separation required for illuminating only 3-4 fiber cores would incur large – and possibly unacceptable – variations in input coupling efficiencies for different VCSELs across the FIG input facet. This would also reduce fiber redundancy, an advantage of FIGs over individually coupled fibers.

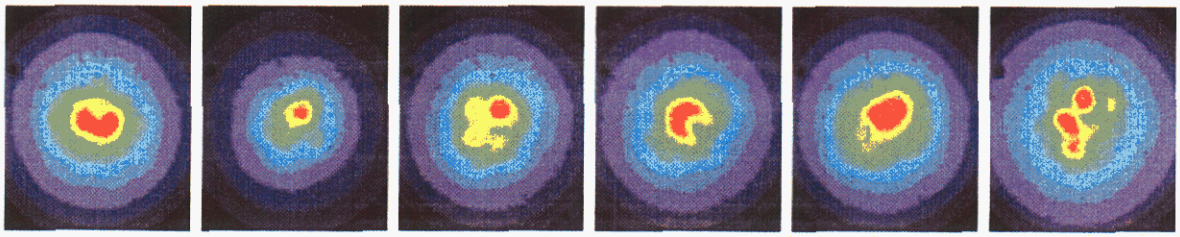

Figure 13 Output far-field patterns showing transverse modes generated with positional variations of a butt-coupled NA = 0.55 FIG. VCSEL current was 0.45 mA, at the onset of stimulated emission. The maximum extent of lateral displacement of fiber-core center to VCSEL center was ± 2 μm from the central position. These patterns did not change with time.

Far-Field Patterns

Far-field patterns were recorded using an f-θ lens made by Coherent. An f-θ lens maps angle of emitted light linearly upon the receiving plane, such as a CCD camera or other focal plane array. This gives one-to-one correspondence between the x- and y-locations in the camera and the angle of emission. The x- and y-axes recorded in this case had total angular widths respectively of 62° and 72°, which corresponds to a diagonal angular field of about 94°. Fig. 9 shows far-field patterns for the three FIGs, all for butt-coupled conditions, at VCSEL input current of 2.50 mA. At this input current, the maximized (VCSEL aligned to one fiber core), the detected optical power at the output facet was ~ 1 mW (see Fig. 7). When the VCSEL is aligned to one fiber core, both NA = 0.55 and 1.00 FIGs transmitted single mode light, but the NA = 0.25 FIG did not. This is surprising but consistent throughout all of our experiments. There may be transfer of sizeable optical power to other fibers or cladding that interferes at the output to produce this pattern (top-left in Fig. 9). This anomaly adds to another anomaly for the near-field pattern: many near-neighbor cores were lit up at the output even though the VCSEL was aligned to only one core at z = 0 μm.

Far-field patterns for minimized (VSCEL aligned in-between three fiber cores) conditions (bottom row, Fig. 9) produced very grainy patterns for 0.25 FIG, less grainy but with a central hole pattern for 0.55 FIG and a more diffused pattern for 1.00 FIG with the central hole almost completely gone. That multiple interference peaks formed indicates that the coherence is still maintained after 20 cm of transmission, although heavily multimoded [47]. This is not surprising if we are to assume the coherence length to be on the order of 30 mm [44], because the differential path lengths cannot exceed the maximum Δn multiplied with the FIG length. The appearance of central 'holes' for NA = 0.55 and 1.00 FIGs probably suggests the cladding modes with large divergence angles are interfering along conical surfaces. The actual reasons would not be ascertained until cladding mode analyses followed with far-field pattern determination (Fourier transformation) are carried out numerically.

Far-field patterns were very similar for all six cases at z = 100 μm (Fig. 10). This suggests that for an approximate 40 μm diameter output patch the FIGs do not significantly add divergence angles to the original VCSEL emission full angle of 22°. It should be borne in mind, however, that all these far-field patterns (as well as the near-field patterns) were taken with neutral density filters to keep the amount of light falling upon the CCD camera below saturation. A little more than 50% of the light incident upon the FIG input facet is coupled into the clad and the ASG. The lateral extent of their rambling is large, extending almost to the perimeter of the entire 1.8 mm wide hexagonal FIG. Their influence upon the far-field pattern does not show up due to their relatively low intensities. However, when 64 or 1000 VCSELs would be simultaneously operated upon the input facet of the FIG, there would be proportional increase to this 'diffuse' background. This, we believe, is the true performance-limiting cross-talk source for FIGs for applications to massively parallel optical interconnects.

BPM Simulation of FIGs

FIGs with NA = 0.25 and 1.00 were simulated. Fig. 11 shows results for maximized (aligned to core) and minimized (aligned to the ASG in between three cores) for NA = 0.25 for z = 100 μm. The results for z = 100 μm exemplify how light would become coupled into different possible modes in general. Since the termination distance for the simulations were limited to 600 μm, not all modes could be seen for z = 0 μm conditions. The 10 μm diameter for Gaussian 1/e (amplitude) beam waist at 850 nm would expand to about 40 μm diameter upon entry at distance z = 100 μm. Light would be coupled to the core as well as to the adjoining clad and ASG – see Fig. 11 (a). This light would also penetrate

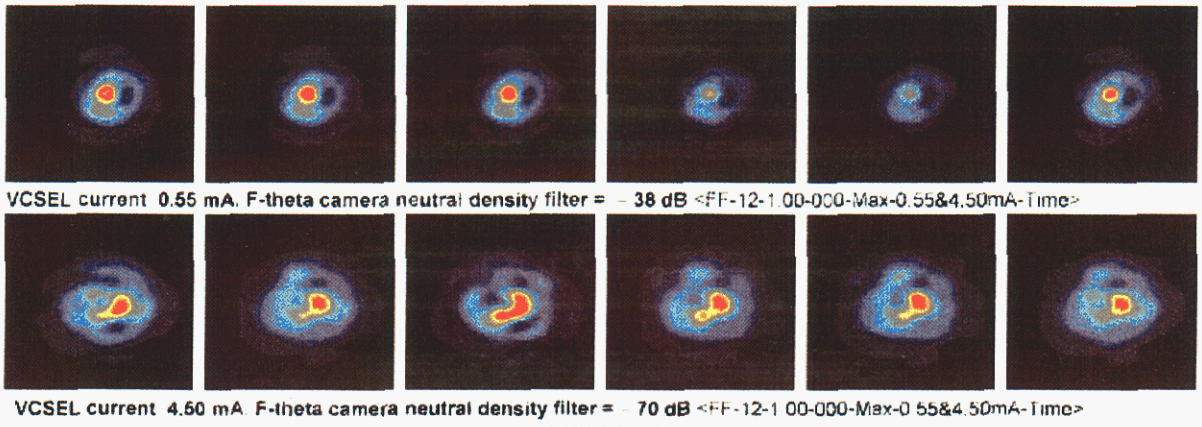

Figure 14 Temporal variation of far-field pattern for 4 μm x4 μm aperture, oxide confined nominally single-mode VCSEL when butt-coupled to NA = 1.00 FIG. The sequence is approximately consecutive in the way the patterns appeared, and it repeats itself over 3-5 seconds period. The top row was taken at just above threshold (0.55 mA) and the bottom row at high injected current (4.50 mA) just below the thermal turnover peak in the L-I curve (see Fig. 7). The VCSEL was not modulated.

into adjacent cores, especially for the tail ends of the Gaussian profile for which the emission angles are larger than the acceptance angle (half angle 15°) for this relatively weekly guided fiber. Fig. 11 (b) shows definite indication of modes carried by the ASG itself with its high refractive index of 1.61 surrounded by the clad of r.i. = 1.559 and the 'core' now acting like a second cladding with r.i. = 1.580. Note both are lower than 1.61. There are indications of focusing of light through the cores, and the three cores that surround the central ASG waveguide have large amounts of couples light from the 10 μm diameter Gaussian beam input. There appear as much possibilities for cladding modes to form here as there are for core-modes. In contrast, the simulations for NA = 1.00 showed definite creation of cladding modes at the expense of core-modes. These were seen more easily for z = 0 μm.

Cladding modes were also found to form for 1-D slab waveguide having the same linear (lateral) distribution of refractive indices as in the FIG. This was true for simulations at both Schott [45] and at Sandia [43], using different simulation codes. It suggests that the cladding or the ASG materials do not have to be contiguous to each other to form a connected matrix as in a 2-D cross-section of an FIG for cladding modes to appear. Cladding modes form through long distance coupling of light through the core region. We are exploring its behavior using coupled leaky mode theory for strongly guided waveguides with high refractive index differences [48-50].

VCSEL Instability due to Optical Feedback

We observed effects of CW optical feedback upon VCSEL performance for all three types of FIG. Their manifestations, however, were uniquely different. For FIG with NA = 0.25, the VCSEL stimulated light power became significantly larger for a value of current (0.55 mA) slightly higher than the threshold current of about 0.52 mA. Fig. 12 plots L_{min}/L_{max} as a function of VCSEL input current for a number of distances between the NA = 0.25 FIG input facet and the VCSEL surface. Here, L_{min} is the optical power detected at the output when the VCSEL is aligned to the center in between three fiber cores – the so-called worst aligned condition. L_{max} is the corresponding detected output light power when the VCSEL is aligned to the center of one fiber core – the so-called best aligned condition. Fig. 12 shows that for z = 0 μm the ratio becomes greater than unity at 0.55 mA, implying a large L_{min}.

For the FIG with NA = 0.55, for the maximized condition at z = 0 μm, we could see the formation of higher order transverse modes by moving the center of the fiber core around the center of the VCSEL – see Fig. 13. The distance between the two was always brought back to zero after each lateral re-positioning. These far field patterns were stable over time.

The far-field patterns for FIG with NA = 1.00 for maximized condition at z = 0 μm were temporally unstable. Far-field pattern shapes varied slowly over time and standard video sampling rates could be used to observe the changes. Since the capture time is no less then 1/100 second, each pattern is stable at least over this time duration. Moreover, the change from one pattern to the next was gradual, indicating a slow internal change within the VCSEL as against a fast

change due to optical reflections from e.g., interfaces within the FIG. For a 20 cm FIG with a maximum continuous refractive index (that of the core) of 1.8, the longest possible return time after reflection at the output facet is 2.4 nanoseconds. These fluctuations do not appear to be related to optical time of flight, but rather to other slowly varying internal mechanisms, such as localized thermal effects.

Spectral Measurements

The L-I data for butt-coupled condition showed small ups and downs not seen in the free-space L-I curves for the VCSELs. These localized peaks and valleys are easily discernable at around 6 mA in Fig. 7 for the second curve from top; but these start to appear at current values as low as 1 mA. These small peaks and valleys appeared consistently at the same values of input current, most certainly after leaving the experimental setup alone for hours or even days, and often after re-alignment. These were observed only for butt-coupled ($z = 0$ μm) condition. We investigated these with spectral analyses using an Acton Research 0.75 m spectrometer with diode-array output as in an optical multichannel analyzer (OMA). With a 1200 grooves per mm grating each pixel separation corresponded to 0.012 nm of spectral resolution.

For the NA = 1.00 FIG, at 2.730 mA (a valley position in the L-I curve) two spectral lines were observed at 848.75 nm (small in magnitude) and 849.77 nm (large in magnitude). Upon changing the current to 2.795 mA (a peak position in the L-I curve), these two changed to 848.78 nm (small in magnitude) and 849.83 nm (large in magnitude). We also observed switching of the two peaks – the lower wavelength peak became larger in magnitude than the higher wavelength peak. Moreover, a gradual increase in wavelength with increased current, consistent with VCSEL cavity length increase, can be seen. We believe that the FIG with its core, clad and ASG acts as a spatial filter which, together with optical feedback, causes these miniature peaks and valleys to appear. The peaks and valleys could be due as much to the changing wavelength as to the switching of magnitude between the two wavelengths. Although not experimentally verified, the appearance of two wavelengths, and their occasional switching, are consistent with the creation of first order transverse modes, observed in this work in the far-fields. The issue of spatial filtering was further exemplified when we conducted L-I-V tests at the end of the multimode fiber used to carry the light from the output facet of the FIG to the input aperture of the spectrometer. The L-I curves showed significantly enhanced peak-and-valley ratios, often with as much as 75% variation, at the end of the multimode fiber. This can be qualitatively explained with the multimode fiber, with its own acceptance angle (numerical aperture), filtering the FIG output spatially according the angular (and spatial) distribution of the modes carried by the FIG. Such variations have been observed elsewhere [40]. In one example of FIG link [34] the output of the FIG is connected to multiple multimode fibers using microlenses that are separately taken to their respective destinations. In such link-solutions modal spatial filtering by the FIG, all the intermediate lenses, and the final multimode fiber, should be relevant issues.

CONCLUSION

In conclusion, we accomplished the following. (i) We qualitatively described the many possible feedback sources for the VCSEL and observed some feedback effects. (ii) We experimentally studied the optical terminal characteristics and observed some of the roles played by the separate transmission media that constitute the FIG. (iii) We carried out initial simulations in attempting to understand cladding mode propagation. (iv) We observed the influence of feedback effects upon the spectra and spectral influence upon transmission properties, including spatial filtering by the transmission media. The FIG appears to be an interesting, albeit a formidable, medium for full understanding – more work is required. Future work on VCSEL-FIG links would most likely progress along two parallel paths. One, exploration and establishment of designable parameter for not only the FIG-link as a whole, but also the designable features and variabilities in the process of manufacturing FIGs. The other, cost-, weight- and system-conscious implementation analyses for the applicability of FIGs into link systems that duly compete, and win, against the traditional fiber-ribbon and individually-aligned-fiber-based parallel links currently available in the market.

The authors thank M. Warren and S. Kemme for technical discussions and constructive criticisms. The work was supported by internal funds at Sandia National Laboratories, Albuquerque, New Mexico, USA and Linköping University, Norrköping, Sweden. Sandia is a multiprogram laboratory operated by Sandia Corporation, a Lockheed Martin Company, for the United States Department of Energy under Contract DE-AC04-94AL85000.

REFERENCES

1. N. Savage and S.K. Moore, "Linking with light." IEEE Spectrum Magazine, August 2002, pp. 32-36.
2. Xanoptix, Inc., http://www.xanoptix.com.
3. Y-M Wong, et.al., (AT&T), "Technology development of a high-density 32-channel 16-Gb/s optical data link for optical interconnection applications for the OptoElectronic Technology Consortium (OETC)." IEEE J Lightwave Technol. 13 (1995) 995-1016.
4. Y.M. Wong, et.al.,(OETC – Lucent, IBM & Honeywell), "OptoElectronic Technology Consortium (OETC) parallel optical data link: components, system applications, and simulation tools." IEEE – 46th Electronics Components and Technology Conference – ECTC (1996) pp. 269-278.
5. J. Bristow, J. Lehman, M. Hibbs-Brenner, Y. Liu, T. Marta, W. Goldberg, E. Kalweit, C. Sullivan, S. Mukherjee, R. Walterson, D. Singh, B. Tyrone and T. Ireland, (OETC - Honeywell & GE), "Packaged AlGaAs waveguide modulator array at 830 nm wavelength." IEEE J Lightwave Technol. Vol. 13 (1995) 1041-1056.
6. W.S. Ishak, K.H. Hahn, B.L. Booth, C. Mueller, A.A.J. Levi and R. Craig, (HP), "Optical interconnects – The POLO approach", Proc. SPIE vol. 2400 (Optical Interconnects III) (1995) pp. 214-221.
7. K. Hahn, et.al., (HP), "Gigabytes/s data communications with the POLO parallel optical link." IEEE – 46th Electronics Components and Technology Conference – ECTC (1996) pp. 301-307.
8. P. Rosenberg, et.al., (HP), "The PONI-1 parallel optical link." IEEE – 49th Electronics Components and Technology Conference – ECTC (1999) pp. 763-769.
9. M. Lebby, C.A. Gaw, W. Jiang, P.A. Kiely, C.L. Shieh, P.R. Claisse, J. Ramadani, D.H. Hartman, D.B. Scwartz and J. Grula, (Motorola – OPTOBUS), "Use of VCSEL arrays for parallel optical interconnects." Proc. SPIE vol. 2683 (Fabrication, Testing and Reliability of Semiconductor Laser) (1996) pp. 81-91.
10. M. Lebby, et.al., (Motorola - OPTOBUS), "Characteristics of VCSEL arrays for parallel optical interconnects." IEEE – 46th Electronics Components and Technology Conference – ECTC (1996) pp. 279-291.
11. L.J. Norton, et.al., (Motorola) "OPTOBUS™ I: a production parallel fiber optical interconnect." IEEE – 47th Electronics Components and Technology Conference – ECTC (1997) pp. 0204-0209.
12. J. Ai, et.al., (NEC & Motorola), "100 x 100 optoelectronic cross-connect interconnects using OPTOBUS®." IEEE J Lightwave Technol. 17 (1999) 765-770.
13. J.D. Crow, et.al., (IBM), "The Jitney parallel optical interconnect." IEEE – 46th Electronics Components and Technology Conference – ECTC (1996) pp. 292-300.
14. M.S. Cohen, et.al., (IBM), "Packaging aspects of the Jitney parallel optical interconnect." IEEE – 48th Electronics Components and Technology Conference – ECTC (1998) pp. 1206-1215.
15. F. Freitag, et.al., (IBM), "Packaging aspects of the Litebus ™ parallel optoelectronic module." IEEE – 50th Electronics Components and Technology Conference – ECTC (2000) pp. 1259-1265.
16. S. Swirhun, et.al., (Vixel Corp.), "The P-VixeLink™ multichannel optical interconnect." IEEE – 46th Electronics Components and Technology Conference – ECTC (1996) pp. 316-320.
17. H. Karstensen, et.al., (Siemens), "Parallel optical link (PAROLI) for multichannel gigabit rate interconnections." IEEE – 48th Electronics Components and Technology Conference – ECTC (1998) pp. 747-754.
18. T. Nagahori, et.al.,(NEC), "1-Gbyte/s array transmitter and receiver modules for low-cost optical fiber interconnection." IEEE – 46th Electronics Components and Technology Conference – ECTC (1996) pp. 255-258.
19. N. Tanaka, et.al., (NTT), "3.5 Gb/s x 4 ch optical interconnection module for ATM switching system." IEEE – 47th Electronics Components and Technology Conference – ECTC (1997) pp. 0210-0216.
20. K. Katsura, et.al., (NTT), "Packaging for a 40-channel parallel optical interconnection module with an over 25-Gb/s throughput." IEEE – 48th Electronics Components and Technology Conference – ECTC (1998) pp. 755-761.
21. A. Miura, et.al., (Hitachi), "Reliable, compact, CMOS interface, 200 Mbit/s x 12-channel optical interconnects using single-mode fiber arrays." IEEE – 47th Electronics Components and Technology Conference – ECTC (1997) pp. 0225-0230.
22. Stratos Lightwave, http://www.stratoslightwave.com/
23. L.J. Sargent, et.al., "Simple technique for bandwidth enhancement of multimode fiber links using controlled spatial emission from vertical cavity surface emitting lasers." Electron. Letts. 34 (1998) 2038-2039.
24. R. Dandliker, et.al., "How modal noise in multimode fibers depends on source spectrum and fiber dispersion." IEEE J Lightwave Technol. 3 (1985) 7-12.
25. J. Jahns, et.al. "Diffractive optics and micro-optics: introduction to the feature issue." Applied Optics IP36 (1997) 4633, and papers therein.

26. R.F. Carson, et.al., (Sandia), "Low-power modular parallel photonic data links." IEEE – 46th Electronics Components and Technology Conference – ECTC (1996) pp. 321-326.
27. (a) Y. Liu, et.al., "Smart-pixel array technology for free-space optical interconnects." Proc. IEEE 88 (2000) 764-768. (b) M.W. Haney, et.al., "Description and evaluation of the 'FAST-Net' smart pixel-based optical interconnection prototype." Proc. IEEE 88 (2000) 816-828.
28. F. Lacroix, et.al., "Experimental and numerical analyses of misalignment tolerances in free-space optical interconnects." Applied Optics IP39 (2000) 704-713.
29. D.F. Brosseau, et.al., "Design, implementation, and characterization of an kinematically aligned, cascaded spot-array generator for a modular-based free-space optical interconnect." Applied Optics IP39 (2000) 733-745.
30. Y. Li, et.al., "Fiber-image-guide-based bit-parallel optical interconnects." Applied Optics IP35 (1996) 6920-6833.
31. H. Kosaka, M. Kajita, Y. Li and Y. Sugimoto, "A two-dimensional optical parallel transmission using a vertical-cavity surface-emitting laser array module and an image fiber," IEEE Photonics Technol. Lett. 9 (1997) 253-255.
32. Y. Li, et.al., "Distributed crossbar interconnects with vertical-cavity surface-emitting laser – angle multiplexing and fiber image guides." Applied Optics IP37 (1998) 254-263.
33. H.F. Ghaemi, et.al., "Fiber image guide with subwavelength resolution." Appl. Phys. Letts. 72 (1998) 1137-1139.
34. S. Kawai, et.al., "Skew-free optical interconnections using fiber image guides for petabit-per-second computer networks." Jpn. J. Appl. Phys. 37 (1998) 3754-3758.
35. T. Maj, A. Kirk, D. Plant, J. Ahadian, C. Fonstad, K. Lear, K. Tatah, M. Robinson and J.A. Trezza, "Interconnection of a 2D VCSEL array to a receiver array via a fiber image guide," Optics in Computing OC-1999, Abstracts, Snowmass, Aspen, CO, USA, April 13-16, 1999, paper PD2-1.
36. T. Maj, et.al., "Interconnection of a two-dimensional array of vertical cavity surface emitting lasers to a receiver array by means of a fiber image guide." Applied Optics IP39 (2000) 683-689.
37. D.M. Chiarulli, et.al., "Optoelectronic multi-chip modules based on imaging fiber bundle structures." SPIE Vol. 4089 (Optice in Computing 2000) (2000) pp. 80-85.
38. D.M. Chiarulli, et.al., "Demonstration of a multichannel optical interconnection by use of imaging fiber bundles but coupled to optoelectronic circuits." Applied Optics IP39 (2000) 698-703.
39. (a) R.K. Kostuk and J. Carriere, "Interconnect signal channel density of fiber imaging guides." IEEE Conf. Proceedings on Parallel Interconnects (PI'99) (Previously MPPOI or Massively Parallel Processing using Optical Interconnects) (1999) pp.157-164. (b) R.K. Kostuk and J. Carriere, "Interfaces to fiber image guide bundles for high density optical interconnects." SPIE Vol. 4089 (Optics in Computing 2000) (2000) pp. 987-992.
40. R.K. Kostuk and J. Carriere, "Interconnect characteristics of fiber image guides." Applied Optics 40 (2001) 2428-2434.
41. S.D. Mukherjee, K.M. Geib, K.D. Choquette and M. Robinson, "Input Coupling Measurements for Parallel Optical Interconnects using Imaging Fiber Bundles and VCSEL Arrays," Conference Digest 2000 CLEO-Europe (Conference on Lasers and Electro-Optics, Europe), 10-15 September 2000, Nice, France, paper CWJ2, pp. 267.
42. K.D. Choquette, V.M. Hietala, K.M. Geib, S.D. Mukherjee, and A.A. Allerman. "Hybrid Integrated VCSEL and Driver Arrays for Optical Interconnects." LEOS Annual Meeting, Optical Interconnects and Processing Systems, Puerto Rico, 13-16 November 2000.
43. S.D. Mukherjee, K.D. Choquette, K.M. Geib, G.R. Hadley, T.R. Carter, A.J. Fischer, C.T. Sullivan and K. Tatah, "Characterization of Crosstalk Sources in Massively Parallel Datalinks Using VCSEL Arrays and Fiber Image Guides" Optics in Computing OC-2001 (OSA and SPIE), January 9-11 2001, Lake Tahoe, Nevada, USA.
44. S.A. Kemme, et.al., "Dynamic coherence measurements of index- and gain-guided VCSELs." IEEE Photonics Technol. Letts. 9 (1997) 554-556.
45. K. Tatah, et.al., "Performance measurements of fiber image guides and fiber bundles in optical interconnect applications." Optic in Computing – OC'99, Technical Digest, OSA, (1999) pp. 115-117.
46. K.D. Choquette, K.M. Geib, A.A. Allerman, D.K. Serkland, J.A. Nevers and J.J. Hindi, paper STuA3-1, Technical Digest, Spatial Modulators and Integrated Optoelectronic Arrays, Snowmass, Aspen, CO, USA, April 12-14, 1999. ISBN 1-55752-601-X (1999) pp. 59-61.
47. S.A. Kemme and R.K. Kostuk, "Scalar diffraction theory approach to estimating multimode-waveguide field-amplitude mode distribution." Applied Optics 37 (1998) 4399-4404.
48. G.R. Hadley, "Index-guided arrays with a large index step." Optics Letts. 14 (1989) 308-310.
49. G.R. Hadley, "Two-dimensional waveguide modeling of leaky mode arrays." 14 (1989) 859-861.
50. G.R. Hadley, "Two-dimensional coupled-mode theory for modeling leaky-mode arrays." Optics Letts. 15 (1990) 27-29.

Two Dimensional Guided Wave Optical Interconnect

Hai Ping Chen[1], Kent D. Choquette[1], Vincent M. Hietala[2], and Kent M. Geib[3]

[1]Electrical and Computer Engineering Dept.
University of Illinois
Urbana-Champaign

[2] Quellan, Inc.
Address??

[3] Sandia National Laboratory
Albuquerque, NM

Abstract:

The characterization of a 2-dimensional optical interconnect system composed of arrays of vertical cavity surface-emitting lasers, drivers, and photoreceivers is reported. The light outputs are spatially transmitted employing a butt-coupled fiber image guide. We separately examine the hybridly integrated driver and VCSEL chips which comprise the transmitter array, as well as the receivers composed of monolithically integrated photodetectors and amplifying circuits. Separately, a single channel of the transmitter component exceeded 1.25 Gbits/s while the receiver component reached 155 Mbits/s. A single channel of the overall system employing the transmitter array, fiber image guide, and receiver array operated at 80 Mbits/s.

I. INTRODUCTION

With the looming bandwidth bottleneck of contemporary electrical interconnects, high-density optical parallel interconnects will be needed to meet the increasing appetite of next-generation computing applications. An optical interconnect is a viable solution because of its innate high bandwidth per optical path, low latency, electrical isolation and immunization from electromagnetic interference (EMI), and immunity to frequency dependent loss or crosstalk [1]. Currently, commercial optical fiber data links are dominated by a single fiber or fiber ribbon cables, which are suitable for applications that require tens of channels. However, computer bus widths are continuously increasing, and an interconnect that requires 128 channels or more will be required in the future [2]. Moreover, because of their linear nature, fiber ribbons do not scale well, while two-dimensional (2-D) approaches may be a feasible alternative. Short-distance interconnections are very cost sensitive and tend to be dominated by packaging costs. Using a guided wave approach to link 2-dimensional vertical cavity surface-emitting laser (VCSEL) transmitters with receiver arrays can potentially reduce the packaging costs on a per channel basis. Thus, optical spatial division multiplexing (SDM) may find application in switching and computing environments.

In this paper, we investigate the performance of an optical interconnect system comprising of an 8x8 VCSEL array transmitting light through a fiber image guide (FIG) onto a symmetric photoreceiver array. First, an overview of SDM and the characteristics of the fiber image guide used in this experiment are described in Section II. Next, the design and characteristics of the transmitter and receiver array are explained in sections III and IV, respectively. In section V, the setup and experimental result of the overall optical interconnect system are described.

II. SPATIAL DIVISION MULTIPLEXING

Optical SDM offers a viable solution to short-distance links such as chip-to-chip and board-to-board interconnections. A simple SDM link can be formed in free space by using a lens or lenslet array to image an array of lasers onto an array of photodetectors. However, a lens-based system requires critical alignment of each element of the transmitter array to each element of the photoreceiver array. An alternative guided wave approach is to use a fiber image guide (FIG) as the optical channel between the transmitter and receiver [2, 3]. This approach allows a large number of channels to be transmitted, where the alignment is fixed at the ends of the bundle but in between the interconnect can be flexible [2, 4]. SDM can offer simplified interface electronics due to lower modulation rate per channel as compared to time division multiplexing approaches, and it offers simplified optics as compared to wavelength division multiplexing approaches. However, SDM creates demands on integration complexity, power dissipation, channel-to-channel skew, signal uniformity, and crosstalk due to its many parallel channels.

The fiber image guide used in this experiment is manufactured by Schott Fiber and has a numerical aperture (NA) of 0.55. This NA was chosen because it yields low crosstalk between channels due to less power in cladding modes and possible spatial filtering in the air-separated flexible region [4]. The FIG is formed from 15379 fiberlets embedded in acid soluble glass, where each fiberlet diameter is 9.1 μm and the pitch is 13.5 μm .The FIG is 25 cm long and has two rigid end facets and a flexible midsection for easy maneuverability. When optical alignment is achieved at each facet, an optical light signal can be spatially multiplexed down the FIG. Shown in Fig. 1 is an example image of the FIG butt-coupled to the transmitter array (note the light spot in Fig. 1 appears large due to saturation of the camera).

III. VCSEL/DRIVER ARRAY

A top view of transmitter component is shown in Fig. 2, where the center chip is an 8 x 8 selectively oxidized VCSEL array, operating at 850 nm wavelength where the lasers are on 250-μm pitch. Surrounding the VCSEL array are 4 metal-semiconductor-field-effect-transistors (MESFETs) driver chips each containing 16 channels. Since VCSELs have low operating current and voltage, they can be directly driven by silicon complementary metal-oxide-silicon (CMOS). However, driving them with GaAs MESFETs driver circuits can potentially achieve even higher modulation speed, in excess of 1 Gbit/s [5]. Each driver is comprised of two current sources and a differential switch [6]. The low current source was designed to provide a tunable bias current of up to 3.5 mA, and the high current source can provide a modulation current of up to 10 mA. These relatively high current values permit high light output VCSEL designs, which in turn can enable lower power photoreceiver designs. The differential switch is made from large depletion-mode MESFETs, where the gate size is optimized to maximize small-signal gain while maintaining a reasonable switching speed.

A plot of the VCSEL light output power versus the switch input voltage with incremental modulation current is shown in Fig. 3. In Fig. 3 the bias current is set to zero, while the VCSEL threshold current is 2.7 mA; thus lasing output is achieved with a modulation current > 3mA. Gunning transceiver logic (GTL) is expected for the input to the driver circuit, where a logic "low" is below 0.4 V and a logic "high" is above 1.2 V.

When the transmitter array was tested separately using a butt-coupled fiber to one VCSEL channel and a commercial high-speed detector on the other end, a modulation speed in excess of 1.25 Gbits/s was achieved as shown in Fig. 4. The rise and fall times were measured to

be 31 ps and 219 ps, respectively, with a bias current of 1 mA and a 9 mA modulation current. The bit-error-rate for the driver/VCSEL component was measured to be 2.496×10^{-10}.

IV. RECEIVER ARRAY

The receiver array consists of an 8 x 8 metal-semiconductor-metal (MSM) photodetector array monolithically integrated with amplifier circuitry around the periphery [6]. The MSM detectors were fabricated monolithically with MESFET circuitry and are 100 μm square and placed on a 250-μm pitch to ease alignment as well as to spatially match the transmitter array, respectively. The detector was fabricated directly on the semi-insulating (SI) GaAs wafer, which presents less than an ideal MSM detector configuration due to slow hole transport in GaAs and the resulting suboptimal photo carrier collection, but is sufficient for speeds up to 1 Gbit/s [6]. The monolithic MSM detector used here have a -3dB bandwidth over 2.5 GHz [6].

The primary design considerations for the receiver circuits were speed, power dissipation, and size, with low power dissipation and small size being serious constraints because of the large number of channels. The circuit characteristics can be found in reference [6]. The receiver array was also tested separately using a commercial VCSEL as the optical source. The maximum speed obtained was limited to 155.52 Mbits/s because of impedance mismatch and the resulting signal reflection at the channel output of the photoreceiver.

V. OPTICAL INTERCONNECT SYSTEM

A block diagram of the experimental setup for the overall interconnect system is detailed in Fig. 5. The modulated input signal is fed into one channel of the transmitter array. The transmitter and receiver array is butt-coupled to a fiber image guide. To achieve alignment for a

single channel, the transmitter and receiver packages were mounted onto translation stages, while the ends of the FIG were fixed. Alignment of multiple channels will also require control of the angular position of each component. The output from the receiver array is then daisy-chained to an external load circuit and an oscilloscope. The external circuit is necessary for the receiver array to produce correct output voltages and has an inductor included to prevent the RF and DC signals from coupling to each other. An eye diagram of this optical interconnection system is shown in Fig. 6 with a maximum speed of 80 Mbits/s.

VI. CONCLUSION

In this paper, we report the characteristics of a 2-dimensional optical interconnect system comprised of a fiber image guide and 8x8 VCSEL and photodetector array. This system has been designed for a computer databus application, such as linking a computer processor to memory. An overall modulation speed of 80 Mbits/s was achieved for a single channel of the system, although faster operation speeds were achieved by the individual components. Presently, the limiting factor for the system is impedance mismatch and signal reflection at the output of the photodetector array. To overcome these electrical limitations and to enable optical alignment of multiple channels, more packaging efforts appropriate for a specific application will be necessary. Nevertheless, given the separate capabilities of VCSEL devices and MESFET circuits, much higher modulation rates are feasible enabling extremely high aggregate data rates for future optical switching and computing applications.

Figure captions

Figure 1. View of the 2-dimensional VCSEL array in a fiber image guide with one laser operating.

Figure 2. Top view of the hybridly integrated transmitter array with a VCSEL arrays surrounded by four driver chips.

Figure 3. Light output for one VCSEL channel as switching voltage is varied for different modulation currents.

Figure 4. Eye diagram of transmitter array at 1.25 Gbits/s with $2^{31}-1$ length pseudo random bit stream.

Figure 5. Block diagram of experimental setup to characterize the optical interconnect system.

Figure 6. Eye diagram of a single channel of the optical interconnect system with maximum speed of 80 Mbits/s.

Fig. 1

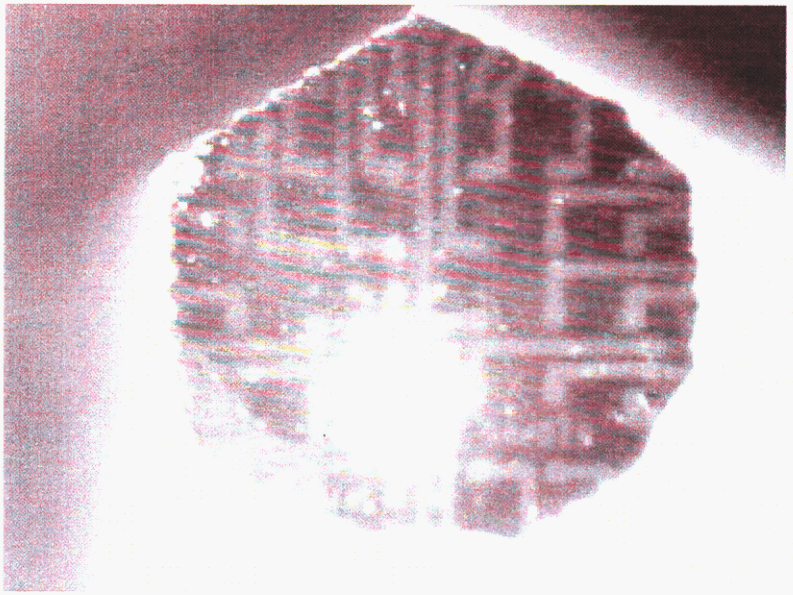

Fig. 2

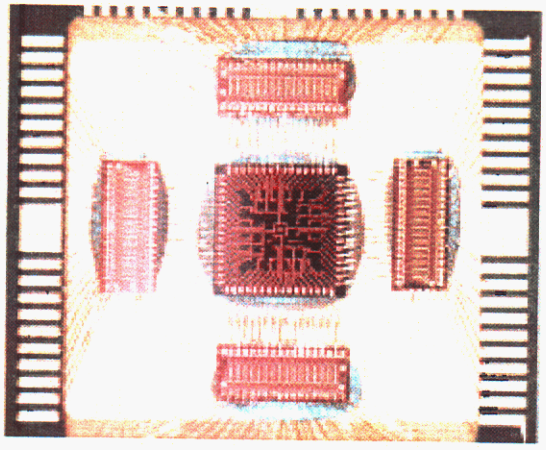

Fig. 3

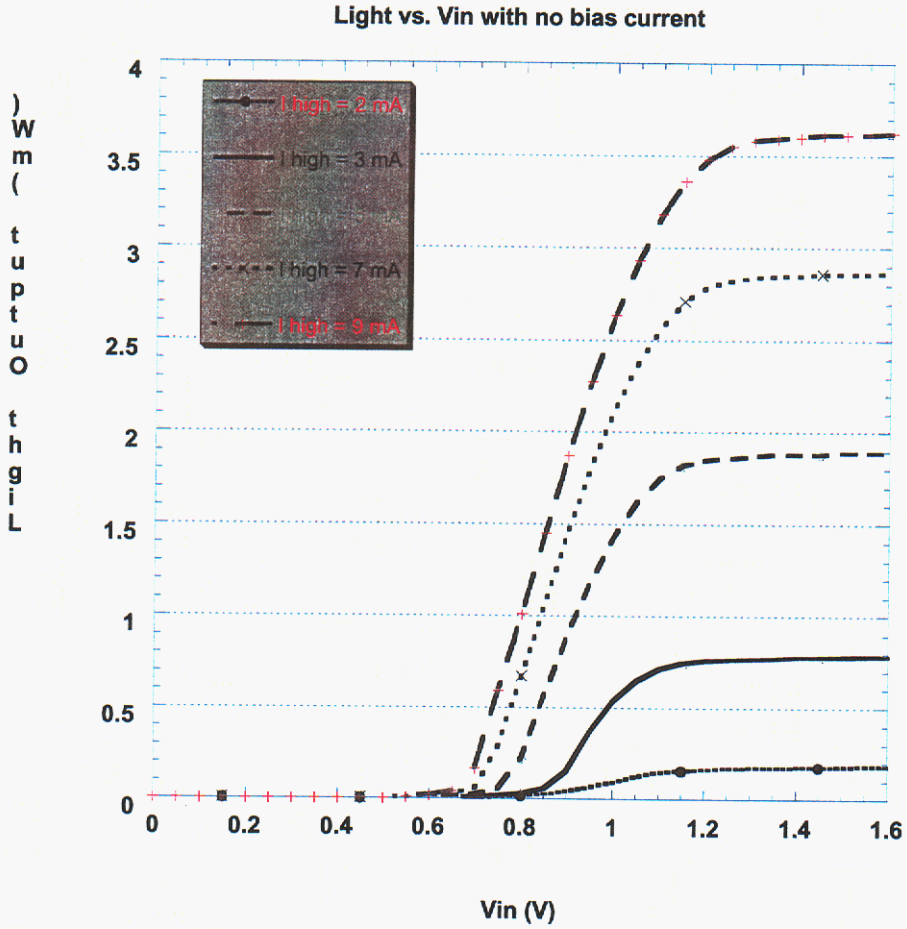
Light vs. Vin with no bias current
Light Output (mW)
I high = 2 mA
I high = 3 mA
I high = 7 mA
I high = 9 mA
0
0.5
1
1.5
2
2.5
3
3.5
4
0
0.2
0.4
0.6
0.8
1
1.2
1.4
1.6
Vin (V)

Fig. 4

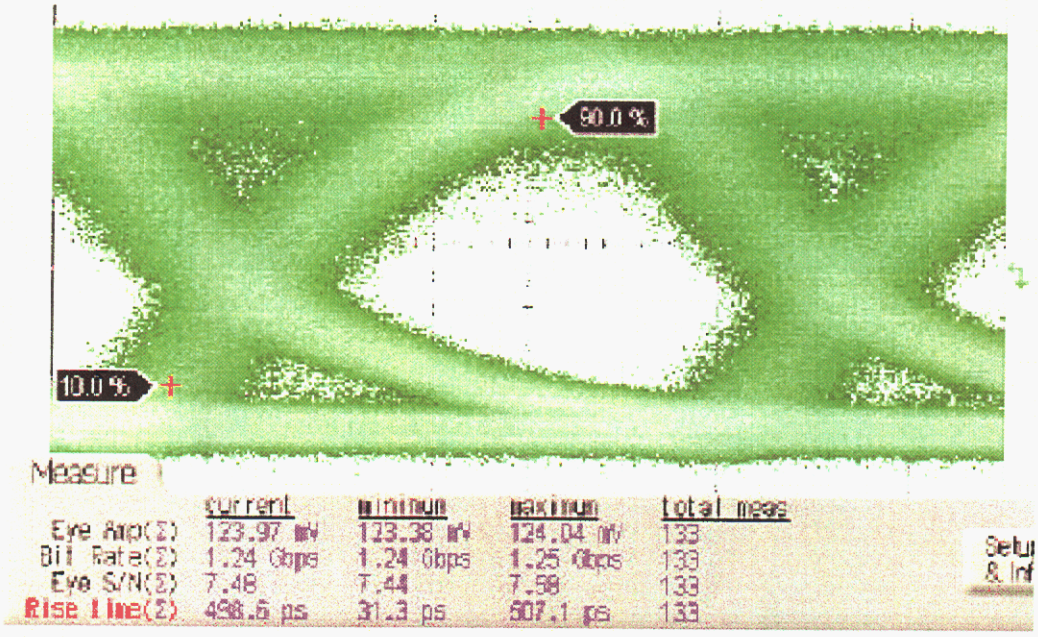
90.0 %
10.0 %
Measure
current
minimum
maximum
total meas
Eye Amp(Σ) 123.97 mV 123.38 mV 124.04 mV 133
Bit Rate(Σ) 1.24 Gbps 1.24 Gbps 1.25 Gbps 133
Eye S/N(Σ) 7.48 7.44 7.50 133
Rise Time(Σ) 498.6 ps 314.3 ps 807.1 ps 133

Fig. 5

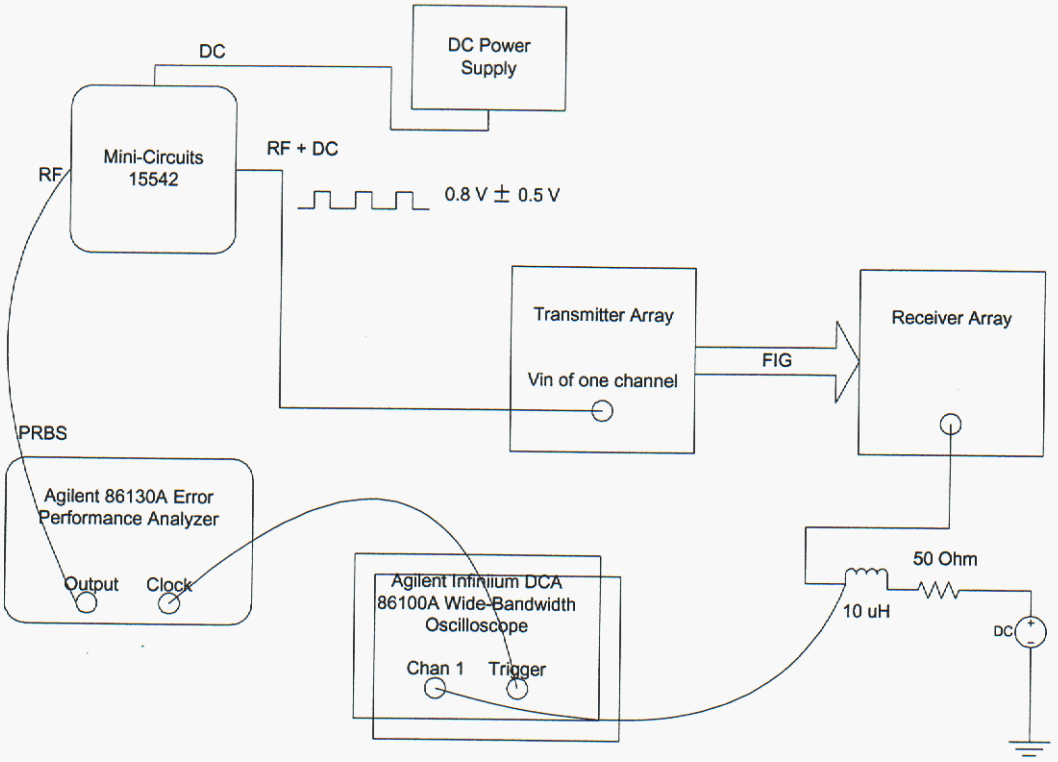
DC
DC Power Supply
Mini-Circuits 15542
RF
RF + DC
0.8 V ± 0.5 V
Transmitter Array
Vin of one channel
FIG
Receiver Array
PRBS
Agilent 86130A Error Performance Analyzer
Output
Clock
Agilent Infiniium DCA 86100A Wide-Bandwidth Oscilloscope
Chan 1
Trigger
50 Ohm
10 uH
DC

Fig. 6

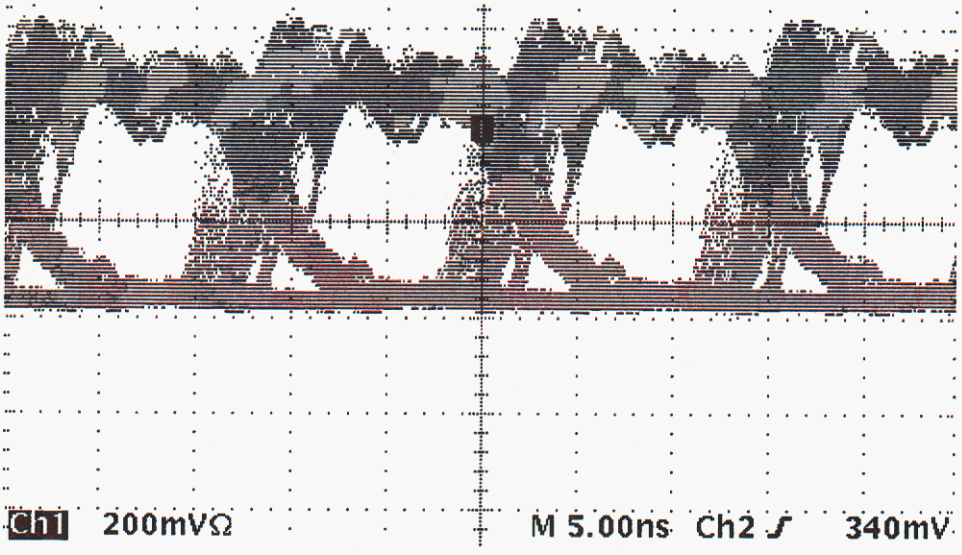

Reference

[1] K. Iga, "Surfacing-emitting laser—Its birth and generation of new optoelectronic fields," *IEEE Journal on Selected Topics in Quantum Electronics,* vol. 6, no. 6, pp. 1201 – 1215, 2000.

[2] T. Maj et al., "Interconnection of a two-dimensional array of vertical cavity surface-emitting lasers to a receiver array by means of a fiber image guide," *Applied Optics,* vol. 39, no. 5, pp. 683-689, 2000.

[3] Y. Li, T. Wang, H. Kosaka, S. Kawai, and K. Kasahara, "Fiber-image-guide-based bit-parallel optical interconnects," *Applied Optics*, vol. 35, no. 35, pp. 6920-6933, 1996.

[4] S. D. Mukherjee, K D. Choquette, K. M. Geib, G. R. Hadley, T. R. Carter, A. J. Fischer, C. T. Sullivan, and K. Tatah, "Characterization of crosstalk sources in massively parallel datalinks using VCSEL arrays and fiber image guides," in *SPIE, IEEE, OSA Proc. Opt. Computing,* Lake Tahoe, NV, Jan. 9-11, 2001, OC-2001.

[5] K. D. Choquette, V. M. Hietala, K. M. Geib, S. Mukherjee, and A. A. Allerman, "High performance vertical cavity laser, driver, and receiver arrays for optical interconnects," in *Lasers and Electro-Optics Society 2000 Annual Meeting*, vol. 2, 2000, pp. 424-425.

[6] V. M. Hietala, "Two-dimensional 8 x 8 photoreceiver array and VCSEL drivers for high-throughput optical data links," *IEEE Journal of Solid-State Circuits,"* vol.36, no. 9, pp. 1292-1302, 2001.

Biographies

Hai Ping Chen was born in Canton, China, in 1978. He received the Bachelor of Science in electrical engineering with high honor from the University of California at Davis in 2000. He received his Master of Science degree in Electrical and Computer Engineering from the University of Illinois at Urbana-Champaign in 2002. His research involved the use of vertical cavity surface-emitting lasers for optical interconnect and switching applications.

Kent D. Choquette received B.S. degrees in engineering physics and applied mathematics from the University of Colorado-Boulder in 1984 and M.S. and Ph.D. degrees in materials science from the University of Wisconsin-Madison in 1985 and 1990, respectively. From 1990 through 1992 he held a postdoctoral appointment at AT&T Bell Laboratories at Murray Hill, NJ and in 1993 he joined Sandia National Laboratories in Albuquerque, NM. He became a Professor in the Electrical and Computer Engineering Dept. at the University of Illinois at Urbana-Champaign in 2000. His research centers around the design, fabrication and characterization of vertical-cavity surface emitting lasers (VCSELs), photonic crystals, and other optoelectronic devices. His research interests include novel fabrication technologies, hybrid integration techniques, and nano-fabrication processes. From 2000-2002 he was a IEEE/LEOS Distinguished Lecturer. Professor Choquette has authored over 100 publications and 2 book chapters, and has presented numerous invited talks and tutorials on VCSELs. He is an Associate Editor of the *Journal of Quantum Electronics*, a Senior member of IEEE/Lasers and Electro-Optics Society, and a member of the Optical Society of America.

Appendix D

Monolithic Integration of Vertical-Cavity Surface-Emitting Lasers and Wavelength-Shifted Resonant-Cavity Photodetectors, D.K. Serkland, K.M. Geib, A.A. Allerman, and T.W. Hargett, in IEEE LEOS 2001 Annual Meeting: 11/12/01 thru 11/15/01, La Jolla, CA (2001).

Fabrication and Performance of Large (64x64) Arrays of Integrated VCSELs and Detectors, K.M. Geib, K.D. Choquette, D.K. Serkland, A.A. Allerman, and T.W. Hargett, in Vertical Cavity Emitting Lasers Symposium SPIE Photonics West 2002: 1/20/02 thru 1/25/02, San Jose, CA (2002).

Fabrication and Performance of Two-Dimensional Matrix Addressable Arrays of Integrated Vertical-Cavity Lasers and Resonant Cavity Photodetectors, K.M. Geib, K.D. Choquette, D.K. Serkland, A.A. Allerman, and T.W. Hargett, IEEE Journal of Selected Topics in Quantum Electronics, Vol. 8, No. 4, July/Aug, pp. 943-947 (2002).

High Density Interleaved VCSEL-RCPD Arrays for Optical Information Processing, K.M. Geib, D.K. Serkland, A.A. Allerman, T.W. Hargett, and K.D. Choquette in VCSELs and Optical Interconnects SPIE Photonics Fabrication Europe 2002: 10/28/02 thru 11/1/02, Brugge, Belgium (2002).

Monolithic Integration of Vertical-Cavity Surface-Emitting Lasers and Wavelength-Shifted Resonant-Cavity Photodetectors

Darwin K. Serkland, K. M. Geib, A. A. Allerman, and T. W. Hargett
Sandia National Laboratories, PO Box 5800, MS 0603, Albuquerque, NM 87185
Tel. 505-844-5355, Fax. 505-844-8985, E-mail: dkserkl@sandia.gov

Monolithically integrated photodetectors and vertical-cavity surface-emitting lasers (VCSELs) are desirable for many applications. The resonant-cavity photodetector (RCPD) is a natural choice for integration with VCSELs, since the RCPD can be fabricated using the same epitaxial layers as the VCSEL simply by etching away several periods of the top distributed Bragg reflector (DBR).[1] Moreover, the RCPD acts as a filter that accepts light from adjacent VCSELs and rejects signals at other wavelengths.[2] However, as a VCSEL heats up with increasing drive current its wavelength red-shifts away from the center of the RCPD passband, as shown in Fig. 1(a).[3] In this paper we report on a novel epitaxial design that red-shifts the RCPD resonance relative to the cold-cavity VCSEL wavelength such that as the laser heats with increasing drive current its wavelength shifts into resonance with the RCPD.

Figure 2 schematically shows how our epitaxial structure differs from that of a standard VCSEL. Rather than having all layers in the top DBR of the VCSEL be exactly a quarter wavelength in thickness, we make the high-index top layer of the RCPD slightly thicker than a quarter wavelength, which causes a corresponding red-shift of the RCPD wavelength by up to a few nanometers. In order to compensate for this thicker top RCPD layer, we make the next layer above it (a low-index layer) thinner than a quarter wavelength, such that the total optical thickness of these two modified layers adds to equal a half wavelength. Hence, the VCSEL wavelength is the same as it would be if the two layers were not modified from their usual quarter-wavelength thickness.

Figure 3(a) shows light-versus-current (LI) data from a 4-μm-square-oxide-aperture VCSEL that indicate the range of operating currents from threshold (1.1 mA) to thermal rollover (8 mA). Figure 3(b) shows the responsivity of the RCPD versus wavelength and the fundamental-transverse-mode spectra of the 4-μm-aperture VCSEL at four operating currents between threshold and thermal rollover. Notice that the VCSEL wavelength shifts from the blue to the red side of the RCPD resonance as it is driven from threshold up to thermal rollover. Hence,

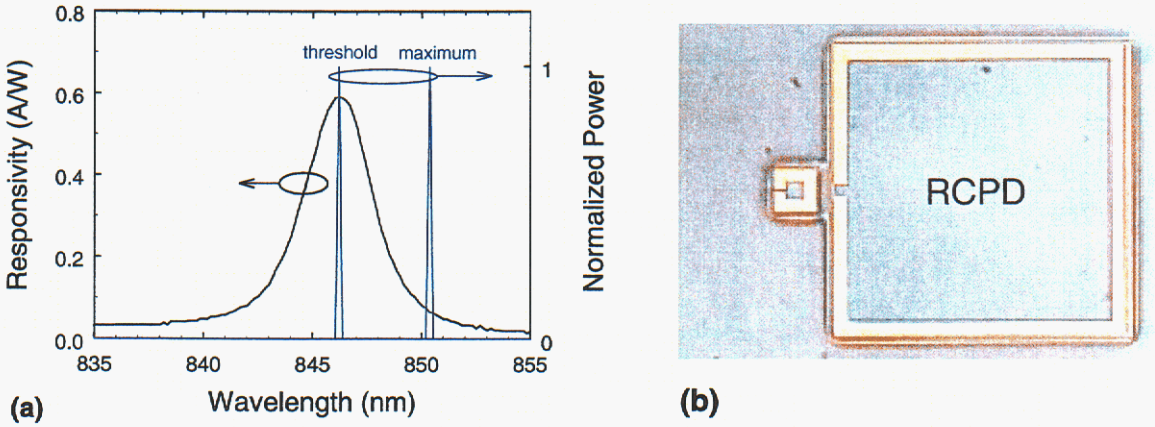

Fig. 1. (a) Responsivity of an RCPD and spectra of a VCSEL obtained with a standard VCSEL/RCPD design. At threshold the VCSEL wavelength coincides with the RCPD resonance, but at maximum output power the VCSEL wavelength is red-shifted away from the RCPD resonance. (b) Photograph of a 30-μm VCSEL mesa next to a 225-μm RCPD mesa.

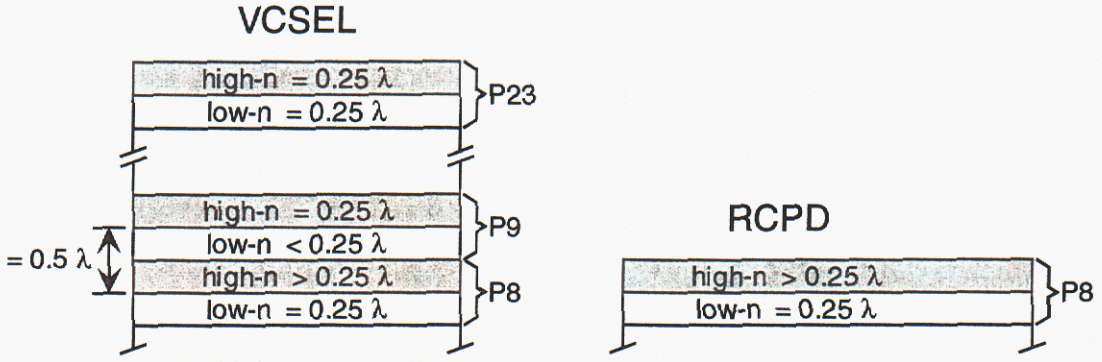

Fig. 2. Schematic cross section of the wavelength-shifted RCPD/VCSEL structure. The 8th, 9th, and 23rd periods of the top DBR are illustrated.

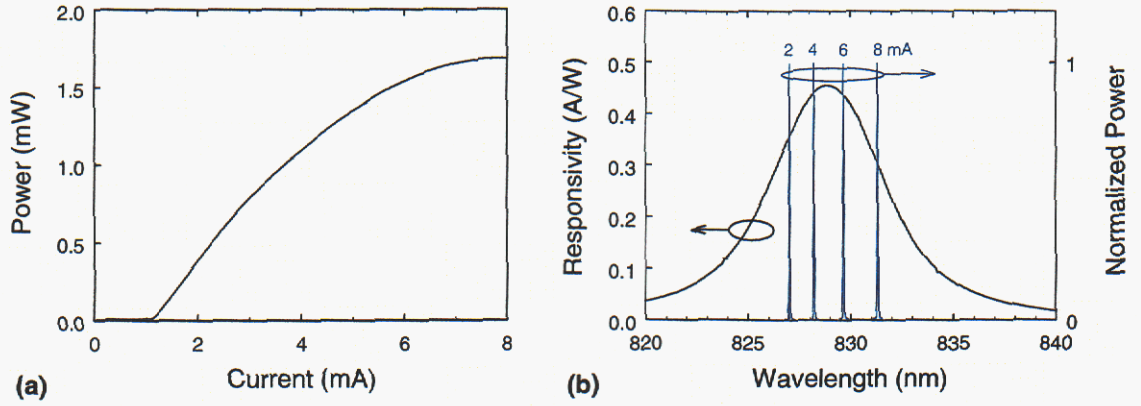

Fig. 3. (a) Light-versus-current data from a 4-μm-aperture VCSEL. (b) Normalized fundamental-mode spectra of the same VCSEL at drive currents of 2, 4, 6, and 8 mA compared with the responsivity data of the adjacent wavelength-shifted RCPD.

over the full range of operating currents, the alignment between the VCSEL wavelength and the RCPD resonance is improved as compared to the typical alignment shown in Fig. 1. For the devices reported here, the top RCPD layer ($Al_{0.16}Ga_{0.84}As$) is grown 20 nm thicker than a quarter wavelength, which is theoretically expected to red-shift the RCPD wavelength by 2 nm from the VCSEL wavelength.

In summary, we have demonstrated monolithically integrated RCPDs and VCSELs using a novel epitaxial design that red-shifts the RCPD wavelength with respect to the cold-cavity VCSEL wavelength. The advantage of this design is that at typical operating currents the VCSEL wavelength is better aligned with the RCPD resonance than with a typical VCSEL/RCPD structure.

Sandia is a multiprogram laboratory operated by Sandia Corporation for the United States Department of Energy under contract No. DE-AC04-94AL85000.

References:

[1] G. G. Ortiz, C. P. Hains, J. Cheng, H. Q. Hou, J. C. Zolper, Electron. Lett. **32**, 1205 (1996).

[2] S. Q. Luong, G. G. Ortiz, Y. Zhou, J. Lu, C. P. Hains, J. Cheng, H. Q. Hou, G. A. Vawter, IEEE Photon. Technol. Lett. **10**, 642 (1998).

[3] K. M. Geib, K. D. Choquette, A. Allerman, J. J. Hindi, J. Nevers, B. E. Hammons, LEOS 1998 Annual Meeting, paper ThC3 (1998).

Fabrication and performance of large (64x64) arrays of integrated VCSELs and detectors

Kent M. Geib*[a], Kent D. Choquette[b], Darwin K. Serkland[a],
Andrew A. Allerman[a], Terry W. Hargett[a]
[a]Sandia National Laboratories, Albuquerque, NM 87185; [b]University of Illinois, Electrical and Computer Engineering Dept., Urbana, IL 61801

ABSTRACT

Vertical-cavity surface-emitting lasers (VCSELs) are uniquely suited for applications requiring high-density 2-dimensional arrays of lasers, such as massively parallel interconnects or imaging applications. We have successfully fabricated 64x64 arrays containing alternating rows of selectively-oxidized 850 nm VCSELs and resonant-cavity photodetectors (RCPDs) on semi-insulating GaAs. In order to reduce the input/output pin count, we employed a matrix addressable architecture, where all the VCSELs (or RCPDs) in each row are connected by a common metal trace at the base of their mesas. The columns are connected by metal traces that bridge from mesa top to mesa top, connecting every other row (i.e., only VCSELs or only RCPDs). The pitch of devices in the array is 55 microns, and total resistance contributed by the long (up to 3.5 mm) row and column traces is below 50 ohms. The epitaxial design, fabrication and performance of these arrays is discussed.

Keywords: VCSEL arrays, integrated VCSELs and detectors

Introduction

Large 2-dimensional arrays of vertical-cavity surface-emitting lasers (VCSELs) were recognized early in their development as an enabling technology for many applications[1,2]. The inclusion of resonant-cavity photodetectors (RCPDs) within such a VCSEL array[3] will enable a variety of applications including high-density interconnects, position sensors and imaging devices. One of the major challenges to fabricating such arrays is developing an interconnect scheme to individually address each pixel in the array while maintaining a minimum device to device dimension. The matrix addressable wiring scheme shown in Fig. 1, where each element is addressed through a row and column designation, minimizes the chip size and lowers the package pin count, thereby placing more of the addressing complexity in software and less in hardware. In this paper we report the first monolithic integrated 64x64 matrix addressable VCSEL/RCPD array. This 64x64 VCSEL/detector array has been implemented in an anode up configuration and emits at nominally 850 nm using the GaAs/AlGaAs materials system.

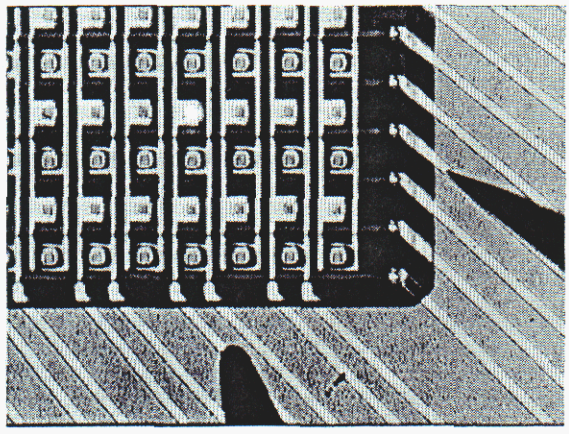

Fig. 1 An implementation of the matrix addressing scheme where a potential is provided between an anode column and a cathode row lighting up the VCSEL at their intersection.

* Correspondence: Email: kmgeib@sandia.gov; Telephone: 505 844 8214

Device Epitaxial Structure

Fabrication of oxide confined VCSELs using mesa isolation[4] requires deep etching to provide a path for the oxidizing species to reach the selective oxidation layer in the VCSEL structure[5]. The matrix addressable architecture requires electrically isolated cathodes and anodes. Thus, the epitaxial material was grown on semi-insulating GaAs using $Al_{0.16}Ga_{0.84}As/Al_{0.92}Ga_{0.08}As$ layers for the distributed Bragg reflectors (DBRs) and a GaAs active region. The deep mesa etching was done in a parallel plate reactive ion etching (RIE) system using a Cl_2-BCl_3 plasma which results in vertical mesa sidewalls. However, maintaining very accurate etch depth uniformity is important for positioning the electrical contacts of the array on the correct epitaxial layers. To overcome even a slight degree of etch depth nonuniformity requires the insertion of an etch-stop layer to precisely define the contact location within the DBR[6].

The following discussion of the epitaxial structure will proceed from the substrate upwards with a schematic diagram of the complete VCSEL/RCPD epitaxial structure being shown in Fig. 2. The mesa etch depth required for complete cathode isolation is nearly 9 μm for the 850 nm VCSEL if a complete n-type conducting DBR is used. Uniform etch depths for such high aspect ratio devices on a close spacing is difficult and is exacerbated by the variation in mesa density particularly near the array edge. due to the required wirebond pad area. Thus, an InGaP etch-stop layer and a 9/4 wavelength thick $Al_{0.16}Ga_{0.84}As$ n-type contact layer were placed only 7 mirror pair below the active layer in the n-type DBR forming an intra-mirror contact leaving the remaining 29 pairs undoped. This provides both low resistance contacts and good current spreading in the intra-mirror contact while greatly reducing the demands on the isolation etch. The InGaP etch-stop layer, however, must not adversely affect the optical or electrical properties of the mirror and it must also be uniformly removed prior to the cathode row isolation etch. Electrical and optical confinement for the VCSEL was provided by selective wet thermal oxidation of an AlAs layer located just below the active layer in the n-DBR.

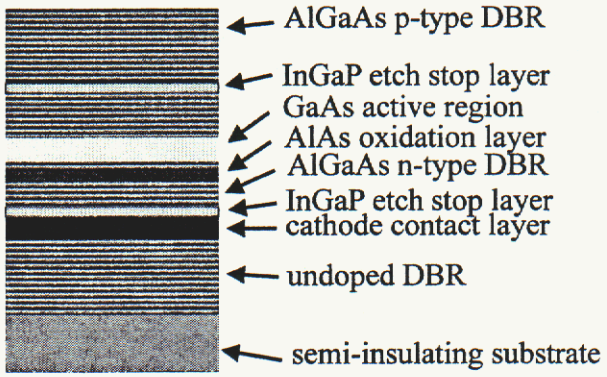

Fig. 2 Schematic representation of the epitaxial layers required to fabricate the matrix addressable array.

The number of top mirror pairs in the RCPD have a strong effect on the responsivity of the detector[7]. Thus, an InGaP etch-stop layer was inserted into the p-DBR to precisely define the top of the RCPD at 6 DBR pair above the active cavity. Although more than 6 top DBR pairs would have yielded a higher responsivity, only 6 pairs were used to obtain a wider spectral bandwidth.

The etch-stop layer developed for both the RCPD anode and the cathodes of both the VCSELs and RCPDs is an InGaP layer that is highly doped and surrounded by appropriately graded AlGaAs layers for good electrical performance. The InGaP layer fits within the quarter wavelength layer of the low-index portion of the DBR. An $Al_{0.16}Ga_{0.84}As$ contact layer was used below the RCPD anode etch-stop in order to minimize optical absorption. Although $Al_{0.16}Ga_{0.84}As$ may yield a higher contact resistance than GaAs, it is not as harmful to the low current RCPD as it would be to the high current VCSEL. A highly doped 9/4 wavelength thick $Al_{0.16}GaAs$ layer with a thin GaAs contact layer is grown as the uppermost layer for the high current VCSEL cathode which also serves as the RCPD cathode.

Fabrication

The basic fabrication process is shown in Fig. 3. The VCSEL anode metal and alignment targets are electron beam deposited Ti/Pt/Au (200 Å/200 Å/2000 Å) using a standard lift-off processes. The VCSEL mesa tops are protected with plasma deposited SiN_x and photoresist while the exposed surface is RIE etched down to the RCPD etch-stop layer. The mesas are 20 μm square on a 55 μm pitch in both directions with the critical lateral dimensions being indicated in Fig. 3a.

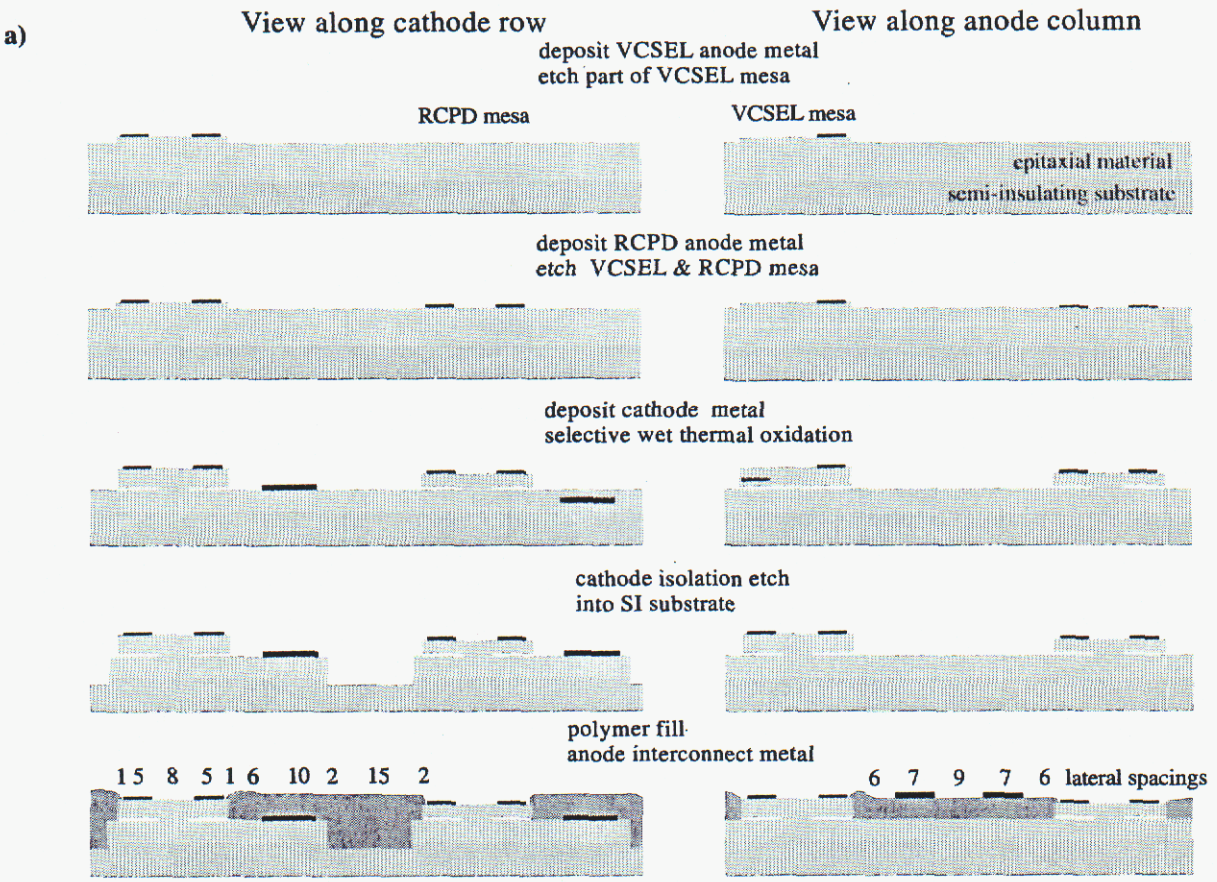

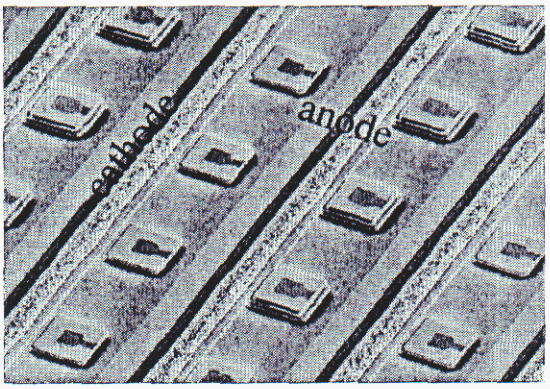

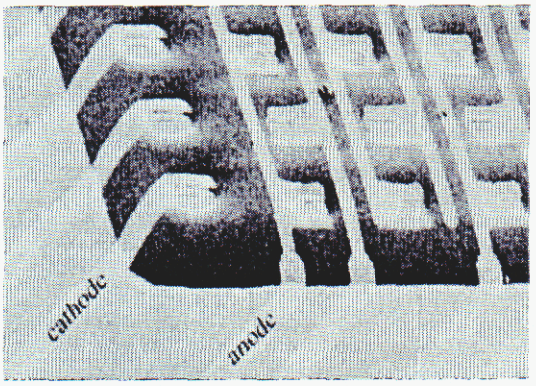

Fig. 3 a) Cross section of the major process steps viewed along the column and row directions b) SEM photo of the sample prior to polymer planarization c) and after completion.

After removing the InGaP layer in a HCl solution, another standard metal lift-off process is used to define the anode contacts for the RCPDs again using Ti/Pt/Au. Both the VCSEL and RCPD mesas are protected with plasma deposited SiN_x and photoresist and the exposed surface is etched down to the cathode etch-stop layer. After removing the InGaP layer, a similar metal lift-off process is used to define the cathode row contacts for both the VCSELs and RCPDs using Ge/Au/Ni/Au (260 Å/540 Å/200 Å/2500 Å). Although the contact layer is highly doped, it's conductivity is not sufficient for efficient low voltage operation and a common metal contact is deposited along the entire length of the cathode row providing a low resistance contact.

The cathodes of all devices (VCSELs or RCPDs) in each row are connected by a metal trace, but adjacent rows must be electrically isolated for proper matrix addressable operation. Trenches between adjacent cathode rows are photolithographically defined and RIE etched through the remaining DBR down to the GaAs substrate. This not only assures good electrical isolation between device rows but also allows wirebond pads to be deposited directly onto the substrate providing good bond pad adhesion to the substrate. Figure 3b is a SEM photomicrograph of the array prior to second level metalization providing a good perspective of the VCSELs, RCPDs, cathode metal and trenches that isolate the rows from each other. The arrays are then placed in the wet thermal oxidation furnace to laterally oxidize the current confinement layer and anneal the ohmic contacts. The arrays are planarized using spin on polymers that are reflowed at elevated temperature to provide good metal step coverage over the ~10 micron topology from the bondpad on the substrate to the top of the VCSEL mesa. The Ti/Au bond pad metal is deposited again using a lift-off process. The SEM image in Fig. 3c shows the interconnect metal step coverage at the edge of the completed array. A low magnification optical micrograph of the packaged array is shown in Fig. 4.

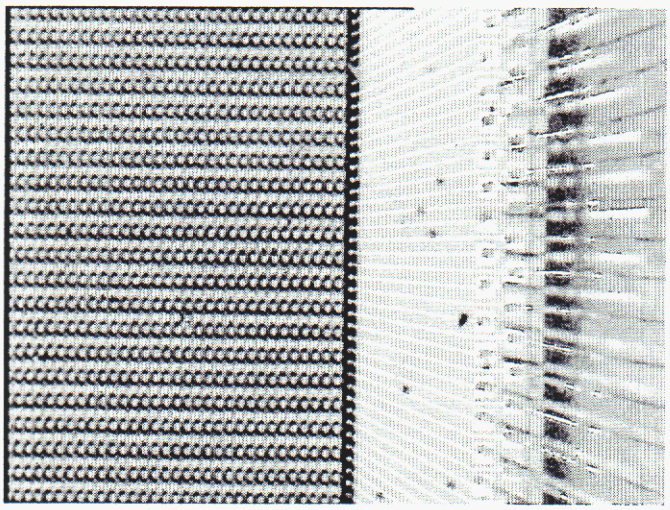

Fig. 4 Optical micrograph of a portion of the packaged array.

Device performance

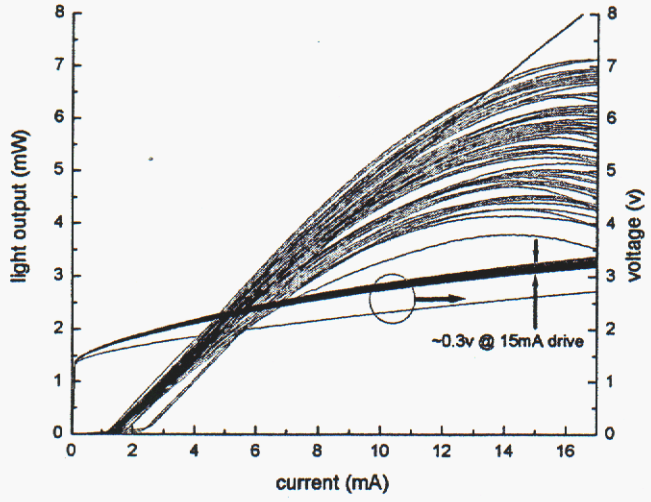

Fig. 5 Light-current-voltage curves for one cathode row in the center of the array. Note the low voltage variation at 15mA drive current.

The oxide confined VCSELs had square current apertures approximately 6 μm on a side with multimode emission at 853 nm. Figure 5 contains LIV data from 64 lasers along a typical row of the array. The laser threshold currents ranged from 1 to 2 mA and the peak output powers ranged from 4 to 7 mW. There are 2 curves showing unusually high output powers and low voltages. These data are from shorted devices where 2 lasers are connected in parallel. This can be seen readily in Fig. 6 which is a plot of the current required for 1mW of output power from all of the lasers in the array. The bright spots indicate where two or more VCSELs are connected in parallel. The two bright columns result from their anodes being shorted together due to faulty bond wires. The bright rows result from accidental connection of adjacent rows during testing. Also clearly observable in Fig. 6 are 3

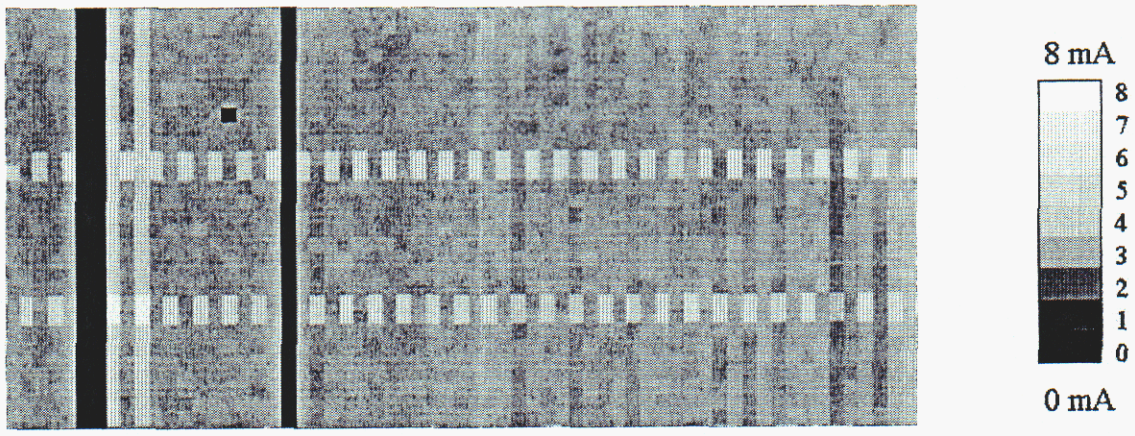

Fig. 6 A gray scale map of the drive current required to achieve 1mW light output for each laser (a 64x32 array).

columns of lasers that have no output due to poor wire bonds resulting in an electrical open circuit of the anode wire. Even though there is a significant spread in the peak output powers shown in Fig. 5, operation at a level of 1mW provides output uniformity sufficient for many applications. The VCSEL output nonuniformity results from uncharacteristic variation in the oxide aperture sizes and the cause is currently being investigated.

The voltage drop along the VCSEL cathode row in a matrix addressable device could potentially be excessive. In an effort to reduce this excess voltage drop, a relatively thick gold contact layer was deposited to aid the conduction through the cathode epitaxial material. Also, the metal trace is contacted to the package at both ends resulting in a voltage variation of only 0.3 volts at 15 mA drive current (R=20 ohms) for the lasers shown in Fig. 5.

The data in Fig. 7 is a typical RCPD photoresponse curve obtained using a wavelength tunable laser source focused into the detector anode aperture. The detector exhibited a peak responsivity of ~0.21 A/W at 853 nm with a full width at half maximum of 4.75 nm. The detector spectral bandwidth can be increased, but only with an accompanying decrease of the responsivity of a RCPD with decreasing mirror reflectivity[7]. For these matrix addressable arrays we chose to trade off responsivity for a wider acceptance bandwidth which provides less variation of the RCPD responsivity over the operating range of VCSEL wavelengths. This is an advantage for integrated RCPD/VCSEL structures, since with increased injection current, the VCSEL wavelength increases due to junction heating, while the reverse biased RCPD wavelength remains constant.

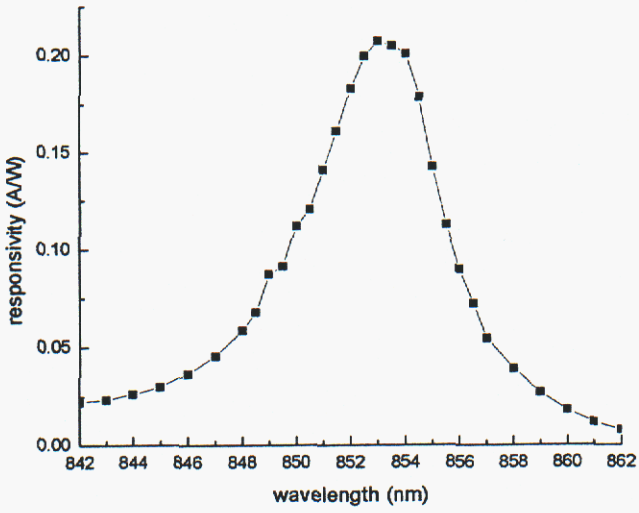

Fig. 7 Responsivity versus wavelength for a single RCPD in the center of the array.

Conclusions

We have demonstrated the feasibility of fabricating dense matrix addressable high count arrays of integrated VCSELs and RCPDs with performance suitable for many applications. VCSEL output uniformity and RCPD responsivity

improvements can be expected with additional growth and processing refinements. Contact resistances to devices in the central region of the matrix addressable array have been reduced to ~20 ohms through the use of both a metal cathode contact and redundant cathode trace to package contacts. Fabrication of the 4096 element matrix addressable array on a 55 μm pitch was made possible by the incorporation of InGaP etch-stop layers at the contact layers within both the upper and lower DBRs. We find the device pitch is limited by the etch aspect ratio that is possible using the parallel-plate RIE tool in combination with the photolithographic resolution possible given the 10 μm mesa topology.

Acknowledgements

Sandia is a multiprogram laboratory operated by Sandia Corporation for the United States Department of Energy under Contract DE-ACO4-94AL85000.

References

1. M. Orenstein, A. Von Lehmen, C. Chang-Hasnain, N. Stoffel, J. Harbison, and L. Florez, "Matrix addressable vertical cavity surface emitting laser array," *Electron. Lett.* **27**, pg 437 (1991).
2. A. Von Lehmen, C. Chang-Hasnain, J. Wullert, L Carrion, N. Stoffel, L. Florez, and J. Harbison, "Independently Addressable InGaAs/GaAs Vertical Cavity Surface Emitting Laser Arrays," *Electron. Lett.* **27**, 583 (1991).
3. K.M. Geib, K.D. Choquette, A.A. Allerman, D.K. Serkland, J.J. Hindi, J.A. Nevers, and B.E. Hammons, "Monolithically Integrated VCSELs and Photodetectors for Microsystems Applications," in *IEEE Lasers and Electro-Optics Society 1998 Annual Meeting*: 12/1/98 thru 12/4/98, Orlando, Florida: (1998).
4. K.D. Choquette, R.P. Schneider, Jr., K.L. Lear, and K.M. Geib, "Low threshold voltage vertical-cavity lasers fabricated by selective oxidation," *Electron. Lett.* **30**, 2043-2044 (1994)
5. K.M. Geib, K.D. Choquette, A.A. Allerman, R.D. Briggs, and J.J. Hindi, "Comparison of fabrication approaches for selectively oxidized VCSEL arrays," in *Vertical-Cavity Surface-Emitting Lasers IV*, K.D. Choquette and Chun Lei, eds. **3946**, 36-40, SPIE (2000).
6. M. Tayahi, N. Dutta, W. Hobson, D. Vakhshoori, J. Lopata, and J. Wynn, "High power InGaAs/GaAsP/InGaP surface emitting laser" *Electron. Lett.* **33**, 1794 (1997).
7. T. Knodl, H. Choy, J. Pan, R. King, R. Jager, G. Lullo, J. Ahadian, R. Ram, C. Fonstad, Jr., and K. Ebeling, "RCE Photodetectors based on VCSEL structures," *IEEE Photon. Tech. Lett.* **11**, 1289 (1999).

Fabrication and Performance of Two-Dimensional Matrix Addressable Arrays of Integrated Vertical-Cavity Lasers and Resonant Cavity Photodetectors

Kent M. Geib, Kent D. Choquette, *Senior Member, IEEE*, Darwin K. Serkland, *Member, IEEE*, Andrew A. Allerman, and Terry W. Hargett

***Abstract*—Massively parallel interconnects and scannerless imaging are applications that would benefit from high-density two-dimensional arrays of lasers. Vertical-cavity surface-emitting lasers (VCSELs) are uniquely suited for these applications due to their small size and high efficiency. We have successfully fabricated 64 × 64 element arrays containing alternating rows of selectively-oxidized 850 nm VCSELs and resonant-cavity photodetectors (RCPDs) monolithically integrated on semi-insulating GaAs substrates. In order to reduce the input and output connections to the array, we employ a matrix addressable architecture, where all the VCSELs (or RCPDs) in each row are connected by a common metal trace at the base of their mesas. The columns are connected by metal traces that bridge from mesa top to mesa top, connecting every other row (i.e., only VCSELs or only RCPDs). The pitch of devices in the array is 55 μm, and the total resistance contributed by the long (up to 3.5 mm) row and column traces is below 50 Ω. The design, fabrication, and performance of these arrays are discussed.**

***Index Terms*—Integrated VCSELs and detectors, VCSEL arrays.**

I. Introduction

EARLY in the development of vertical-cavity surface-emitting lasers (VCSELs), large two-dimensional (2-D) arrays were recognized as an enabling technology for many applications [1], [2]. The inclusion of resonant-cavity photodetectors (RCPDs) within such a VCSEL array [3] will enable a variety of applications including high-density interconnects, position sensors, and imaging devices. One of the major challenges to fabricating such large arrays is developing an interconnect scheme to individually address each pixel in the array while maintaining a minimum separation distance between devices. The matrix addressable architecture is illustrated in the scanning electron microscope (SEM) image in Fig. 1, where each element can be addressed through a row and column connection, minimizing the chip size and lowering the number of connections to the array from the package, thereby placing more of the addressing complexity in software and less in hardware. In this paper, we report the first monolithically integrated 64 × 64 element matrix addressable VCSEL/RCPD array. This 2-D array has been implemented in an anode up configuration and emits at nominally 850 nm using the GaAs/AlGaAs materials system grown by metalorganic vapor phase epitaxy.

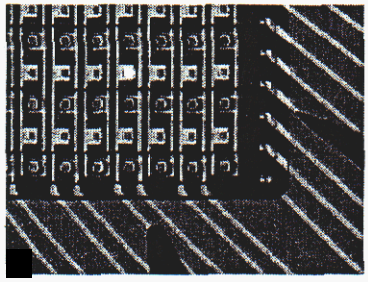

Fig. 1. Implementation of the matrix addressing scheme where a potential is provided between an anode column and a cathode row lighting up the VCSEL at their intersection.

Although the matrix addressable architecture is less flexible than that of an independently addressable array, it reduces the connections to a $N \times N$ array from N^2 to $2N$ [4]. Minimizing the number of electrical connections between the VCSEL array and the electronic circuitry will become very important for high-count arrays, even using advanced packaging techniques such as flip-chip bonding. For the 64 × 64 arrays that we discuss here, the number of bond pads required is reduced from 4096 to 128. Note that our application required separate anode contacts for the VCSELs and RCPDs in each column, thereby necessitating an additional 64 bond pads. Another important issue for matrix addressable VCSEL arrays is the larger effective series resistance. To reduce the electrical resistance of the long (3.5 mm) cathode traces, bond pads were provided at both ends of each cathode row increasing the total number of required bond pads to 256. In addition, we employed metal runners along the rows to augment the conductivity.

We first discuss the fabrication procedure that we developed to integrate VCSELs and RCPDs into the matrix addressable arrays. An important issue is the use of a selective etch stop for accurate delineation of the detector facet and device contacts. We next discuss the performance of both the VCSELs and detectors in our arrays. We conclude with a discussion of the limitations

Manuscript received April 10, 2002; revised May 20, 2002. Sandia is a multiprogram laboratory operated by Sandia Corporation for the United States Department of Energy under contract DE-ACO4-94AL85000.

K. M. Geib, D. K. Serkland, A. A. Allerman, and T. W. Hargett are with the Sandia National Laboratories, Albuquerque, NM 87185 USA (e-mail: kmgeib@sandia.gov).

K. D. Choquette is with the Electrical and Computer Engineering Department, University of Illinois, Urbana, IL 61801 USA.

Digital Object Identifier 10.1109/JSTQE.2002.801691.

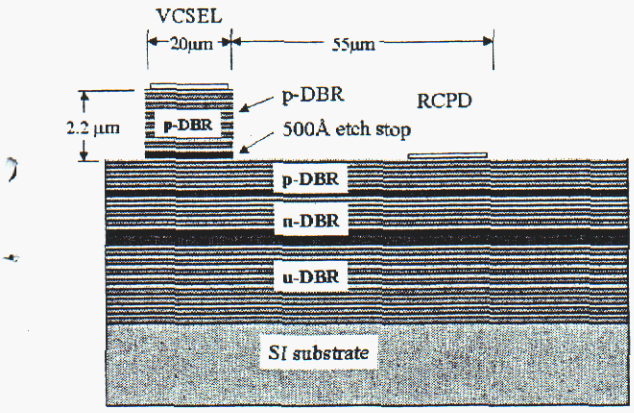

Fig. 2. Schematic cross section after etching to the RCPD anode layer.

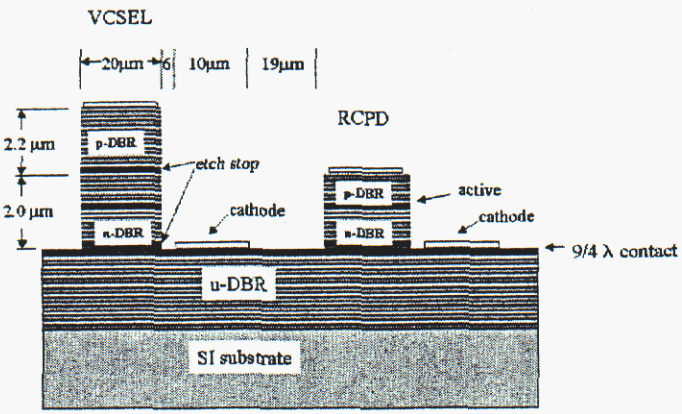

Fig. 3. Intramirror cathode contact location.

of our fabrication process for higher count and higher density (closer pitch) 2-D arrays.

II. Fabrication

The array fabrication process is shown schematically in Figs. 2–5. We begin by depositing Ti–Pt–Au (200 Å/200 Å/2000 Å) for the VCSEL anode metal and alignment marks using electron beam deposition and a standard liftoff process. Next, the VCSEL mesa tops are protected with plasma deposited SiN_x and photoresist, while the exposed surface is etched by reactive ion etching (RIE) through 15 distributed Bragg reflector (DBR) pairs to the RCPD anode etch-stop layer. The RIE system uses a parallel plate design and a Cl_2/BCl_3 plasma with *in situ* reflectance monitoring for precise identification of the etch depth. A slight variation in the thickness of the RCPD mirror termination layer has a dramatic impact on the detector responsivity [5]. To overcome possible array nonuniformities introduced by this etch, we found the use of an ~500- Å-thick ($1/4\lambda$) InGaP etch stop layer incorporated into the epitaxial stack [6] to be necessary to allow precise definition of the RCPD input mirror. In our design, we retained six DBR pairs above the active region.

After removing the InGaP etch stop layer in hydrochloric acid, another standard metal liftoff process is used to define the anode contacts for the RCPDs again using Ti–Pt–Au on a moderately doped $Al_{0.16}Ga_{0.84}As$ contact layer. Note that

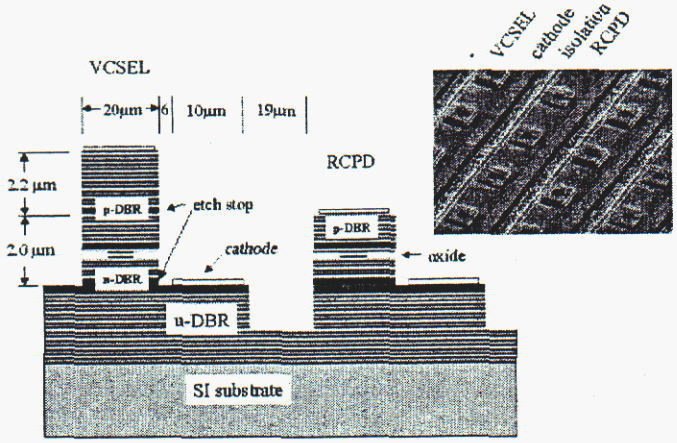

Fig. 4. Trench isolation etch and oxidation.

a low impedance contact is not essential for the anode of the reverse biased low current RCPD. Both the VCSEL and RCPD mesas are protected with plasma deposited SiN_x and photoresist, then the exposed surface is again etched by RIE to the cathode etch-stop layer (Fig. 3) located seven DBR pairs below the cavity. This InGaP etch-stop is located on a highly doped 200-Å-GaAs contact layer in the lower n-type mirror. Just below the contact layer is a 9/4 wavelength thick layer of highly doped $Al_{0.16}Ga_{0.84}As$. Under this highly doped layer, the remainder of the lower DBR is undoped, which is of course necessary to achieve device isolation between the VCSEL and detector elements in the array. The intramirror ohmic contact provides low resistance for optimum VCSEL operation while minimizing the required etch depth for device isolation. We found that minimizing the overall topology was critical to achieving close pitch arrays. Thus, by using an intramirror contact and an undoped (insulating) lower DBR, the device pitch is significantly reduced. After removing the InGaP layer, another metal liftoff process is used to define the cathode row contacts for both the VCSELs and RCPDs using Ge–Au–Ni–Au (260 Å/540 Å/200 Å/5000 Å). Although the cathode epitaxial contact layer is highly doped, its conductivity alone is not sufficient to provide a low-resistance path to devices in the center of the array. Thus, for efficient low-voltage operation across the entire array, a common metal contact is deposited along the entire length of the cathode row to provide a low resistance path to devices in the middle of the array.

The cathodes of all devices (VCSELs or RCPDs) in each row are connected by a metal trace, but adjacent rows must be electrically isolated for proper matrix addressable operation. As shown schematically in Fig. 4, trenches between adjacent cathode rows are photolithographically defined and the field between arrays is etched by RIE through the remaining 29 DBR layers down to the semi-insulating GaAs substrate. This not only assures good electrical isolation between device rows as well as exposing the aperture layers for oxidation [7] but also allows wirebond pads to be deposited directly onto the substrate providing good pad adhesion for wirebonding. The inset of Fig. 4 is a SEM photomicrograph of the array prior to final interconnect metallization providing a good perspective of the VCSELs, RCPDs, cathode metal, and trenches that isolate the rows from each other. Note

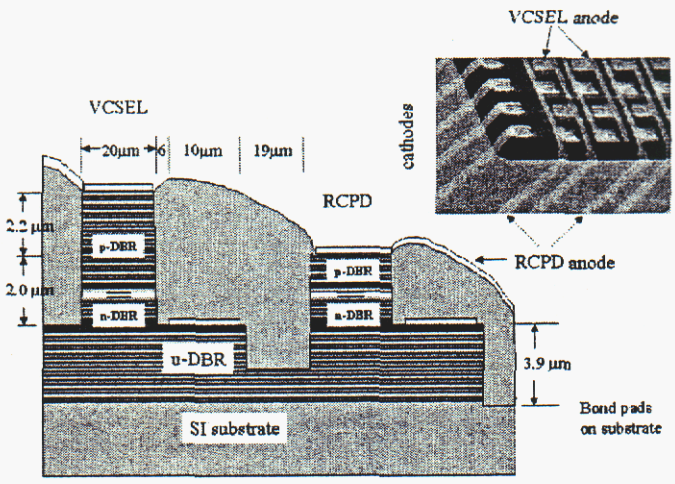

Fig. 5. Device planarization and anode interconnect metallization.

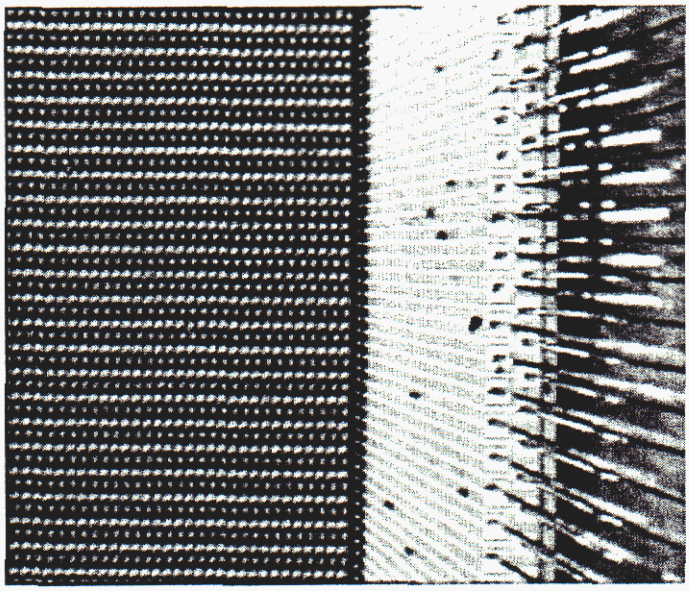

Fig. 6. Optical micrograph of a portion of the packaged array.

that because the aspect ratio during RIE limits the trench depth to less than that in the field, we must insure that the trenches are etched into the undoped portions of the bottom DBR. After this etch step, the arrays are then placed in the wet thermal oxidation furnace to laterally oxidize the current confinement layer [8] and simultaneously anneal the ohmic contacts. Although we require oxide confinement within the VCSELs, large area detectors are desirable to maximize the responsivity. The effective area of the RCPD would be decreased by lateral oxidation due to the shift in cavity resonance wavelength where the oxide is formed. Hence, to prevent the formation of a current aperture in the RCPD during VCSEL oxidation, the RCPD mesas are protected with photoresist to prevent lateral oxidation. After oxidation at 420° C, the hard-baked photoresist is removed in an oxygen plasma.

The arrays are planarized (Fig. 5) using spin-on polymers that are reflowed at elevated temperature. Reflow of the polymer film insures good metal step coverage over the nearly 10-μm topology between the bondpad on the substrate and the top of the VCSEL mesa, while maintaining good anode to cathode electrical isolation. Special photolithographic techniques using two layers of nominally 4-μm-thick photoresists were developed in order to provide the planarization necessary to achieve good lateral resolution over such extreme topologies. The final step is to deposit the Ti–Au bond pad metal using a liftoff process. The SEM image inset in Fig. 5 shows the interconnect metal step coverage at the edge of the completed array. The samples were finally mounted into a ceramic 256 pin grid array package for testing. A low-magnification optical micrograph of the packaged and wirebonded array is shown in Fig. 6.

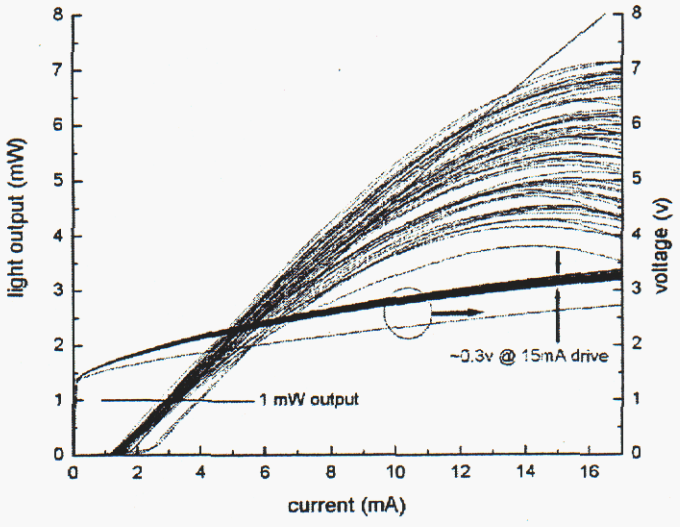

Fig. 7. Light-current-voltage curves for one cathode row in the center of the array. Note the low-voltage variation at 15-mA drive current.

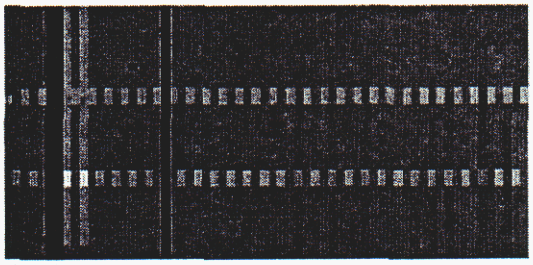

Fig. 8. Gray scale map of the drive current required to achieve a 1-mW light output for each laser (a 64 × 32 array).

III. Device Performance

The oxide confined VCSELs had square current apertures approximately 6 μm on a side with multimode emission at 853 nm. Fig. 7 contains LIV data from 64 lasers along a typical row of the array. The laser threshold currents ranged from 1.2 to 1.8 mA and the peak output powers ranged from 4 to 7 mW. There are two curves showing unusually high output powers and low voltages. These data are from shorted devices where two lasers are connected in parallel. These parallel connected VCSELs are readily apparent in Fig. 8, which is a plot of the current required for 1 mW of output power from all of the 2048 lasers in the array. The bright spots indicate where two or more VCSELs are connected in parallel. The two bright columns result from two anode interconnect traces being shorted together by faulty bond

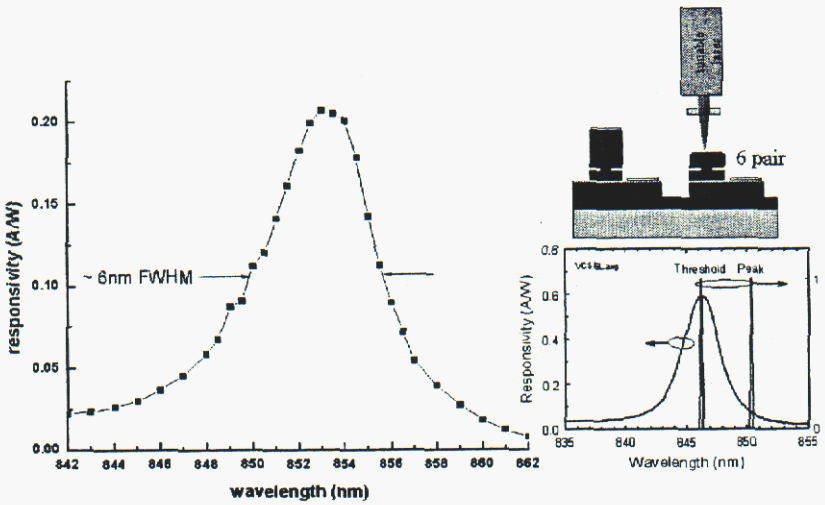

Fig. 9. Responsivity versus wavelength for a single RCPD in the center of the array as measured with the apparatus shown in the inset. The second inset shows the red shift of the VCSEL wavelength with injection current.

wires. The bright rows result from accidental connection of adjacent rows during testing. In addition, clearly observable in Fig. 8 are three columns of lasers that have no output due to bad wire bonds resulting in an electrical open circuit of the anode wire. Even though there is a significant spread in the peak output powers shown in Fig. 7, operation at a level of 1 mW provides output uniformity sufficient for many applications. The VCSEL output nonuniformity results from uncharacteristic variation in the oxide aperture sizes.

The voltage drop along the VCSEL cathode row in a matrix addressable device could potentially be quite large and could severely hamper the application. In an effort to reduce this excess voltage drop, a relatively thick gold contact layer was deposited along each row to enhance conduction. In addition, the metal trace is contacted to the package at both row ends resulting in a voltage variation of only 0.3 V at 15-mA drive current ($R = 20\,\Omega$) for the lasers shown in Fig. 7. The typical differential resistance (dV/dI) of the individual VCSELs is 149 Ω at 3-mA drive (~1 mW) and 88 Ω at 10 mA (~4 mW). The up to 4-mm-long, 10-μm-wide metal traces contribute a significant parasitic inductance, which we theoretically predict to be on the order of 6 nH. In the worst case, where both the anode and cathode address lines are this long, we estimate that the parasitic inductance will limit the small signal modulation bandwidth of the VCSELs to 2 GHz.

The data in Fig. 9 is a typical RCPD photoresponse curve obtained using a wavelength tunable laser source focused into the detector anode aperture as schematically depicted in the inset. The detector exhibited a peak responsivity of 0.21 A/W (~30% quantum efficiency) at 853 nm and a full-width at half-maximum of 5.75 nm, which closely match the previously reported values of 40% and 5.75 nm [9]. The detector spectral bandwidth can be increased by decreasing the top mirror reflectivity, but with an accompanying decrease of the responsivity [9]. For these matrix addressable arrays, we chose to trade off responsivity for a wider acceptance bandwidth which provides less variation of the RCPD responsivity over the operating range of VCSEL wavelengths. This is an advantage for integrated RCPD/VCSEL structures since with increased injection current the VCSEL wavelength red shifts due to junction heating while the reverse biased RCPD experiences no heating and the peak response wavelength remains constant as shown in the inset of Fig. 9.

IV. Conclusion

We have demonstrated the feasibility of fabricating dense matrix addressable high-count arrays of monolithically integrated VCSELs and RCPDs with performance suitable for many applications. VCSEL output uniformity and RCPD responsivity improvements can be expected with additional growth and processing refinements. Series resistances arising from the long metal traces to the VCSELs in the central region of the matrix addressable array have been reduced to ~20 Ω through the use of a metal cathode contact trace and redundant package contacts at each row end. Fabrication of the 4096 element matrix addressable array on a 55-μm pitch was made possible by the incorporation of two InGaP etch-stop layers: one at the top contact layer of the RCPD and one at the lower contact of both the RCPD and the VCSEL. Using the fabrication process that we have developed for matrix addressable arrays, we find the device pitch is limited by the etch aspect ratio achieved using the parallel-plate RIE tool in combination with the reduced photolithographic resolution due to the severe 10-μm mesa topology. Nevertheless, we have obtained viable VCSEL performance from the largest number of VCSELs contained within a single die achieved to date. The development of these high-count VCSEL arrays will enable new VCSEL applications in the areas of imaging, sensing, and communication, offering potential benefits to markets ranging from health care to computing.

References

[1] M. Orenstein, A. V. Lehmen, C. Chang-Hasnain, N. Stoffel, J. Harbison, and L. Florez, "Matrix addressable vertical cavity surface emitting laser array," *Electron. Lett.*, vol. 27, pp. 437–438, 1991.

[2] A. V. Lehmen, C. Chang-Hasnain, J. Wullert, L. Carrion, N. Stoffel, L. Florez, and J. Harbison, "Independently addressable InGaAs/GaAs vertical cavity surface emitting laser arrays," *Electron. Lett.*, vol. 27, pp. 583–585, 1991.

[3] K. M. Geib, K. D. Choquette, A. A. Allerman, D. K. Serkland, J. J. Hindi, J. A. Nevers, and B. E. Hammons, "Monolithically integrated VCSELs and photodetectors for microsystems applications," presented at the IEEE Lasers Electro-Optics Soc. Annu. Meet., Orlando, FL, Dec. 1–4, 1998.

[4] R. A. Morgan, G. D. Guth, C. Zimmer, R. E. Leibenguth, M. W. Focht, J. M. Freund, K. G. Glogovsky, T. Mullally, F. F. Judd, and M. T. Ason, "Two-dimensional matrix addressed vertical cavity top-surface emitting array display," *IEEE Photon. Technol. Lett*, vol. 6, pp. 913–917, Aug. 1994.

[5] D. K. Serkland, K. M. Geib, A. A. Allerman, and T. W. Hargett, "Monolithic integration of vertical-cavity surface-emitting lasers and wavelength-shifted resonant-cavity photodetectors," presented at the IEEE Lasers Electro-Optics Soc. Annu. Meet., San Diego, CA, Nov. 11–14, 2001.

[6] M. Tayahi, N. Dutta, W. Hobson, D. Vakhshoori, J. Lopata, and J. Wynn, "High power InGaAs/GaAsP/InGaP surface emitting laser," *Electron. Lett.*, vol. 33, pp. 1794–1795, 1997.

[7] K. M. Geib, K. D. Choquette, A. A. Allerman, R. D. Briggs, and J. J. Hindi, "Comparison of fabrication approaches for selectively oxidized VCSEL arrays," in *Vertical-Cavity Surface-Emitting Lasers IV*, K. D. Choquette and C. Lei, Eds. Bellingham, WA: SPIE, 2000, vol. 3946, pp. 36–40.

[8] K. D. Choquette, R. P. Schneider Jr., K. L. Lear, and K. M. Geib, "Low threshold voltage vertical-cavity lasers fabricated by selective oxidation," *Electron. Lett.*, vol. 30, pp. 2043–2044, 1994.

[9] T. Knodl, H. Choy, J. Pan, R. King, R. Jager, G. Lullo, J. Ahadian, R. Ram, C. Fonstad Jr., and K. Ebeling, "RCE Photodetectors based on VCSEL structures," *IEEE Photon. Tech. Lett.*, vol. 11, pp. 1289–1291, Oct. 1999.

Kent M. Geib received the M.S. degree in electrical engineering from Colorado State University (CSU), Ft. Collins.

He has been part of the advanced vertical cavity surface emitting laser (VCSEL) development team at Sandia National Laboratories, Albuquerque, NM, for the past eight years. His current research focus is on the development of advanced processes for the fabrication of novel optoelectronic devices including high-performance VCSELs and VCSEL arrays integrated with high-speed electronics. He was a Research Associate at CSU for 15 years, implementing surface analytical spectroscopies to study the chemical compositions and the development of the interfaces of III-V compound semiconductors with their oxides and/or metals. He has co-authored more than 90 peer reviewed journal articles and one book chapter.

Mr. Geib is a member of the American Vacuum Society and Sigma Xi.

Kent D. Choquette (M'97–SM'02) received B.S. degrees in engineering physics and applied mathematics from the University of Colorado, Boulder, and the M.S. and Ph.D. degrees in materials science from the University of Wisconsin, Madison, in 1984, 1985, and 1990, respectively.

From 1990 to 1992, he was a postdoctoral researcher with AT&T Bell Laboratories, Murray Hill, NJ, and in 1993, he joined Sandia National Laboratories, Albuquerque, NM. He joined the Electrical and Computer Engineering Department, University of Illinois, Urbana, in 2000. His research interests center around the design, fabrication, and characterization of vertical-cavity surface emitting lasers (VCSELs) and other optoelectronic devices. His research interests include novel fabrication technologies, hybrid integration techniques, and nano-fabrication processes. He has authored over 100 publications and two book chapters and has presented numerous invited talks and tutorials on VCSELs. He is an Associate Editor of the IEEE JOURNAL OF QUANTUM ELECTRONICS.

Dr. Choquette is a senior member of the IEEE/Lasers and Electro-Optics Society and a member of the Optical Society of America. From 2000 to 2002, he was an IEEE/LEOS Distinguished Lecturer.

Darwin K. Serkland (M'98) received the B.A. degree in physics and mathematics from Carleton College, Northfield, MN, and the Ph.D. degree in applied physics from Stanford University, Stanford, CA, in 1989 and 1995, respectively. His graduate research focused on the generation of squeezed states of light using periodically poled lithium niobate waveguides.

He was a Post-Doctoral Fellow and then a Research Assistant Professor, studying nonlinear fiber-optic devices using picosecond optical pulses, at Northwestern University, Evanston, IL. In 1998, he joined Sandia National Laboratories, Albuquerque, NM, where he currently leads a team in the design, growth, fabrication, and characterization of compound-semiconductor optoelectronic devices, including photodiodes, electro-absorption modulators, and vertical-cavity surface-emitting lasers.

Andrew A. Allerman received the Ph.D. degree in physics from Auburn University, Auburn, AL, in 1992.

He was a Research Scientist at the Australian National University, Canberra, Australia, and then joined Texas Instruments, Dallas, TX, where he worked on GaAs-based electronic devices. He is currently a Principle Member of Technical Staff at Sandia National Laboratories, Albuquerque, NM. His research projects are now focused on developing MOCVD growth of wide band gap nitride semiconductors for UV emitters and electronic devices. While at Sandia, he has advanced MOCVD growth techniques of antimony-based compound semiconductors for use in midinfrared (3.3 $\rightarrow$ 6.0 μm) lasers and LEDs. He has also studied the growth and properties of novel materials such as InGaAsN and GaAsSbN for long-wavelength (1.3 μm) opto-electronics and high-efficiency solar cells. He has developed vertical cavity surface emitting lasers from 740 nm to 1 μm for a number applications including external cavity frequency doubling.

Terry W. Hargett received the A.A.S. degree in avionics systems from the Community College of the Air Force, and the B.S. degree in business from Wayland Baptist College, Plainview, TX, in 1994 and 1995, respectively.

He retired from the United States Air Force in 1995 and from 1995 to 1998, he was an on-site residual gas analyzer site service engineer at Intel Fab 7, 9, and 11 by MKS Instruments, Albuquerque, NM. In 1998, he joined Sandia National Laboratories, Albuquerque, NM, as an MOCVD grower technician on a D-125 Emcore reactor. He supports numerous projects through growth and materials characterization including vertical-cavity surface-emitting lasers, solar cells, photonic integrated circuits, and optical and RF MEMs.

High density interleaved VCSEL-RCPD arrays for optical information processing

Kent M. Geib*[a], Darwin K. Serkland[a], Andrew A. Allerman[a],
Terry W. Hargett[a] , and Kent D. Choquette[b]

[a]Sandia National Laboratories, Albuquerque, NM 87185;
[b]University of Illinois, Electrical and Computer Engineering Dept., Urbana, IL 61801

ABSTRACT

Vertical-cavity surface-emitting lasers (VCSELs) are uniquely suited for massively parallel interconnects and scannerless imaging applications due to their small size, high efficiency and amiability to formation of high-density 2-dimensional arrays. We have successfully fabricated 4096 element arrays (64x64) containing alternating rows of selectively-oxidized 850 nm VCSELs and resonant-cavity photodetectors (RCPDs) on a 55 micron pitch monolithically integrated on semi-insulating GaAs substrates. We employ a matrix addressable architecture to reduce the input and output electrical connections to the array, where all the VCSELs (or RCPDs) in each row are connected by a common metal trace at the base of their mesas. The columns are connected by metal traces that bridge from mesa top to mesa top, connecting every other row (i.e., only VCSELs or only RCPDs). The design, fabrication and performance of these arrays is discussed.

Keywords: VCSEL arrays, integrated VCSELs and detectors

Introduction

Large 2-dimensional arrays of vertical-cavity surface-emitting lasers (VCSELs) have long been recognized as an enabling technology for many applications[1,2]. The inclusion of resonant-cavity photodetectors (RCPDs) within such a VCSEL array[3] will enable a variety of applications including high-density interconnects, position sensors and imaging devices. In this paper we report on the fabrication and performance of a monolithically integrated 64x64 element matrix addressable VCSEL/RCPD array. This 2-dimensional array has been implemented in an anode up configuration and emits at nominally 850 nm using the GaAs/AlGaAs materials system grown by metalorganic vapor phase epitaxy.

One of the major challenges to fabricating such large arrays is developing an interconnect scheme to individually address each element in the array while maintaining a minimum separation distance between devices. Although the matrix addressable (row and column) architecture is less flexible than independent addressing, it reduces the connections to a NxN array[4] from N^2 to 2N. Minimizing the number of electrical connections between the VCSEL array and the electronic circuitry will become very important for high-count arrays, even those using advanced packaging techniques such as flip-chip bonding. For the 64x64 arrays that we discuss here, the number of bond pads required is reduced from 4096 to 128. Note that our application required separate anode contacts for the VCSELs and RCPDs in each column, thereby necessitating an additional 64 bond pads. Another important issue for matrix addressable VCSEL arrays is the larger effective series resistance. To reduce the electrical resistance of the long (3.5 mm) cathode traces, bond pads were provided at both ends of each cathode row increasing the total number of required bond pads to 256.

* kmgeib@sandia.gov; phone 1 505 844-8214; FAX 1 505 844-8985; Sandia National Laboratories, PO Box 5800, MS 0603, Albuquerque, NM, USA 87185-0603

In the following sections, we will discuss the fabrication procedures developed to integrate VCSELs and RCPDs into the matrix addressable arrays. The use of a selective etch stop for accurate delineation of the detector facet and device contacts was an enabling technology for this fabrication. We will next discuss the performance of both the VCSELs and detectors in our arrays along with their performance in an actual system. Finally , we will conclude with a discussion of the limitations of our fabrication process for higher density (closer pitch) 2-dimensional arrays.

Fabrication

The array fabrication process is shown schematically in Figs. 1 through 3. We begin by depositing Ti/Pt/Au (200 Å/200 Å/2000 Å) for the VCSEL anode metal and alignment marks using electron beam deposition and a standard lift-off process. Next, the VCSEL mesa tops are protected with plasma deposited SiN_x and photoresist while the exposed surface is etched by reactive ion etching (RIE) through 15 distributed Bragg reflector (DBR) pairs to the RCPD anode etch-stop layer. The RIE system uses a parallel plate design and a Cl_2/BCl_3 plasma with in-situ reflectance monitoring for precise identification of the etch depth. A slight variation in the thickness of the RCPD mirror termination layer has a dramatic impact on the detector responsivity[5]. To overcome possible array nonuniformities introduced by this etch, we found it essential to use an ~500 Å thick (1/4λ) InGaP etch-stop layer incorporated into the epitaxial stack[6] to allow precise definition of the RCPD input mirror. In our design we retained 6 DBR pairs above the active region.

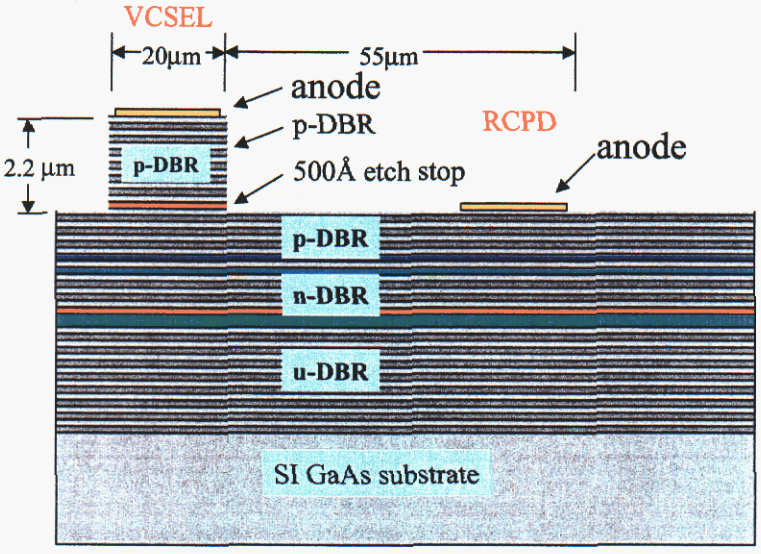

Fig. 1: A schematic cross-section after etching to the RCPD anode layer.

After removing the InGaP etch-stop layer in hydrochloric acid, another standard metal lift-off process is used to define the anode contacts for the RCPDs again using Ti/Pt/Au on a moderately doped $Al_{0.16}Ga_{0.84}As$ contact layer. Note that a low impedance contact is not essential for the anode of the reverse biased low current RCPD. Both the VCSEL and RCPD mesas are protected with plasma deposited SiN_x and photoresist then the exposed surface is again etched by RIE to the cathode etch-stop layer (Fig. 2) located 7 DBR pairs below the cavity. The mesa etch exposes the aperture layers for oxidation[7], provides mesa to mesa electrical isolation and precisely locates the n-type contact on a highly doped 200 Å GaAs contact layer in the lower n-type mirror. Just below the contact layer is a 9/4 wavelength thick layer of highly doped $Al_{0.16}Ga_{0.84}As$. Under this layer, the remainder of the lower DBR is undoped, which is necessary to achieve device isolation between the VCSEL and detector elements in the array. The intra-mirror ohmic contact provides low resistance for optimum VCSEL operation while minimizing the required etch depth for device isolation. We found that minimizing the overall topology was critical to achieving close pitch arrays. Thus, by using an intra-mirror contact and an undoped (insulating) lower DBR the device pitch can be significantly reduced. After removing the InGaP layer, another metal lift-off process is used to define the cathode row contacts for both the VCSELs and RCPDs using Ge/Au/Ni/Au (260 Å/540 Å/200 Å/5000 Å). Although the cathode epitaxial contact layer is highly doped, its conductivity is not sufficient to provide a low resistance path to devices in the center of the array. Thus, for efficient low voltage operation across the entire array, a common metal contact is deposited along the entire length of the cathode row to provide a low resistance path to devices in the middle of the array. This mesa etch also exposes the aperture layers for oxidation[7].

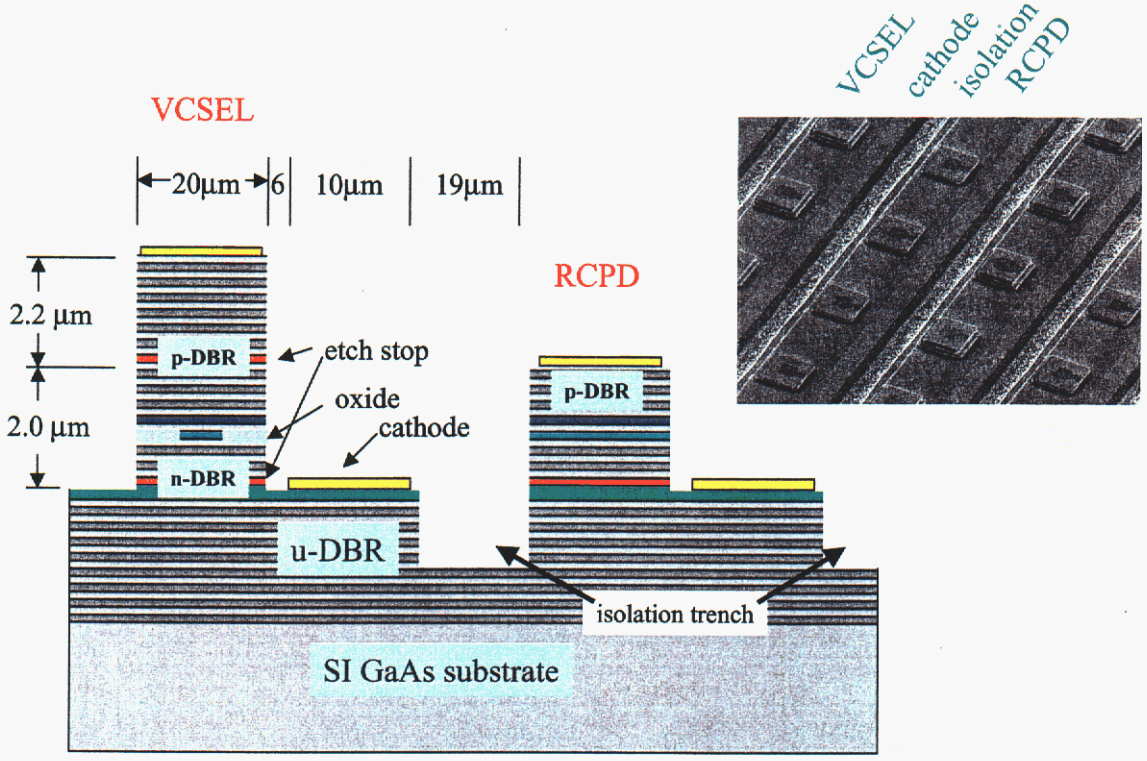

Fig. 2: Intra-mirror cathode contact location and trench isolation etch and oxidation.

The cathodes of all devices (VCSELs or RCPDs) in each row are connected by a metal trace, but adjacent rows must be electrically isolated for proper matrix addressable operation. As shown schematically in Fig. 2, trenches between adjacent cathode rows are photolithographically defined and etched by RIE into the undoped DBR layers. Simultaniously, (at a slightly faster etch rate than the narrow trenches within the array) the field between arrays is etched by RIE through the remaining 29 DBR layers down to the semi-insulating GaAs substrate. This not only assures good electrical isolation between device rows but also allows wirebond pads to be deposited directly onto the substrate providing good pad adhesion for wirebonding. The inset of Fig. 2 is a SEM micrograph of the array prior to final interconnect metalization providing a good perspective of the VCSELs, RCPDs, cathode metal and trenches that isolate the rows from each other. Note that because the narrow trench openings limit their etch rate to less than that in the field between arrays, we must insure that the trenches are etched into the undoped portions of the bottom DBR to achieve electrical isolation. After this etch step the arrays are then placed in the wet thermal oxidation furnace to laterally oxidize the current confinement layer[8] and simultaneously anneal the ohmic contacts. Although we require oxide confinement within the VCSELs, it is not desired in the RCPDs. The effective area of the RCPD would be decreased by lateral oxidation due to the shift in cavity resonance wavelength where the oxide is formed. Hence to prevent the formation of a current aperture in the RCPD during VCSEL oxidation, the RCPD mesas are protected with photoresist to prevent lateral oxidation. After oxidation at 420°C the hard baked photoresist covering the RCPDs is removed in an oxygen plasma.

The arrays are planarized (Fig. 3) using spin-on polymers that are reflowed at elevated temperature. Reflow of the polymer film insures good metal step coverage over the nearly 10 μm topology between the bondpads on the substrate and the tops of the VCSEL mesas, while maintaining good anode to cathode electrical isolation. Special photolithographic techniques using two layers of nominally 4 μm thick photoresist were developed in order to provide the planarization necessary to achieve good lateral resolution over such extreme topologies. The final step is to deposit the Ti/Au bond pad metal using a lift-off process. The SEM image inset in Fig. 3 shows the interconnect metal step

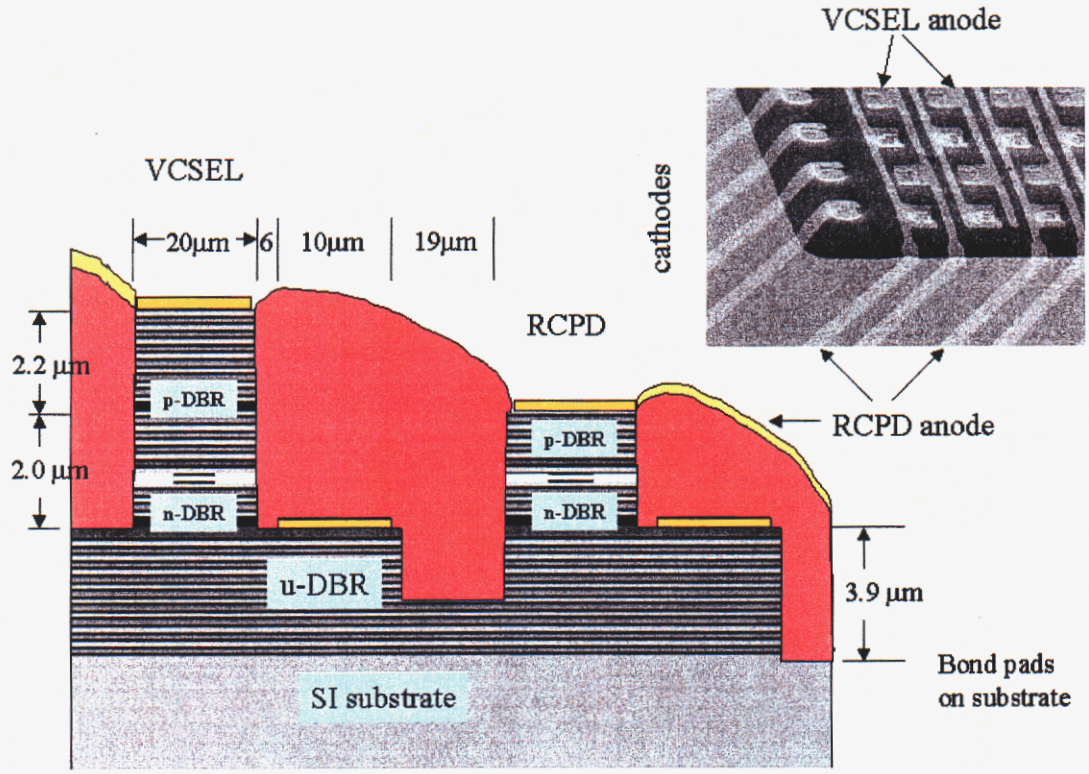

Fig. 3: Device planarization and anode interconnect metalization.

coverage at the edge of the completed array. Each array was finally mounted into a ceramic 256 pin grid array package for testing.

Device performance

Shown in Fig. 4 is a plot of the current required for 1mW of output power from all of the 2048 lasers in the array. The bright spots indicate where two or more VCSELs are accidentally connected in parallel. The two bright columns result from two anode interconnect traces being shorted together by faulty bond wires. The bright rows result from accidental connection of adjacent rows during testing. Also clearly observable in Fig. 4 are 3 columns of lasers that have no output due to bad wire bonds resulting in an electrical open circuit of the anode wire. Even though there is a spread in the VCSEL peak output powers, operation at a level of 1mW provides output uniformity sufficient for many applications such as the one shown below.

The data in Fig. 5 is a typical RCPD photoresponse curve obtained using a wavelength tunable laser source focused into the detector anode aperture. The detector exhibited a peak responsivity of 0.21 A/W (~30% quantum efficiency) at 853 nm and a full width at half maximum of 5.75 nm, which closely match the

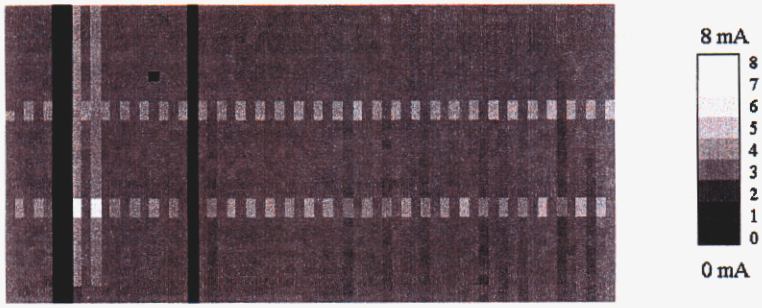

Fig. 4: A gray scale map of the drive current required to achieve 1mW light output for each laser (a 64x32 array).

previously reported values[9] of 40% and 5.75 nm. The detector spectral bandwidth can be increased by decreasing the top mirror reflectivity, but with an accompanying decrease of the responsivity[9]. For these matrix addressable arrays we chose to trade off responsivity for a wider acceptance bandwidth which provides less variation of the RCPD responsivity over the operating range of VCSEL wavelengths. This is an advantage for integrated RCPD/VCSEL structures since with increased injection current the VCSEL wavelength red shifts due to junction heating while the reverse biased RCPD experiences no heating and the peak response wavelength remains constant as shown in the inset of Fig. 5.

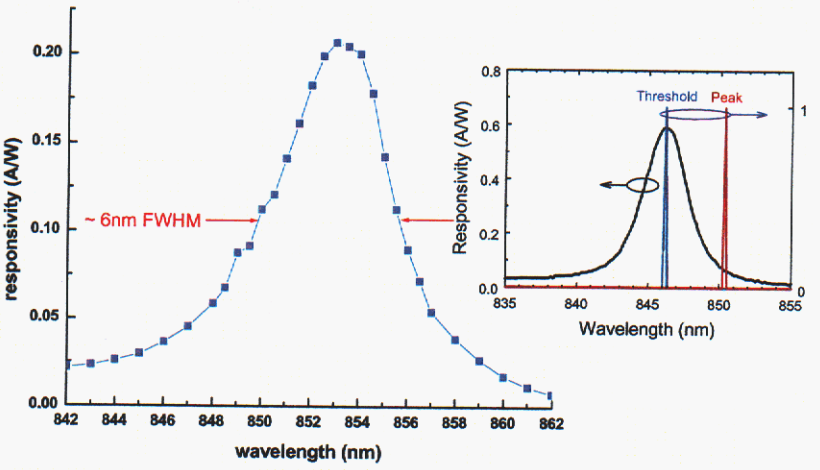

Fig. 5: Responsivity versus wavelength for a single RCPD in the center of the array. The inset shows the red shift of the VCSEL wavelength with injection current.

The prototype chip was developed for the scannerless imaging system of New Dimension Research, Inc. (Woburn, Massachusetts) that uses the chip as both the source and detector. A photograph of an image resolution target obtained from this system is shown in Fig. 6. The device-to-device pixelization is clearly visible at the high magnification. The pixelization can be minimized by reducing the device pitch. The 55 μm pitch used here is conservative to serve as proof of principle and Fig. 7 shows part of a test array that performed nicely with a 40 μm pitch. The minimum device pitch is dictated by the achievable isolation etch aspect ratio and the lithographic resolution possible over the large surface topology.

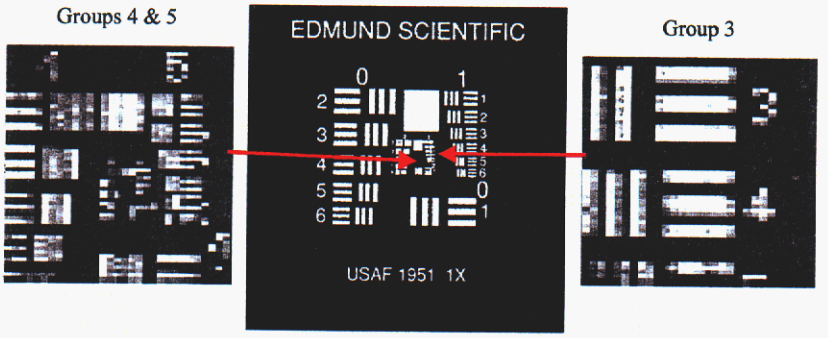

Fig. 6: Scannerless images of a resolution target using the matrix addressable array to demonstrate ~12 μm lateral resolution. Images courtesy of New Dimension Research, Inc. of Woburn, Massachusetts.

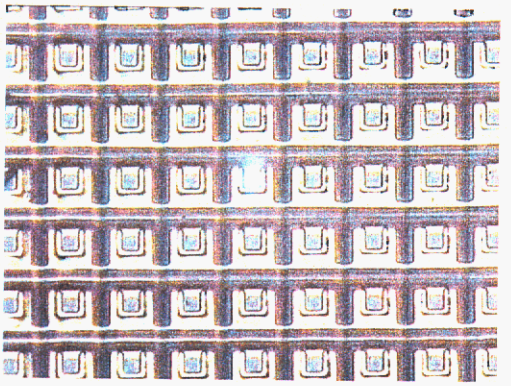

Fig. 7: An optical micrograph of a portion of a 10x16 VCSEL test array on a 40 μm pitch with the center element illuminated.

Conclusions

We have demonstrated the feasibility of fabricating dense matrix addressable high-count arrays of monolithically integrated VCSELs and RCPDs with performance suitable for many applications.

VCSEL output uniformity and RCPD responsivity improvements can be expected with additional growth and processing refinements. Fabrication of the 4096 element matrix addressable array on a 55 μm pitch was made possible by the incorporation of two InGaP etch-stop layers, one at the top contact layer of the RCPDs and one at the lower contact of both the RCPD and the VCSEL. Using the fabrication process that we have developed for matrix addressable arrays, we find the device pitch is limited by the etch aspect ratio achieved using the parallel-plate RIE tool in combination with the reduced photolithographic resolution due to the severe 10 μm mesa topology. Nevertheless, scannerless images with ~12 μm lateral resolution have been obtained using the VCSEL illuminators and RCPD detectors. The development of these high-count VCSEL/RCPD arrays will enable new VCSEL applications in the areas of imaging, sensing, and communication, offering potential benefits to markets ranging from health care to computing.

Acknowledgements

Sandia is a multiprogram laboratory operated by Sandia Corporation for the United States Department of Energy under Contract DE-ACO4-94AL85000. This work was partially supported by National Institutes of Health under the Small Business Innovation Research grants RR12279 and EY12067.

References

1. M. Orenstein, A. Von Lehmen, C. Chang-Hasnain, N. Stoffel, J. Harbison, and L. Florez, "Matrix addressable vertical cavity surface emitting laser array," *Electron. Lett.* **27**, pg 437 (1991).
2. A. Von Lehmen, C. Chang-Hasnain, J. Wullert, L Carrion, N. Stoffel, L. Florez, and J. Harbison, "Independently Addressable InGaAs/GaAs Vertical Cavity Surface Emitting Laser Arrays," *Electron. Lett.* **27**, 583 (1991).
3. K.M. Geib, K.D. Choquette, A.A. Allerman, D.K. Serkland, J.J. Hindi, J.A. Nevers, and B.E. Hammons, "Monolithically Integrated VCSELs and Photodetectors for Microsystems Applications," in *IEEE Lasers and Electro-Optics Society 1998 Annual Meeting*: 12/1/98 thru 12/4/98, Orlando, Florida: (1998).
4. R. A. Morgan, G. D. Guth, C. Zimmer, R. E. Leibenguth, M. W. Focht, J. M. Freund, K. G. Glogovsky, T. Mullally, F.F. Judd, and M. T. Ason, "Two-Dimensional Matrix Addressed Vertical Cavity Top-Surface Emitting Array Display," IEEE *Photon. Tecl. Lett* **6**, pg 913 (1994).
5. Darwin K. Serkland, K.M. Geib, A.A. Allerman, and T.W. Hargett, "Monolithic integration of vertical-cavity surface-emitting lasers and wavelength-shifted resonant-cavity photodetectors," in *IEEE Lasers and Electro-Optics Society 1998 Annual Meeting*: 11/11/01 thru 11/14/01, San Diego, California: (2001).
6. M. Tayahi, N. Dutta, W. Hobson, D. Vakhshoori, J. Lopata, and J. Wynn, "High power InGaAs/GaAsP/InGaP surface emitting laser" *Electron. Lett.* **33**, 1794 (1997).
7. K.M. Geib, K.D. Choquette, A.A. Allerman, R.D. Briggs, and J.J. Hindi, "Comparison of fabrication approaches for selectively oxidized VCSEL arrays," in *Vertical-Cavity Surface-Emitting Lasers IV*, K.D. Choquette and Chun Lei, eds. **3946**, 36, SPIE (2000).
8. K.D. Choquette, R.P. Schneider, Jr., K.L. Lear, and K.M. Geib, "Low threshold voltage vertical-cavity lasers fabricated by selective oxidation," *Electron. Lett.* **30**, 2043 (1994).
9. T. Knodl, H. Choy, J. Pan, R. King, R. Jager, G. Lullo, J. Ahadian, R. Ram, C. Fonstad, Jr., and K. Ebeling, "RCE Photodetectors based on VCSEL structures," *IEEE Photon. Tech. Lett.* **11**, 1289 (1999).

Distribution:

1	MS 9018	Central Technical Files, 8945-1
2	MS 0899	Technical Library, 9616
1	MS 0612	Review & Approval Desk, 9612
1	MS 0188	D. Chavez, LDRD Office, 1030
6	MS0603	K. M. Geib, 1742
1	MS0603	D. K. Serkland, 1742
1	MS0601	A. A. Allerman, 1126
1	MS0603	G. M. Peake, 1742
1	MS0603	T. W. Hargett, 1742
1	MS0603	S. Samora, 1743
1	MS0603	V. M. Montano, 1742
1	MS0603	G. D. Karpen, 1742
1	MS0603	D. J. Rieger, 1763
1	MS0603	R. D. Briggs, 1742
1	MS0603	G. R. Hadley, 1742
1	MS0603	T. R. Carter, 1743
1	MS0601	A. J. Fischer, 1123
1	MS0603	C. T. Sullivan, 1742